Print edition ISSN 2615-5109
Electronic edition ISSN 2621-0541

Publisher:
Center of Technology, Fakultas Teknik, Universitas Hasanuddin

Address:
Engineering Faculty Campus, Hasanuddin University
Jl. Poros Malino km. 6, Bontomarannu
Kabupaten Gowa, Sulawesi Selatan, Indonesia, 92171
Email : epi-ije@unhas.ac.id
Website : cot.unhas.ac.id/journals/index.php/epiije
Telp/Fax : +62-(0)411-58601

EPI International Journal of Engineering
Editorial Board

Foreword

It is with great pleasure that we present the latest edition of the EPI International Journal of Engineering (EPI-IJE), Volume 7, Number 2, August 2024. This issue brings together a diverse range of research studies that contribute to the advancement of engineering knowledge and its practical applications. The selected papers highlight current challenges and innovations across various engineering disciplines, including marketing analysis, mining engineering, structural mechanics, geotechnical engineering, construction management, and renewable energy systems.

The first paper, "The Impact of Viral Stealth Marketing on Consumers' Buying Interest on Cosmetic Products", explores the effectiveness of viral stealth marketing strategies in influencing consumer purchasing behavior in the cosmetics industry. The second paper, "Slope Stability Analysis of Pit X on Nickel Mining Based on Comparison between Design and Actual Mining Condition", examines the stability of a nickel mining slope by comparing theoretical design models with actual field conditions.

The third paper, "Vibration Analysis of Simply Supported Rectangular Plates Constrained by Rotational Edge Springs", presents an analytical study on the vibrational behavior of rectangular plates with rotational constraints. The fourth paper, "Bearing Capacity and Deformation of Timber Pile-Raft Foundation on Soft Soil Deposits", investigates the performance of timber pile-raft foundations in weak soil conditions.

The fifth paper, "Performance and Capabilities of Small Qualification Contractors on the Sustainable Construction Regulations Implementation", assesses the ability of small contractors to comply with sustainable construction regulations. Finally, the sixth paper, "Performance Investigation of Solar Water Heating System with Flat-plate Absorber Integrated with Thermal Storage", explores the efficiency of solar water heating systems incorporating thermal storage technology.

We extend our gratitude to all the authors, reviewers, and editorial team members who have contributed to this issue. We hope that the research findings presented in this volume will inspire further studies and technological advancements in their respective fields.

Sincerely,

Dr. Faisal Mahmuddin
Editor-in-Chief of EPI-IJE

TABLE OF CONTENTS

EPI International Journal of Engineering
Volume 7, Number 2, August 2024, pp. 44-48
DOI: 10.25042/epi-ije.082024.01

*p*ISSN 2615-5109
*e*ISSN 2621-0541

The Impact of Viral Stealth Marketing on Consumers' Buying Interest on Cosmetic Products

Andi Dian Sry Rezki Natsir[a,*], Riskawati[b], Rianti Indah Lestari[c], Fitri Junianti[d], Anita Wardana[e]

[a]Agricultural Industrial Engineering, Polytechnic ATI Makassar, Makassar, Indonesia. Email: andidiansryrezki@atim.ac.id
[b]Agricultural Industrial Engineering, Polytechnic ATI Makassar, Makassar, Indonesia. Email: riskawati@atim.ac.id
[c]Agricultural Industrial Engineering, Polytechnic ATI Makassar, Makassar, Indonesia. Email: indahrianty@atim.ac.id
[d]Chemical Engineering, Polytechnic ATI Makassar, Makassar, Indonesia. Email: fitrijuanianti@atim.ac.id
[e]Public Relation Unit, Polytechnic ATI Makassar, Makassar, Indonesia. Email: anitawardana@atim.ac.id

Abstract

The concept of viral stealth marketing has been actively used by marketers to make products well-received in society. Stealth marketing is one of the digital marketing strategies that advertises a product or service to someone without them realizing that they are becoming a marketing object. Stealth marketing is more commonly found on social media platforms today, such as Facebook or Instagram, than traditional advertising media, such as newspaper, TV, and radio broadcasts. Influencers as service providers are becoming more general in this method of marketing. Cosmetic products are products that are often marketed with the viral stealth marketing method. Recommendations of cosmetic products from people we know will be easier to accept. Data collection was carried out by conducting a survey on the age group of Gen Z. Data processing using paired t-test and F-test. The results of the paired t-test found that there was a difference in the buying interest of consumers who received product promotion treatment (B1) with the group of consumers who received agent recognition treatment (B2) with a significance value of 0.000. Meanwhile, the results of the F-test show that the presence of agent recognition treatment affects consumers' buying interest in indicators of seeking information, trying products, knowing more, and the desire to own products. This result indicates a change in the buying interest of consumers in cosmetic products when they are aware of the use of viral stealth marketing promotion methods.

Keywords: Customer, viral marketing, viral stealth marketing, t-test and F-test

1. Introduction

In line with the development of communication technology, competition between marketers is getting tougher and unavoidable [1]. Every day, marketers have to do more, work smarter and harder, be creative and have to have many ways to convince consumers to make their communication messages more audible [2]. Advertising is one of the ways used by marketers to send messages to consumers to communicate company products [3]. The traditional communication strategy that has been built by companies with their consumers has begun to change [4], [5], where in influencing consumers or in their marketing communications, marketers try to create a strategy that as much as possible, uses a more subtle way of persuading consumers [6], [7] so as to avoid defense mechanisms as an initial reaction to consumers that can hinder the achievement of these marketing communication goals [8].

One of the factors that causes traditional marketing techniques, such as advertising on TV, tabloid newspapers, radio, and other media, to be shifted due to the ineffectiveness of conventional advertising today due to the huge advertising costs and also the decreasing opportunities for consumers to pay attention to existing advertisements [9], [10]. Marketing techniques are moving more toward digital with more subtle word-of-mouth communication methods [11], [12]. One that is quite famous is viral stealth marketing (VSM). Alkhafagi and ALsiede [13] stated that stealth marketing methods show a positive effect on customer engagement. The development of social media that has entered all levels of society has also caused conventional methods to be considered ineffective. The linkage between social networks and marketing is formed by the relationship of the world's communication and society [14].

The target market that is very relevant to marketing new models through viral stealth marketing is Generation Z, who have excellent digital literacy. From [15] in their book Marketing to Gen Z, they state that a special approach is needed to be able to sell products to Generation Z. They have a liberal relationship, are based on the strength of numbers or group acceptance, are oriented towards entrepreneurial skills, and think globally without forgetting their locality.

Cosmetic products become unique products for sale. Marketers must be smart in influencing potential consumers to gain consumer buying interest [16]. Cosmetic products that are applied to the consumer's body

*Corresponding author. Tel.: +62 822 1035 2784
Jalan Sunu No. 220, Makassar
South Sulawesi, Indonesia

cause consumers to be very selective in choosing cosmetic products that are suitable for them. Cosmetics have become a basic necessity for women in beautifying themselves in a fast way. The increasing need for women to beautify themselves has made the cosmetics industry increase rapidly in Indonesia [17]. This is what causes a new marketing technique to become more popular, especially for the target market of Gen Z. Techniques that use a more refined approach, attract more attention, and can reduce advertising costs are needed to know consumers' buying interest. Based on the description above, researchers tried to raise the title The Impact of Viral Stealth Marketing on Consumer Buying Interest in Cosmetic Products.

2. Research Methodology

The tools and materials used in this study are questionnaires, examples of cosmetic products (face wash soap), product promotional videos and promotional agent recognition videos as treatment tools given to respondents.

The type of research used is experimental research. The experimental research approach aims to identify cause-and-effect relationships between variables [18]. Experimentation is an objective observation of phenomena that are made to occur in a highly controlled situation in which one or more factors are allowed to vary while others are allowed to be constant [19]. The stages of conducting laboratory experimental research with the data collection method using this questionnaire are as follows:

1. Preparation of data retrieval instruments.
   The data collection instrument in the form of a questionnaire is made based on the results of the literature review regarding consumer buying interest indicators.
2. Creation of treatment videos.
   There are 2 videos of treatment given in this study, firstly a promotional video that tells the experience of the agent in using cosmetic product X. Second the video of the agent's recognition that the experience of using cosmetic product X that was previously told was not based on his personal reference but the scenario obtained from cosmetic product company X and the agent got paid from cosmetic product company X.
3. Division of respondent groups.
   The data collection process begins by dividing the group of respondents into two groups of respondents, namely group A as the group of respondents control and group B as the group of treatment respondents.
4. Giving treatment to the respondent group.
   The treatment was given in two sessions. The first session was given a treatment using product promotional videos for each group (A1 and B1). The second session was given the same product promo video in the first session for group A (A2) and the agent recognition video treatment for group B (B2).
5. Data collection using questionnaires for each group of respondents.
   A questionnaire measuring the buying interest of Generation Z consumers was given to each group in each session with the following variables:
   Y1 = looking for information
   Y2 = consider buying
   Y3 = interested in trying
   Y4 = want to know
   Y5 = want to have

   The Likert scale with a range of choices strongly agrees to the point of strongly disagreeing. The scores for each of the answer choices are as follows:
   SA = Strongly Agree; Score 5
   A = Agree; Score 4
   LS = Less Agree; Score 3
   DA = Disagree; Score 2
   SDA = Strongly Disagree; Score 1
6. Data processing.
   The data obtained were then processed using paired t-test samples for groups A1-A2 (Pair 1), B1-B2 (Pair 2), A1-B1 (Pair 3), and A2-B2 (Pair 4). This is done to find out the differences between the groups paired in the test. In this study, the F test was also used to determine which variables distinguished the control group (A) and the treatment group (B).

3. Results and Discussion

3.1. Results

This study involved 30 respondents who were divided into two groups of 15 people each. Group A is the control group, and group B is the group that is given treatment. Respondents were selected by a random purposive method based on a group of Generation Z consumers between the ages of 20 and 21. Statistical data on pairs of groups of respondents can be seen in Table 1.

In Table 1, it can be seen that there are 4 pairs of groups paired, namely A1-A2 (Pair 1), B1-B2 (Pair 2), A1-B1 (Pair 3), and A2-B2 (Pair 4). All groups had a sample count (N) of 15 data each. This indicates that the amount of data entered on the data processing is the same for each test group and has been completed [20]. Pair 1 compares the A1 data group with A2 where it shows the average data spread, standard deviation, and standard mean error have the same values for both groups (A1-A2). The display of the results of this preliminary data can be expected for the two groups, but there is no difference in consumer buying interest. Pair 2 compared the B1 and B2 groups with their average values, standard deviations, and average standards to be quite different, so we can guess that the group of B1 respondents who got the cosmetic product promotion treatment with the group of B2 respondents who got the recognition treatment, had different buying interests.

Table 1. Paired samples statistics

		Mean	N	Std. Deviation	Std. Error Mean
Pair 1	A1	4.160	15	.2414	.0623
	A2	4.160	15	.2414	.0623
Pair 2	B1	3.840	15	.5082	.1312
	B2	3.067	15	.7118	.1838
Pair 3	A1	4.160	15	.2414	.0623
	B1	3.840	15	.5082	.1312
Pair 4	A2	4.160	15	.2414	.0623
	B2	3.067	15	.7118	.1838

Pair 3 comparison between groups A1 and B1 shows that the average value of the respondents' data distribution is not much different, namely 4.160 (A1) and 3,840 (B1). It is alleged that the two groups had relatively similar buying interests after receiving promotional treatment for cosmetic products. The average answer that respondents had was around a score of 4, which means that consumer interest in cosmetic products is quite good. The average respondent chose to agree to the buying interest variable (Y 1, Y 2, Y 3, Y 4, and Y 5). Pair 4 compared groups A2 and B2, where the two groups had different treatments. Group A2 (group A, session 2) received the same promotional video treatment in the first session as the control group. Group B2 (group B session 2) received a video recognition treatment. In Table 1, groups A2 and B2 have quite different average values, standard deviations, and standard mean errors. The average choice of respondents in group A2 had a score of 4 (agree), while in group B2, it was in group 3 (less agree). It can be presumed that there are differences in consumer buying interest from the two groups of respondents [21].

The paired data are then processed by conducting a t-test for each group of respondents. The results of data processing using SPSS can be seen in Table 2.

In Table 2, we can see that with a significance level of less than 0.05, pair 1 (A1-A2) shows an insignificant value (1,000). This can be interpreted as the two groups being equal or not having a difference in buying interest in both the first session and in the second session [22]. This control group showed that the promotion treatment given in session 1 (A1) and session 2 (A2) was consistent. Pairs 2, 3, and 4 produce signification values of less than 0.05 i.e., 0.001, 0.033, and 0.000, respectively. This shows that between the groups for each of their partners have different buying interests. The existence of a video of the agent's recognition treatment affects consumers' buying interest in the cosmetic products offered [23].

The F test is used to determine what variables most distinguish the group that gets the promotion treatment (B1) from the group that gets the agent recognition treatment (B2). The following are the results of processing F test data:

In Table 3, the significance values that are less than 0.05 are the variables Y1, Y 3, Y 4, and Y 5. Y 1 of 0.013, Y 3, Y 4, and Y5 are 0.000 each. This suggests that the presence of agent recognition treatment affects consumers' buying interest in the indicators of seeking information, trying products, knowing more, and the desire to own products [24].

3.2. Discussion

The results showed that there was no difference in the buying interest of respondents in the control group (A) both in session 1 and in session 2 (A1 and A2). The control group consists of respondents who only get product promotion videos and without agent recognition videos related to the Viral Stealth Marketing (VSM) promotion method in sessions 1 and 2. Respondents' buying interests remained the same, and the same treatment was used in different sessions. Consumer buying interest was different in the group of respondents who received a video of agent recognition related to the VSM promotion method in session 2. This can be seen in pairs 2, 3, and 4, showing significantly different values of less than 0.05, namely 0.001, 0.033, and 0.000, respectively.

Table 2. Paired samples t-test

		Mean	Std. Deviation	Std. Error Mean	95% Confidence Interval of the Difference		t	Df	Sig. (2-tailed)
					Lower	Upper			
Pair 1	A1 - A2	.00	.2268	.0586	-.1256	.126	.00	14	1.000
Pair 2	B1 - B2	.77	.7245	.1871	.3721	1.175	4.13	14	.001
Pair 3	A1 - B1	.32	.5226	.1349	.0306	.609	2.37	14	.033
Pair 4	A2 - B2	1.09	.7741	.1999	.6646	1.522	5.47	14	.000

Table 3. F-test

		Sum of Squares	Df	Mean Square	F	Sig.
Y1	Between Groups	6.533	3	2.178	3.909	.013
	Within Groups	31.200	56	.557		
	Total	37.733	59			
Y2	Between Groups	3.333	3	1.111	2.102	.110
	Within Groups	29.600	56	.529		
	Total	32.933	59			
Y3	Between Groups	20.867	3	6.956	13.401	.000
	Within Groups	29.067	56	.519		
	Total	49.933	59			
Y4	Between Groups	17.250	3	5.750	8.718	.000
	Within Groups	36.933	56	.660		
	Total	54.183	59			
Y5	Between Groups	18.983	3	6.328	8.714	.000
	Within Groups	40.667	56	.726		
	Total	59.650	59			

The average score of consumers buying interest in session 2 in the group that received treatment was lower than the average score of consumers buying interest in session 1. This decrease in the average value shows that consumers' buying interest decreases after knowing that the products offered use the viral stealth marketing method [25], [26]. Significant indicators of consumer buying interest in the respondent group are indicators of seeking information, trying products, knowing more, and the desire to own products. This can be seen from the results of the F test with a significance value for each attribute of Y1 of 0.013, Y3, Y4, and Y5 of 0.000 each. Consumer interest decreases to find information related to products, try products, find out more about the product, and the desire to own products with the VSM promotion method [27].

4. Conclusion

Research on the impact of viral stealth marketing on the buying interest of consumers from the Generation Z age group in cosmetic products, it can be concluded that from the paired t-test results, it is known that there is a difference in the buying interest of consumers who get product promotion treatment (B1) with the group of consumers who get agent recognition treatment (B2) with a significance of 0.000. Meanwhile, the results of the F test show that the presence of agent recognition treatment affects consumers' buying interest in indicators of seeking information, trying products, knowing more, and the desire to own products. This result replicates a change in the buying interest of consumers of cosmetic products when they learn about the use of viral stealth marketing promotion methods.

Acknowledgments

The author would like to express his deepest gratitude to all parties who have provided assistance, direction, and knowledge during this research process.

References

[1] H. Guven, “Industry 4.0 and Marketing 4.0: In Perspective of Digitalization and E-Commerce,” in *Agile Business Leadership Methods for Industry 4.0*, B. Akkaya, Ed., Emerald Publishing Limited, 2020, pp. 25–46.

[2] M. Rabindranath and A. K. Singh, “Advertising Campaign and Media Planning,” in *Advertising Management: Concepts, Theories, Research and Trends*, Springer Nature Singapore, 2024, pp. 121–152.

[3] J. M. Juska, *Integrated Marketing Communication: Advertising and Promotion in a Digital World*. Routledge, 2021.

[4] J. Moisander, E. Närvänen, and A. Valtonen, “Interpretive Marketing Research: Using Ethnography in Strategic Market Development,” in *Marketing Management*, Routledge, 2020, pp. 237–253.

[5] M. Ahearne, Y. Atefi, S. K. Lam, and M. Pourmasoudi, “The Future of Buyer–Seller Interactions: A Conceptual Framework and Research Agenda,” *J. Acad. Mark. Sci.*, vol. 50, pp. 22–45, 2022.

[6] S. Das, “A Systematic Study of Integrated Marketing Communication and Content Management System for Millennial Consumers,” in *Innovations in Digital Branding and Content Marketing*, IGI Global, 2021, pp. 91–112.

[7] A. Braca and P. Dondio, “Developing Persuasive Systems for Marketing: The Interplay of Persuasion Techniques, Customer Traits and Persuasive Message Design,” *Ital. J. Mark.*, pp. 369–412, 2023.

[8] T. Hilken *et al.*, “Disrupting Marketing Realities: A Research Agenda for Investigating the Psychological Mechanisms of Next-Generation Experiences with Reality-Enhancing Technologies,” *Psychol. Mark.*, vol. 39, no. 8, pp. 1660–1671, 2022.

[9] M. B. von Rimscha and R. Riemann, “13 Developments in Advertising Markets and Their Effects on Media Companies,” in *De Gruyter Handbook of Media Economics*, De Gruyter, 2024, p. 185.

[10] A. S. Bist, V. Agarwal, Q. Aini, and N. Khofifah, “Managing Digital Transformation in Marketing: ‘Fusion of Traditional Marketing and Digital Marketing,’” *Int. Trans. Artif. Intell.*, vol. 1, no. 1, pp. 18–27, 2022.

[11] K. K. Batth, “Digitization of Word-of-Mouth,” in *Handbook on Tourism and Social Media*, Edward Elgar Publishing, 2022, pp. 256–264.

[12] S. Robledo, P. Duque, and A. M. G. Aguirre, “Word of Mouth Marketing: A Scientometric Analysis,” *J. Scientometr. Res.*, vol. 11, no. 3, pp. 436–446, 2022.

[13] Y. A. M. Alkhafagi and Y. A. H. ALsiede, “Role of Stealth Marketing in Customer Engagement,” *Webology*, vol. 19, no. 1, pp. 6267–6291, 2022.

[14] L. Zollo, R. Filieri, R. Rialti, and S. Yoon, “Unpacking the Relationship Between Social Media Marketing and Brand Equity: The Mediating Role of Consumers’ Benefits and Experience,” *J. Bus. Res.*, vol. 117, pp. 256–267, 2020.

[15] J. Fromm and C. Garton, *Marketing to Millennials: Reach the Largest and Most Influential Generation of Consumers Ever*. Amacom, 2013.

[16] J.-L. Chen and A. Dermawan, “The Influence of YouTube Beauty Vloggers on Indonesian Consumers’ Purchase Intention of Local Cosmetic Products,” *Int. J. Bus. Manag.*, vol. 15, no. 5, pp. 100–116, 2020.

[17] M. Aisyah, “Consumer Demand on Halal Cosmetics and Personal Care Products in Indonesia,” *Al-Iqtishad J. Ilmu Ekon. Syariah*, vol. 9, no. 1, pp. 125–142, 2017.

[18] S. Em, “Exploring Experimental Research: Methodologies, Designs, and Applications Across Disciplines,” English Academy Essay.

[19] P. Pandey and M. M. Pandey, “Research Methodology Tools and Techniques,” Buzau, 2015.

[20] M. J. Curtis *et al.*, “Planning Experiments: Updated Guidance on Experimental Design and Analysis and Their Reporting III,” *Br. J. Pharmacol.*, vol. 179, no. 15, pp. 3907–3913, 2022.

[21] V. A. Nasir, A. C. Keserel, O. E. Surgit, and M. Nalbant, “Segmenting Consumers Based on Social Media Advertising Perceptions: How does Purchase Intention Differ Across Segments?,” *Telemat. Informatics*, vol. 64, 2021.

[22] D. Koehn, S. Lessmann, and M. Schaal, “Predicting Online Shopping Behaviour from Clickstream Data Using Deep Learning,” *Expert Syst. Appl.*, vol. 150, 2020.

[23] N. Gelati and J. Verplancke, “The Effect of Influencer Marketing on The Buying Behavior of Young Consumers: A study of How The Purchase Intention of Young Consumers is Affected by

Brands within The Fashion and Beauty Industries," Linköping University, 2022.

[24] W. Zhang, P. K. Chintagunta, and M. U. Kalwani, "Social Media, Influencers, and Adoption of an Eco-Friendly Product: Field Experiment Evidence from Rural China," *J. Mark.*, vol. 85, no. 3, pp. 10–27, 2021.

[25] M. L. E. Alcantara *et al.*, "Examining the Impact of Guerilla Advertising Content on Consumer Purchase Intention of Gen Z," *Int. J. Multidiscip. Res.*, vol. 2, no. 1, pp. 649–668, 2024.

[26] J.-H. Shao, E. Zhang, Y. Xiang, and R.-Z. Jing, "Efficient Combinations of Dual Incentives on Social Networks to Achieve Viral Spread," *Electron. Commer. Res.*, vol. 15, no. 1, pp. 1–24, 2023.

[27] M. A. R. Alfarez, "Pengaruh Viral Marketing, Brand Awareness, dan Distribution Intensity terhadap Purchase Decision melalui Brand Preference pada Konsumen Minuman Kekinian," Universitas Negeri Jakarta, 2024.

EPI International Journal of Engineering
Volume 7, Number 2, August 2024, pp. 49-57
DOI: 10.25042/epi-ije.082024.02

*p*ISSN 2615-5109
*e*ISSN 2621-0541

Slope Stability Analysis of Pit X on Nickel Mining Based on Comparison between Design and Actual Mining Condition

Tegar Abadi[a], Purwanto[b,*]

[a]Mining Engineering Department, Faculty of Engineering, Hasanuddin University Email: tegarabadi31@gmail.com.
[b]Mining Engineering Department, Faculty of Engineering, Hasanuddin University. Email: purwanto@unhas.ac.id

Abstract

The nickel laterite mining on the slopes of pit X uses the open-cast mining method with material strength conditions similar to soil. Slope stability considerations under temporary conditions such as earthquakes and increased groundwater levels due to rain need to be reviewed as a precaution against landslides. Limonite and saprolite materials have varying cohesion and phi values that affect the safety factor value. The probability function describes the distribution of a random variable to estimate the probability value of a parameter. The limit equilibrium method can indicate the probability of failure. The pit X slope is designed with a bench height of 10 meters, a bench width of 7 meters, and a single slope inclination of 45˚, but after mining, the slope geometry and material distribution conditions change. Stability analysis of the pit X by comparing design and actual conditions after mining is conducted to determine the safety factor comparison under various soil conditions in both design and actual states. The analysis is performed using the Unified Soil Classification System (USCS) classification method and the Morgenstern-Price (MP) limit equilibrium method. All sections meet the slope stability criteria based on the minimum safety factor standards of 1.30 for static conditions, 1.10 for dynamic conditions, 1.0 for saturated soil conditions, and a probability of failure of <5%. However, based on the results of physical property tests, slope stability needs to be reviewed periodically due to the potential for landslides. Sections A-A' and D-D' have steeper overall slopes in the actual condition, resulting in lower safety factors than in the design condition. Sections B-B' and C-C' have gentler overall slopes in the actual condition, resulting in higher safety factors than in the design condition.

Keywords: Slope stability, landslide, limit equilibrium method, safety factor, overall slope

1. Introduction

Nickel laterite is a high-value economic mineral material. The distribution of nickel ore and differences in the characteristics of soil and rock masses affect slope geometry, which impacts safety factors. Lateritic nickel deposits are mined while considering slope stability to ensure the ore extraction process follows mining engineering principles. Slope stability is a consideration in mining activities. Inappropriate pit slope geometry can cause slope failures. The potential impact of slope failures depends greatly on the type of soil and rock mass and the formed slope geometry [1].

Slope stability is a crucial concept in geotechnical engineering regarding the stability of natural and artificial slopes. Slope stability analysis involves calculating safety factors and is followed by the development of geotechnical computations. Various parameters such as slope geometry, physical data of geological materials, and shear strength factors, as well as pore water pressure, play significant roles in slope stability evaluation. Slope stability is also characterized by numerous uncertainties such as soil properties, loads, and water pressure [2]. The basic characteristics of soil determine the type of structure to be built, and external actions must be taken to ensure that the structure withstands earthquakes, water seepage, and other external factors [3].

The open-pit mining system uses the open-cast mining method, by cutting the side of the hill from the top downwards following its contour lines with shallow excavation depth. Stripping is done in a stepped form. There are three materials: limonite, saprolite, and bedrock. Limonite and saprolite are materials containing nickel ore with strengths almost approaching soil, while bedrock is a very hard base rock [4].

Nickel laterite mining on the slopes of Pit X uses the open-cast mining method with material strength conditions similar to soil. Slope stability considerations under temporary conditions, such as earthquakes and increased groundwater levels due to rain, need to be reviewed as a precaution against potential landslides. The physical properties of the soil significantly impact slope stability, but no previous studies have compared slope stability analysis with soil physical properties. Limonite and saprolite materials have varying cohesion and phi values influencing the resulting safety factor value. The

*Corresponding author. Tel.: +62-812-4195-9407
Jalan Poros Malino km. 6, Bontomarannu
Gowa, Indonesia, 92171

higher the cohesion and internal friction angle value, the greater the safety factor. The probability distribution function describes the spread of a random variable to estimate the probability value of a parameter. The limit equilibrium method can indicate the probability of failure. The pit slope design includes a bench height of 10 meters, a bench width of 7 meters, and a single slope inclination 45˚. The slope of pit X in the actual mining condition experienced geometry changes due to mining activities. After mining, no analysis was done on the actual conditions.

Limit Equilibrium Analysis is a modern method widely used for slope stability analysis, utilizing the static equilibrium concept and disregarding the slope's stress-strain relationship. It analyzes the comparison between driving forces and resisting forces on the slope. The Morgenstern-Price method is one of the analysis methods based on the limit equilibrium principle, where the analysis process results from the equilibrium of each normal force and moment acting on every slice of the slope's slip surface. The equilibrium conditions that must be met include vertical and horizontal force equilibrium, as well as moment equilibrium. The factor of safety (FoS) provides information on whether the slope is stable or unstable [5]. The Monte Carlo simulation is a flexible method in probabilistic analysis that incorporates significant distribution variations without interpretation and easily models correlations between variables. In the Limit Equilibrium Method, where the FoS is the ratio of resisting forces to driving forces, each parameter is a random variable with uncertainty and a specific probability distribution. Therefore, Monte Carlo simulation is suitable for determining the probability of failure (PoF) from the limit equilibrium analysis [6].

Responding to issues both from plan design and actual conditions of pit slope X, it is considered necessary to conduct further analysis of slope stability. Therefore, a study entitled "Analysis of Slope Stability of Pit X on Nickel Mining Based on Comparison Between Design and Actual Mining Conditions" was conducted to avoid potential hazards that may occur.

2. Literatur Review

Slopes are portions of the Earth's surface that form a certain angle with the horizontal plane. Slopes can be formed naturally or by human activities. Naturally formed slopes include hillsides and riverbanks, while human-made slopes include excavations, embankments, levees, canal banks, and open-pit mine slopes [7].

The possibility of landslides occurring always exists on all types of slopes. Landslides occur when driving forces exceed resisting forces originating from the shear strength of the soil along the failure plane. Technically, it can be said that landslides occur when safety factors do not meet the criteria for each slope [8].

If the value of the safety factor (FK) for a slope is > 1.0 (resisting force > driving force), the slope is considered stable. However, if the value of FK < 1.0 (resisting force < driving force), the slope is considered unstable [6]. The design criteria for determining the stability condition of slopes using Ministry of Energy and Mineral Resources Regulation Number 1827 of 2018 can be seen in Table 1.

Table 1. The values of the safety factor and the probability of landslide in mining slope

Landslide type	Severity of Landslide	Acceptable Criteria		
		Static Safety Factor	Dynamic Safety Factor	Probability of Failure
Bench	Low High	1.1	None	25 – 50%
Interramp	Low	1.15 – 1.2	1	25%
	Moderate	1.2	1	20%
	High	1.2 – 1.3	1.1	10%
Overall	Low	1.2 – 1.3	1	15 – 20%
	Moderate	1.3	1.05	5 -10%
	High	1.3 – 1.5	1.1	<5%

Natural and artificial slope failures occur due to changes in topography, seismic activity, groundwater flow, loss of strength, stress changes, seasons, climate, and weather. External forces acting on the materials forming the slope cause them to tend to slide. The tendency to slide can be resisted by the shear strength of the materials. A slope that has been stable for a long time can become unstable due to several factors such as the type and condition of the soil or rock layers forming the slope, slope geometry, increased water content in the soil (such as seepage or rainfall infiltration), weight and distribution of loads, and vibrations or earthquakes. Factors influencing slope stability can result in shear stress throughout the soil mass, and slope movement will occur unless the shear resistance on every potential failure surface exceeds the shear stress [9].

The Unified Soil Classification System (USCS), as shown in Fig. 1, first proposed by Casagrande and later developed by the United States Bureau of Reclamation (USBR), the United States Army Corps of Engineers (USACE), and subsequently the American Standard Testing of Materials (ASTM), has been adopted as the standard method for classifying soils. In the USCS soil classification system, soils are categorized into two main groups [3]:

1. Coarse-grained soils, consisting of gravel and sand, with less than 50% of the soil passing through a No. 200 sieve (F200 < 50). The group symbol begins with G for gravel or gravelly soil, or S for sand or sandy soil.
2. Fine-grained soils, with more than 50% of the soil passing through a No. 200 sieve (F200 ≥ 50).

The Limit Equilibrium method is highly popular in slope stability analysis. It is also known as the slice method because the failure surface of the slope is divided into several slices. The Limit Equilibrium method is expressed through equilibrium equations of one or several assumed undistorted blocks, which balance unknown forces (reactions from the stable rock mass or inter-block forces), particularly shear forces acting on the selected failure surface. These shear forces represent the entire section where shear strength is assumed to act. The stability condition of slopes using this method is expressed in terms of safety factor indices [1]

UNIFIED SOIL CLASSIFICATION SYSTEM

Major Divisions				Group Symbols	Typical Names	Field Identification Procedures	Laboratory Classification Criteria		Information Required for Describing Soils
1	2			3	4	5	6		7
Coarse grained soils more than half of material is larger than No. 200 sieve size.	Gravels (more than half of coarse fraction is larger than No. 4 sieve size.)	Clean gravels (little or no fines, less than 5%)	Between 5% and 12% fines is borderline and requires dual symbols	GW	Well-graded gravels, gravel-sand mixtures, little or no fines	Wide range in grain size and substantial amounts of intermediate particle sizes	$C_u = \frac{D_{60}}{D_{10}}$ greater than 4 $C_c = \frac{(D_{30})^2}{D_{10}D_{60}}$ between 1 and 3		Give typical name: Indicate approximate percentage of sand and gravel, maximum size, angularity, surface conditions, and hardness of the coarse grains; local or geologic name and other pertinent descriptive information, and symbol in parentheses. For undisturbed soils add information on degree of stratification, degree of compactness, cementation, moisture conditions, and drainage characteristics. Example: Silty sand gravelly, about 20% hard angular gravel particles ½ in. maximum size; rounded and subangular sand grains, coarse to fine; about 15% non plastic fines with low dry strength; well compacted and moist in place; alluvial sand (SM)
				GP	Poorly graded gravels, gravel-sand mixtures, little or no fines	Predominantly one size or a range of sizes with some intermediate sizes missing	Not meeting the requirements for GW		
		Gravels with fines (appreciable amount of fines, greater than 12%)		GM	Silty gravels, poorly graded gravel-sand-silt mixtures	Nonplastic fines	Atterberg limits below "A" line or PI less than 4	Above "A" line with PI between 4 and 7 are borderline cases and require dual symbols	
				GC	Clayey gravels, poorly graded gravel-sand-clay mixtures	Plastic fines	Atterberg limits above "A" line, with PI greater than 7		
	Sands (more than half of coarse fraction is smaller than No. 4 sieve size.)	Clean sands (little or no fines, less than 5%)		SW	Well graded sands, gravelly sands, little or no fines	Wide range in grain sizes and substantial amounts of all intermediate particle sizes	$C_u = \frac{D_{60}}{D_{10}}$ greater than 6 $C_c = \frac{(D_{30})^2}{D_{10}D_{60}}$ between 1 and 3		
				SP	Poorly graded sands, gravelly sands, little or no fines	Predominantly one size or a range of sizes with some intermediate sizes missing	Not meeting the requirements for SW		
		Sands with fines (appreciable amount of fines, greater than 12%)		SM	Silty sands, poorly graded sand-silt mixtures	Non plastic fines	Atterberg limits below "A" line or PI less than 4	Above "A" line with PI between 4 and 7 are borderline cases and require dual symbols	
				SC	Clayey sands, poorly graded sand-clay mixtures	Plastic fines	Atterberg limits above "A" line, with PI greater than 7		
Fine grained soils more than half of material is smaller than No. 200 sieve size		Dry strength	Dilatancy	Toughness *					
	Silts and clays Liquid limit less than 50	None to slight	Quick to slow	None	ML	Inorganic silts and very fine sands, rock flour, silt or clayey fine sands with slight plasticity			Give typical name, indicate degree and character of plasticity, amount and maximum size of coarse grains, color in wet conditions, odor (if any), local or geologic name, and other pertinent descriptive information and symbol in parentheses. For undisturbed soils add information on structure, stratification, consistency in undisturbed and remolded states, moisture and drainage conditions. Example: Clayey silt, brown, slightly plastic; small percentage of fine sand; numerous vertical root holes; firm and dry in place; loess (ML).
		Medium to high	None to very slow	Medium	CL	Inorganic clays of low to medium plasticity, gravelly clays, sandy clays, silty clays, lean clays			
		Slight to medium	None to very slow	Medium	OL	Organic silts and organic silty clays of low plasticity			
	Silts and clays Liquid limit greater than 50	Slight to medium	Slow to none	Slight to medium	MH	Inorganic silts, micaceous or diatomaceous fine sandy or silty soils, elastic silts			
		High to very high	None	High	CH	Inorganic clays of high plasticity, fat clays			
		Medium to high	None to very slow	Slight to medium	OH	Organic clays of medium to high plasticity			
Highly organic soils				Pt	Peat and other highly organic soils				

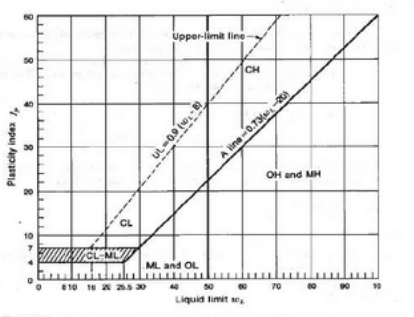

Figure 8-2
Plasticity chart (also called "Casagrande's A-chart") to use with Table 8-1 for the Unified Soil Classification System.

** Dry strength (crushing characteristics); Dilatancy (reaction to shaking); Toughness (consistency near plastic limit)*

Figure 1. The unified soil classification system [3]

The Limit Equilibrium method calculates the safety factor by comparing the shear strength along the failure surface to the required force that can support the slope's equilibrium inclination. Shear failure can be expressed as a Mohr-Coulomb function with shear strength expressed as cohesion and friction angle [10]. Static equilibrium can be achieved in two ways. The first approach involves considering the equilibrium of the entire soil mass and then solving it for only the free body. The second approach divides the soil into many parts, and then each slice must satisfy the equilibrium condition for all forces [11].

The higher the values of cohesion and internal friction angle, the greater the factor of safety, as described in the Mohr-Coulomb equation, both in static and dynamic conditions. The shear strength of the material, which resists the material from causing a slope failure, is expressed in the Mohr-Coulomb failure criterion as follows [12]:

$$\tau = c' + (\sigma_n - u)\tan\emptyset \quad (1)$$

where:

τ = Shear strength
c' = Effective cohesion
ϕ' = Effective friction angle
σ_n = Total normal stress
u = Pore water pressure

The probability distribution function describes the distribution of a random variable used to estimate the probability of occurrence of a parameter. The Limit Equilibrium method can indicate the Probability of Failure (PoF) value. The probability of a landslide can be defined as the ratio between the number of analyzed slope failures (FK < 1) and the total number of analyses (simulation samples), expressed as a percentage. The equation for the PoF function is [13]:

$$PoF = \frac{n\,FK<1}{n\,FK\,total} x\,100 \quad (2)$$

Monte Carlo simulation is a flexible method in probabilistic analysis that combines a significant distribution variation without interpretation and the ability to easily model correlations between variables. The Limit Equilibrium Method, where the value of FK represents the ratio of resisting forces to driving forces, each parameter being an uncertain random variable with a specific probability distribution. Therefore, the use of Monte Carlo simulation is suitable for determining the PoF value from Limit Equilibrium Analysis [6].

3. Research Method

The data collection technique for this research involves gathering topographic data, which is used to draw several sections or cross-sections of the pit under study. Material data composing the slope, physical property test data, and groundwater table data are also collected. Groundwater table data, based on drilling data, indicate a reference point of 12.5 meters for the initial placement of the groundwater table from the top of the limonite. However, several considerations need to be taken into account, such as the distance from the bedrock and the angle of the formed

groundwater table. Data processing includes CU+PWP test results and physical property data such as moisture content, specific gravity, sieve analysis, Atterberg limits, and hydrometer test results. Vulcan software is utilized to process material distribution data, while Geostudio SLOPE/W is used to analyze slope stability.

The soil samples collected are obtained from drilling samples. Soil samples for physical property testing in the laboratory are obtained using Standard Penetration Test samples. Sample preparation is adjusted according to the equipment standards and testing protocols of ASTM system. The moisture content test determines the soil's water content percentage. Moisture content is the ratio of the weight of water in the soil to the total weight of the soil. The specific gravity test is performed to determine the soil's density that passes through a No. 10 sieve using a pycnometer. Soil-specific gravity is the ratio of the weight of soil grains to the weight of distilled water in the air with the same volume at a certain temperature. Sieve analysis and hydrometer tests are conducted to determine the particle size distribution of the soil for soil grain size distribution and classification. Particle size distribution larger than 0.075 mm is determined by sieve analysis, while particle size distribution smaller than 0.075 mm is determined by hydrometer analysis. The purpose of these tests is to determine the values of the liquid limit, plastic limit, and plasticity index in determining the consistency limits of the soil.

The slope stability analysis uses the Morgenstern-Price Limit Equilibrium Method in 2D using the Geostudio SLOPE/W software. The Morgenstern-Price method is chosen because it employs varied assumptions to calculate the resultant forces between slices. The analysis is performed by extracting section designs from the Vulcan software. These designs contain information about the slope geometry, including the slope height based on the Actual topography, overall slope, and individual slopes. The determination of the groundwater level angle based on the overall slope formed is made by calculating the angle from

The initial point at the top of the slope to the toe of the saprolite. The determining the water table. Here is a general approach based on such a reference:

$$a = tan^{-1}(0.65\ tan\ b) \quad (3)$$

where:

a = Water table slope angle (˚)
b = Overall slope angle (˚)

4. Results and Discussion

4.1. The Result of laboratory test data processing

4.1.1. The results of the physical properties test

The data from the physical property tests include moisture content, specific gravity, sieve analysis, Atterberg limits, and hydrometer test, as shown in Table 2.

Table 2. The results of the physical properties test

Height (m)	*Liquid Limit* (%)	*Plastic Limit* (%)	*Indeks Plastic* (%)	*Water content* (%)	*Sand* (%)	*Silt* (%)	*Clay* (%)	*Specific Gravity* (Mg/m^3)
1.55-2	63.19	46.17	17.02	81.40	1.00	88.00	11.00	3.51
3.55-4	84.04	65.16	18.88	69.47	5.90	77.00	17.10	2.80
6-6.45	74.37	51.34	23.03	44.49	2.10	81.40	16.50	3.29
8-8.45	89.67	64.48	25.19	74.83	1.30	87.50	11.20	3.36
11-11.45	75.86	63.36	12.50	75.17	6.30	77.80	15.80	2.62
13-13.45	84.69	57.91	26.78	95.01	1.50	96.00	2.50	3.24
15-15.45	77.84	70.57	7.27	84.68	2.40	86.30	11.30	3.24
17-17.45	63.52	47.43	16.09	80.92	4.20	88.20	7.60	3.22
19-19.45	81.75	59.85	21.90	77.99	1.30	96.20	2.50	3.19
21-21.45	90.80	74.99	15.81	88.32	3.30	86.00	10.70	2.55
23-23.45	119.92	75.31	44.61	85.26	2.80	96.50	0.70	3.12
27-27.45	73.25	42.13	31.12	53.56	6.10	85.00	8.90	3.40

Based on the results of the physical properties test for the soil type, which is silt, the average moisture content is 75.93%, indicating that the moisture content at Pit X is high. This suggests that during rainfall, water will overflow, and there is potential for landslides. The reason is that as the moisture content in the soil increases, the driving force of the soil also becomes stronger. The liquid limit test results show that the soil has high plasticity. High moisture content can cause an increase in pore pressure, a decrease in shear strength, a high swelling factor, and the formation of an interface zone.

The physical properties test data should be considered for slope monitoring because there is still potential for landslides at Pit X. Heavy rainfall causes the soil to absorb water, reducing cohesion and increasing the total weight of the soil mass. This condition makes the soil more prone to landslides. Water infiltrating the soil will increase pore water pressure, reducing the effective strength of the soil and making it more likely to collapse. Slopes exposed to continuous rainfall may deform or crack, potentially triggering larger landslides.

4.1.2. The results of the mechanical properties test

The soil mechanical properties data for slope stability analysis in Geostudio SLOPE/W software refers to the Final Geotechnical Report Engineering for Slope Geometry Based on Updated Parameters at Pit X. This includes the results of the CU+PWP triaxial test, which consists of values for cohesion, phi (friction angle), and unit weight obtained from undisturbed samples, as shown in Table 3.

Table 3. The results of the mechanical properties test

Material	Material Model	Unit Weight (kN/m^3)	Cohesion (kPa)	Friction angle (^{0})
Limonite	Mohr-Coulomb	16.00	10.00	35.00
Saprolite	Mohr-Coulomb	17.00	15.00	35.00
Peridotite	High strength	22.00	-	-

Table 4. Input standard deviation value

Input Material	Standard Deviation	Minimum	Maximum	Mean
Limonite friction angle	1.78	30.99	40.08	35
Limonite cohesion	2.53	10	15	10
Saprolite friction angle	4.71	20.91	40.55	35
Saprolite Cohesi	12.26	7.56	18.52	15

4.2. The results of slope stability

The slope stability analysis of pit X is conducted by comparing the planned design slope condition to the condition after mining activities in 4 sections for each condition based on reference safety factor values and landslide probability. The safety factor values used are a minimum of 1.30 for static conditions, 1.10 for dynamic conditions, and a maximum landslide probability of 5%, referring to the Ministry of Energy and Mineral Resources Regulation Number 1827 of 2018, as shown in Table 1. A safety factor of 1.0 for saturated soil conditions refers to the safety factor value set by pit X.

4.2.1. The results of plan design slope stability analysis

The input analysis used refers to the material data composing the slope and groundwater table. For dynamic conditions, a value of 0.2g is used based on the maximum hazard value for bedrock movement from the Indonesian earthquake hazard map 2017, with a return period of 50 years. For saturated soil conditions, a value of Ru 0.2 is used, derived from the average value observed at the research site. The landslide probability analysis utilizes the standard deviation from 2,000 data points, which were then statistically analyzed by pit X. The used standard deviation values can be seen in Table 4.

1. Section A-A'

The results of the slope stability analysis in the design condition of section A-A' using the Limit Equilibrium Method (LEM) based on Geostudio SLOPE/W can be seen in Fig. 2. Based on the simulation results for various soil conditions with an overall slope of 31.19˚, forming a water table angle of 21.48˚ from Eq. 3, it is obtained that section A-A' has a safety factor value for the static condition of 1.43, for the dynamic condition of 1.16, and for the saturated condition of 1.11. Based on the results of 2,000 simulation safety factors, the landslide probability value yields a PoF value of 1.07%, meaning there is a 1.07% probability of safety factors falling below 1 from the conducted simulations, as shown in Fig. 3.

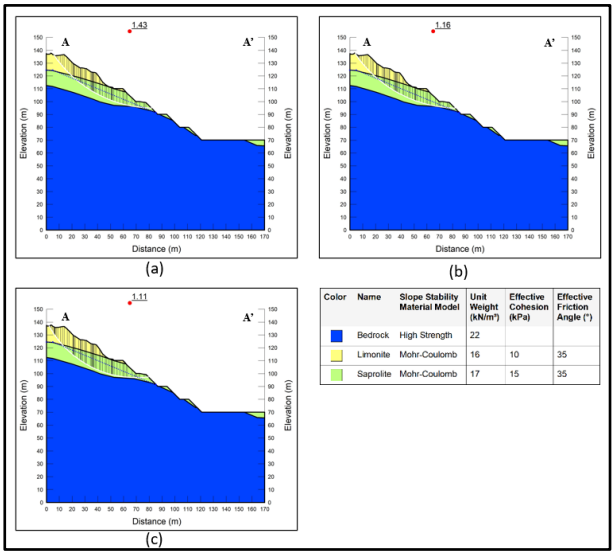

Figure 2. Safety factor for section A-A' design: (a) Static condition, (b) Dynamic condition, and (c) Saturated condition

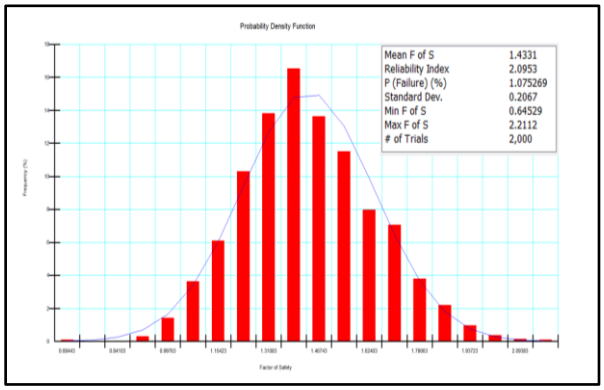

Figure 3. Probability density function section A-A' design

All analysis results meet the slope stability criteria, but based on the physical property data, slope stability needs to be monitored due to the potential for landslides.

2. Section B-B'

The results of the slope stability analysis in the design condition of sections B-B' using the Limit Equilibrium Method (LEM) based on Geostudio SLOPE/W can be seen in Fig. 4.

Based on the simulation results for various soil conditions with an overall slope of 37.74˚, forming a water table angle of 26.71˚ from Equation 3, it is obtained that section B-B' has a safety factor value for the static condition of 1.35 for the dynamic condition of 1.16, and for the saturated condition of 1.16. The landslide probability value based on the results of 2,000 simulation safety factors yields a PoF value of 2.7%, meaning there is a 2.7% probability of safety factors falling below 1 from the conducted simulations, as shown in Fig. 5. All analysis results meet the slope stability criteria. Still, based on the physical property data, slope stability needs to be monitored due to the potential for landslides.

3. Section C-C'

The results of the slope stability analysis in the design condition of section C-C' using the Limit Equilibrium Method (LEM) based on Geostudio SLOPE/W can be seen in Fig. 6.

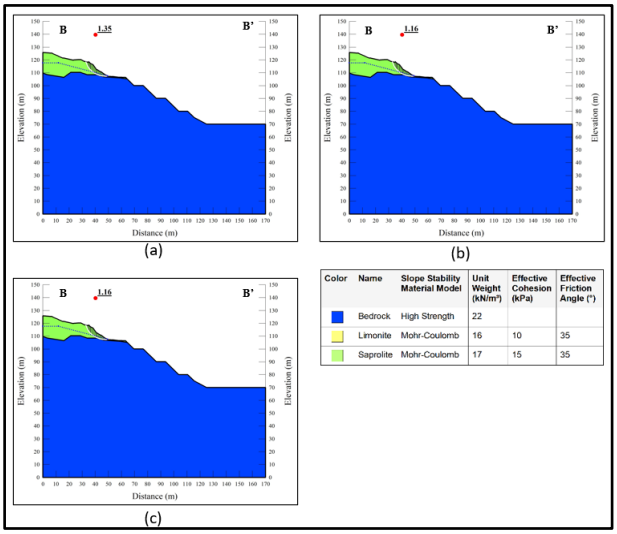

Figure 4. Safety factors for section B-B' design: (a) Static condition, (b) Dynamic condition, and (c) Saturated condition

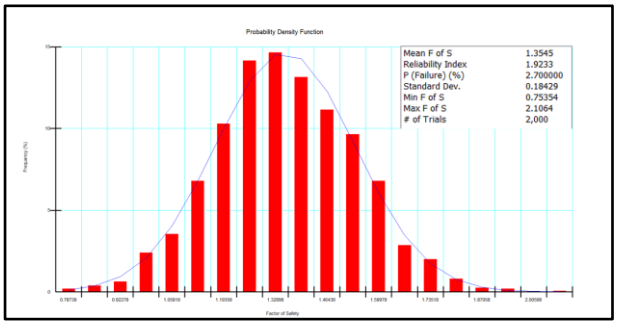

Figure 5. Probability density function section B-B' design

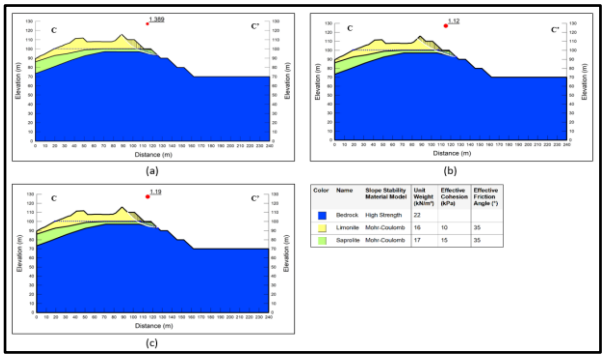

Figure 6. Safety factor for section C-C' design: (a) Static condition, (b) Dynamic condition, and (c) Saturated condition

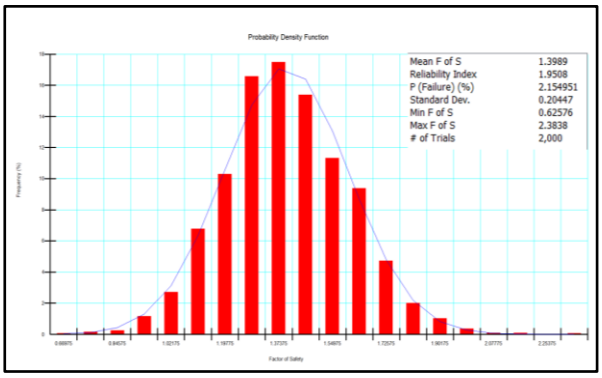

Figure 7. Probability density function section C-C' design

Based on the simulation results for various soil conditions with an overall slope of 32.03˚, forming a water table angle of 22.12˚ from Equation 3, it is obtained that section C-C' has a safety factor value for the static condition of 1.389 for the dynamic condition of 1.12, and for the saturated condition of 1.19. The landslide probability value based on the results of 2,000 simulation safety factors yields a PoF value of 2.15%, meaning there is a 2.15% probability of safety factors falling below 1 from the conducted simulations, as shown in Fig. 7. All analysis results meet the slope stability criteria, but based on the physical property data, slope stability needs to be monitored due to the potential for landslides.

4. Section D-D'

The results of the slope stability analysis in the design condition of sections D-D' using the Limit Equilibrium Method (LEM) based on Geostudio SLOPE/W can be seen in Fig. 8.

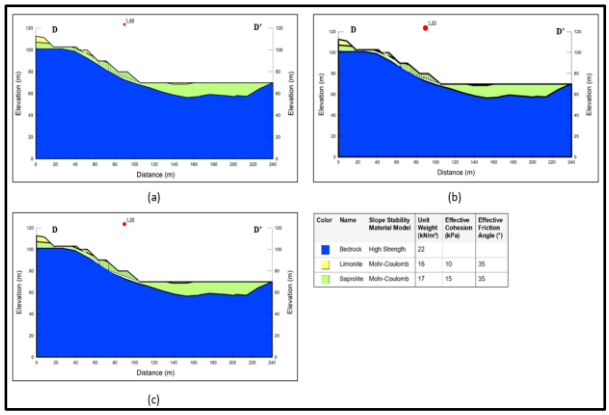

Figure 8. Safety factors for section D-D' design: (a) Static condition, (b) Dynamic condition, and (c) Saturated condition

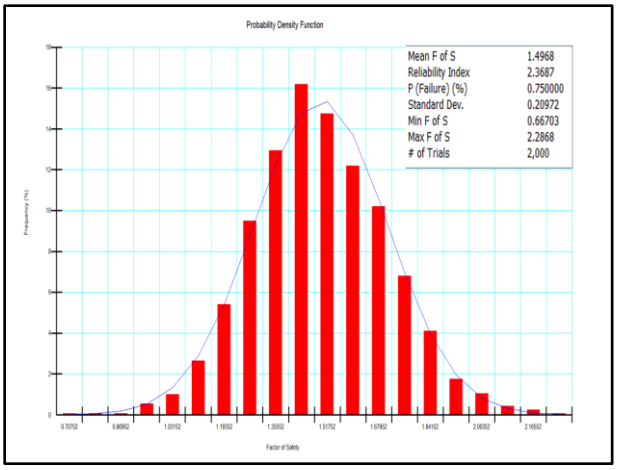

Figure 9. The probability density function section D-D' design

Based on the simulation results for various soil conditions with an overall slope of 27.04˚, forming a water table angle of 18.35˚ from Equation 3, it is obtained that section D-D' has a safety factor value for the static condition of 1.49 for the dynamic condition of 1.20, and for the saturated condition of 1.25. The landslide probability value based on the results of 2,000 simulation safety factors yields a PoF value of 0.75%, meaning there is a 0.75% probability of safety factors falling below 1 from the conducted simulations, as shown in Fig. 9. All analysis results meet the slope stability criteria, but based on the physical property data, slope stability needs to be monitored due to the potential for landslides.

4.2.2 The results of actual slope stability analysis

The actual condition of slope pit X has undergone changes in slope geometry due to mining activities affecting the overall slope formed. The input analysis used refers to the material data composing the slope and groundwater table. For dynamic conditions, a value of 0.2g is used based on the maximum hazard value for bedrock movement from the Indonesian earthquake hazard map 2017 with a return period of 50 years. For saturated soil conditions, a value of Ru 0.2 is used, derived from the average value observed at the research site. The landslide probability analysis utilizes the standard deviation from 2,000 data points, which were then

statistically analyzed by pit X. The standard deviation values used for analysis can be seen in Table 4.

1. Section A-A'

The results of the slope stability analysis in the actual condition of sections A-A' using the Limit Equilibrium Method (LEM) based on Geostudio SLOPE/W can be seen in Fig. 10.

Based on the simulation results for various soil conditions with an overall slope of 32.29˚, forming a water table angle of 22.33˚ from Equation 3, it is obtained that section A-A' has a safety factor value for the static condition of 1.36 for the dynamic condition of 1.10, and for the saturated condition of 1.03. The landslide probability value based on the results of 2,000 simulation safety factors yields a PoF value of 2.47%, meaning there is a 2.47% probability of safety factors falling below 1 from the conducted simulations, as shown in Fig. 11. All analysis results meet the slope stability criteria, but based on the physical property data, slope stability needs to be monitored due to the potential for landslides.

2. Section B-B'

The results of the slope stability analysis in the actual condition of sections B-B' using the Limit Equilibrium Method (LEM) based on Geostudio SLOPE/W can be seen in Fig. 12.

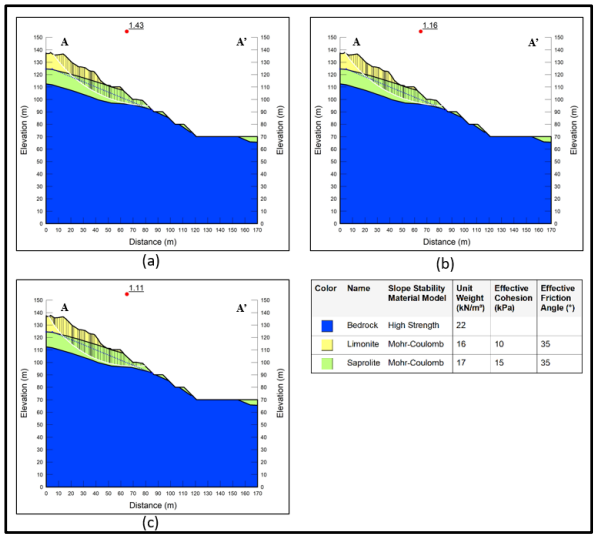

Figure 10. Safety factor for section A-A' actual: (a) Static condition, (b) Dynamic condition, and (c) Saturated condition

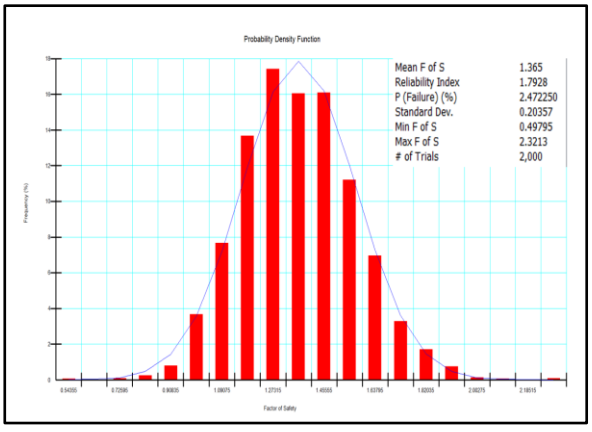

Figure 11. Probability density function section A-A' actual

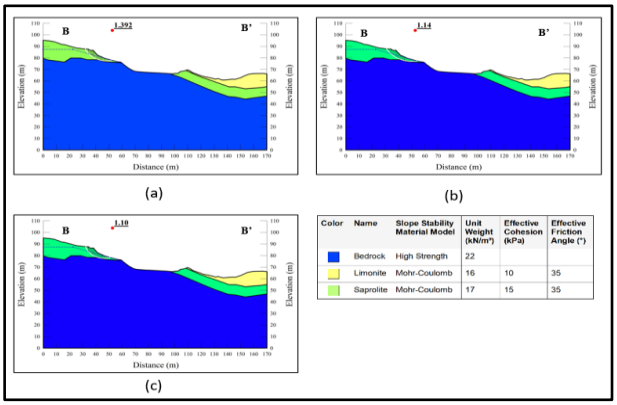

Figure 12. Safety factor for section B-B' actual: (a) Static condition, (b) Dynamic condition, and (c) Saturated condition

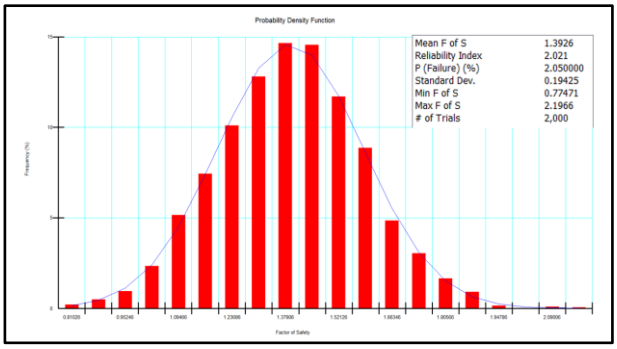

Figure 13. Probability density function section B-B' actual

Based on the simulation results for various soil conditions with an overall slope of 26.47˚, forming a water table angle of 17.93˚ from Equation 3, it is obtained that section B-B' has a safety factor value for the static condition of 1.392 for the dynamic condition of 1.14, and for the saturated condition of 1.10. The landslide probability value based on the results of 2,000 simulation safety factors yields a PoF value of 2.05%, meaning there is a 2.05% probability of safety factors falling below 1 from the conducted simulations, as shown in Fig. 13. All analysis results meet the slope stability criteria, but based on the physical property data, slope stability needs to be monitored due to the potential for landslides.

3. Section C-C'

The results of the slope stability analysis in the actual condition of section C-C' using the Limit Equilibrium Method (LEM) based on Geostudio SLOPE/W can be seen in Fig. 14.

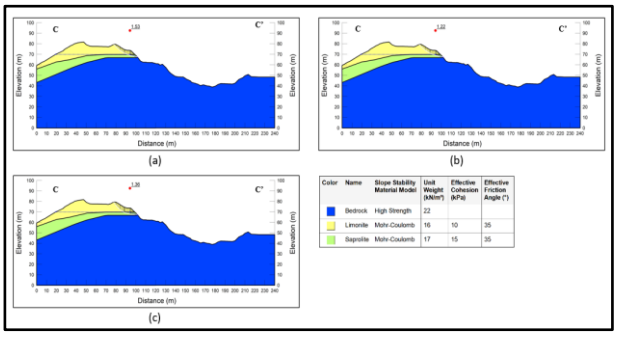

Figure 14. Safety factor for section C-C' actual: (a) Static condition, (b) Dinamic condition, and (c) Saturated condition

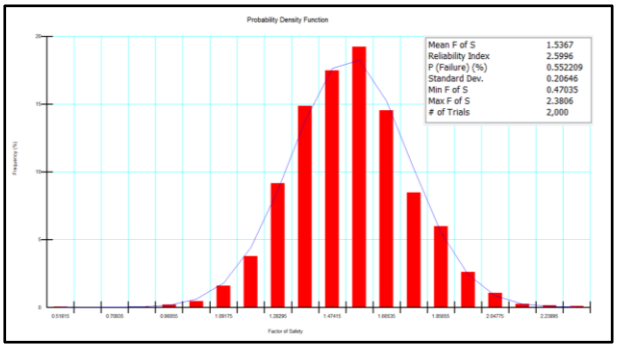

Figure 15. Probability density function section C-C' actual

Based on the simulation results for various soil conditions with an overall slope of 29.34˚, forming a water table angle of 20.07˚ from Equation 3, it is obtained that section C-C' has a safety factor value for the static condition of 1.53, for dynamic condition of 1.22, and for the saturated condition of 1.36. The landslide probability value based on the results of 2,000 simulation safety factors yields a PoF value of 0.55%, meaning there is a 0.55% probability of safety factors falling below 1 from the conducted simulations, as shown in Fig. 15. All analysis results meet the slope stability criteria, but based on the physical property data, slope stability needs to be monitored due to the potential for landslides.

4. Section D-D'

The results of the slope stability analysis in the design condition of sections D-D' using the Limit Equilibrium Method (LEM) based on Geostudio SLOPE/W can be seen in Fig. 16.

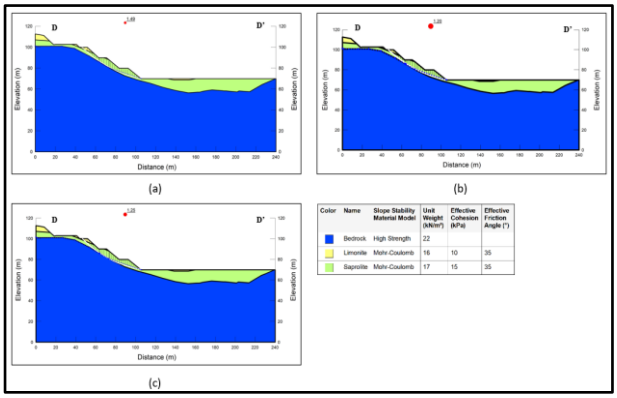

Figure 16. Safety factor for section D-D' actual: (a) Static condition, (b) Dynamic condition, and (c) Saturated condition

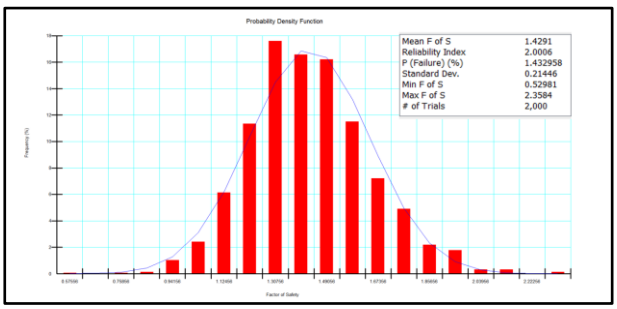

Figure 17. Probability density function section D-D' actual

Table 5. Results of all slope stability analysis

Section	FK Static	FK PGA	FK Saturated	Probability of Failure (%)	Overall Slope (˚)
A - A' Design	1.43	1.16	1.11	1.07	31.19
A - A' Actual	1.36	1.10	1.03	2.47	32.29
B - B' Design	1.35	1.16	1.16	2.7	37.74
B - B' Actual	1.392	1.14	1.10	2.05	26.47
C - C' Design	1.389	1.12	1.19	2.15	32.03
C - C' Actual	1.53	1.22	1.36	0.55	29.34
D - D' Design	1.49	1.20	1.25	0.75	27.04
D - D' Actual	1.42	1.15	1.12	1.43	29.69

Based on the simulation results for various soil conditions with an overall slope of 29.69˚, forming a water table angle of 20.44˚ from Equation 3, it is obtained that section D-D' has a safety factor value for the static condition of 1.42, for dynamic the condition of 1.15, and for the saturated condition of 1.12. The landslide probability value based on the results of 2,000 simulation safety factors yields a PoF value of 1.43%, meaning there is a 1.43% probability of safety factors falling below 1 from the conducted simulations, as shown in Fig. 17. All analysis results meet the slope stability criteria, but based on the physical property data, slope stability needs to be monitored due to the potential for landslides.

Based on the results of the slope stability analysis for both design and actual conditions in Table 5, it can be observed that the factor of safety values is influenced by the overall slope formed at the same sections. The flatter the slope, the higher the factor of safety obtained, as the resisting forces are greater and the driving forces are smaller. Section A-A' in the actual condition has a steeper overall slope compared to the design condition, resulting in a lower factor of safety. Section B-B', on the other hand, has a flatter overall slope in the actual condition, leading to a higher factor of safety. Similarly, Section C-C' also has a flatter overall slope in the actual condition, which results in a greater factor of safety. Conversely, Section D-D' has a steeper overall slope in the actual condition, resulting in a lower factor of safety.

The probability of failure using Monte Carlo simulation is employed to determine the percentage likelihood of landslides based on unsafe conditions (SF < 1.0) against the overall factor of safety using the limit equilibrium method. The probability of landslide occurrence is inversely proportional to the factor of safety obtained; the higher the factor of safety, the lower the potential for landslides. Factors contributing to the slope becoming flatter or steeper in the actual condition include discrepancies in the block model compared to the actual conditions, the presence of high-grade ore in the actual final plan leading to overcutting, and planning priorities that affect the relocation of equipment.

Recommendations from the analysis for maintaining long-term slope stability include conducting routine monitoring of groundwater level changes, slope movements, and signs of deformation such as cracks or changes in soil structure. The importance of regular monitoring allows for early detection of changes in conditions that could lead to landslides, enabling

mitigation measures to be implemented before significant failures occur, thus ensuring the safety of mining operations efficiently. Regular slope stability analyses should be conducted, considering weather conditions, changes in groundwater levels, and additional loads such as mining activities. The existing drainage systems should be properly maintained to ensure that rainwater can be efficiently diverted without causing water accumulation around the slope.

5. Conclusion

Based on the analysis results of pit X under actual mining conditions and design plan, it can be concluded that:

1. The slope stability analysis results under both design and actual conditions, considering various slope conditions using the limit equilibrium method, indicate that all sections meet the stability criteria based on the minimum safety factor standards for different slope conditions: 1.30 for static condition, 1.10 for dynamic condition, and 1.0 for saturated soil condition. However, regular monitoring of slope stability is necessary based on the results of physical property tests due to the presence of landslide potential.
2. The slope stability analysis results based on the probability of failure values under both design and actual conditions using the limit equilibrium method indicate that all sections meet the stability criteria based on the minimum probability of failure standard of less than 5%. Nevertheless, periodic review of slope stability is required based on the results of physical property tests due to the potential for landslides.
3. Comparison of the slope stability analysis results between the design and actual conditions shows that Sections A-A' and D-D' have a steeper overall slope in the actual condition, resulting in a lower factor of safety compared to the design condition. In contrast, Sections B-B' and C-C' have a flatter overall slope in the actual condition, leading to a higher factor of safety than in the design condition. The factors contributing to the slope becoming flatter or steeper in the actual condition include discrepancies in the block model compared to the actual conditions, the presence of high-grade ore in the actual final plan leading to overcutting, and planning priorities that affect the relocation of equipment.

Acknowledgments

The authors would like to thank the Department of Mining Engineering, Hasanuddin University, which has supported the preparation of this research. and all parties involved so that this research can run in accordance with what we expect.

References

[1] G. P. Giani, *Rock Slope Stability Analysis*. Turin: Technical University of Turin, 1988.

[2] S. Suman, S. Z. Khan, S. K. Das, and S. K. Chand, "Slope Stability Analysis using Artificial Intelligence Techniques," *Nat. Hazards*, vol. 84, pp. 727–748, 2016.

[3] D. Panguriseng, *Dasar-dasar Mekanika Tanah*. Yogyakarta: Pena Indis, 2018.

[4] M. A. Azizi, R. N. Hakim, and A. D. Nugraha, "Optimalisasi Geometri Lereng Tambang Nikel Menggunakan Metode Probabilistik pada Hill Pit 05, PT Vale Indonesia Tbk, Sorowako, Kabupaten Luwu Timur, Provinsi Sulawesi Selatan," *J. Geomine*, vol. 7, no. 2, pp. 92–100, 2019.

[5] S. Khodijah, U. S. Monica, J. Ersyari, N. Khoirullah, and R. I. Sophian, "Analisis Kestabilan Lereng Menggunakan metode Kesetimbangan Batas dalam Kondisi Statis dan Dinamis pada Pit X, Tanjung Enim, Sumatra Selatan," *Geosci. J.*, vol. 6, no. 4, pp. 1030–1037, 2022.

[6] I. Arif, *Geoteknik Tambang: Mewujudkan Produksi Tambang yang Berkelanjutan dengan Menjaga Kestabilan Lereng*. Jakarta: PT Gramedia Pustaka Utama, 2016.

[7] A. Halawa, "Analisis Kestabilan Lereng Mine Highwall dengan Metode Bishop dan Software Rockscience Slide Pada Area Penambangan Batubara di Pit 2a Barat PT. Fontana Resources Indonesia) Kab. Barito Utara Kalimantan Tengah," *J. Sains dan Teknol. ISTP*, vol. 11, no. 1, pp. 35–49, 2019.

[8] O. C. P. Rajagukguk, A. E. Turangan, and S. Monintja, "Analisis Kestabilan Lereng dengan Metode Bishop (Studi Kasus: Kawasan Citraland Sta.1000m)," *J. Sipil Statik*, vol. 2, no. 3, pp. 140–147, 2014.

[9] M. Jihad, R. H. K. Putra, and A. S. Sari, "Kajian Stabilitas Lereng pada Lahan Bekas Tambang Andesit," in *Prosiding Seminar Teknologi Kebumian dan Kelautan (SEMITAN II) Institut Teknologi Adhi Tama Surabaya (ITATS)*, 2020.

[10] D. C. Wyllie and C. W. Mah, "Structural Geology and Data Interpretation," in *Rock Slope Engineering*, 4th ed., CRC Press, 2004.

[11] J. M. Duncan, S. G. Wright, and T. L. Brandon, *Soil Strength and Slope Stability*. New York: John Wiley & Sons, 2005.

[12] S. Arief, "Analisis Kestabilan Lereng dengan Metode Irisan," Sorowako, 2008.

[13] F. Atiiqah and B. Heriyadi, "Analisis Kestabilan Lereng Front IV Pit Limit di Area Penambangan Batu Kapur PT. Semen Padang Sumatera Barat," *J. Bina Tambang*, vol. 5, no. 3, pp. 29–38, 2020.

EPI International Journal of Engineering
Volume 7, Number 2, August 2024, pp. 58-67
DOI: 10.25042/epi-ije.082024.03

*p*ISSN 2615-5109
*e*ISSN 2621-0541

Vibration Analysis of Simply Supported Rectangular Plates Constrained by Rotational Edge Springs

Yoshihiro Narita[a,*]

[a]Hokkaido University (Professor Emeritus), N-13, W-8, Sapporo, Japan. Email: ynarita1951@gmail.com

Abstract

Comprehensive and accurate numerical results are presented for natural frequencies of thin isotropic, simply supported rectangular plates additionally constrained by rotational elastic springs on the edges. For complete coverage of combination, the number of all the combinations in boundary conditions of simply supported, rotationally constrained and clamped is calculated by Polya counting theory, and all sets of frequency parameters are tabulated for the lowest five modes. The Ritz method, along with displacements assumed in special polynomial form with boundary index, is used to include the strain energy stored in the rotational springs. Convergence and comparison studies are made to demonstrate accuracy of tabulated results, and the frequency parameters are listed for the fifteen sets of boundary conditions and various spring stiffness of the square plates. Some results are also presented for rectangular plates.

Keywords: Free vibration, natural frequency, simply supported plate, rectangular plate, rotational spring

1. Introduction

Vibration of flat plates has been an important research topic in mechanical, aeronautical and other structure-oriented fields in engineering. A large number of publications has appeared since a monograph was compiled by Leissa [1] in 1969, and some good textbooks were released, for example a book written by Gorman [2] on plate vibration. Among various plate applications, the most typical planform is a rectangle, and Leissa [3] published a paper on frequency parameters to cover all combinations of free, simply supported and clamped edges. These results are updated by the present author in improved accuracy [4].

For rectangular plates elastically constrained along edges, a reasonable number of papers were published because of the importance that plate structural elements are usually attached elastically to the main structure. Up to the year of 2000, Laura and his co-workers published some papers [5-8] to obtain lower frequencies, and other authors [9,10] dealt with plates with springs. A series of notable works were written by Gorman [11-15] on vibration of rectangular plates with elastic edge supports by using a famous method of the superposition method.

In the 2000's, Li [16] and Li [17] presented solutions for predicting frequencies of rectangular plates with generally restrained edges. Eftekhari and Jafari [18] derived a solution for variable thickness plates with elastic edges. Recently, Wan [19] presented an original analysis on the topic, and Zhang and others [20] presented in 2021 some results on plates with free and opposite two adjacent elastic edges. Leng and others [21] studied in 2022 vibration of plates with one corner free and its edges rotationally-restrained. Thus, up to now, the vibration of rectangular plates with elastic edge springs has drawn attentions from researchers, but the purpose of all the previous papers seems to propose analytical methods, and the frequency data presented are still limited to some specific cases.

The present author therefore undertakes to compile comprehensive and organized sets of frequency parameters for the problem, and published already one paper [22] on the free plates elastically supported by translational springs. In this paper, an analysis is extended to simply supported rectangular plates with rotational spring on the edges. These two papers fully encompass elastically supported rectangular plates in a way to cover

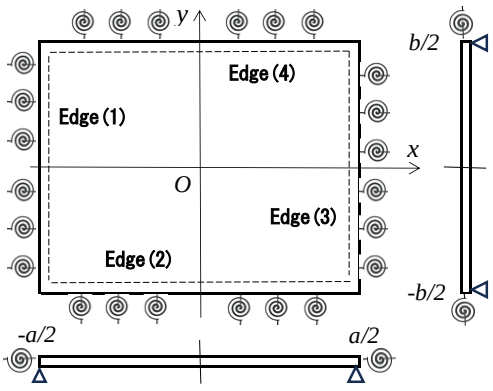

Figure 1. Simply supported rectangular plate with uniform rotational springs on the edges and the coordinate system

*Corresponding author.
N-13, W-8, Kitaku
Sapporo, Japan, 060-8628

from a totally free to a simply supported plate [22] and from there to a totally clamped plate (present paper).

2. Methodology

2.1. Combination of boundary conditions

Figure 1 illustrates an isotropic rectangular plate simply supported along four edges and elastically constrained by additional uniform rotational spring at the edges, and this edge condition is denoted by RS (Rotational Spring) in the paper. The dimension of the plate is given by $a \times b \times h$ (thickness) and the origin of the coordinate system is located in the center. Starting from the left hand edge ($x = -a/2$), four edges are labelled as Edge(1), Edge(2), Edge(3) and Edge(4) in counter-clock-wise, and each spring can have different value of rotational spring stiffness.

When one considers combination of the classical boundary conditions (F, S, C) in an isotropic square plate (a/b=1), there are twenty-one combinations to give distinct sets of the identical natural frequencies and this number can be theoretically determined by use of Polya counting theory [23,24]. In this theory, the number of combinations is determined by a cyclic polynomial

$$Z_G(z) = \frac{1}{8}\left(z^4 + 2z^3 + 3z^2 + 2z\right) \tag{1}$$

where Z_G is the number of distinct combinations to show independent sets of different natural frequencies, *G* denotes "permutation", and *z* is the number of different boundary conditions considered at each edge. For example, when one considers three boundary conditions (Free (F), Simple support (S), Clamp (C)), the number "three" is inserted in Eq.(1) as $Z_G(3) = 21$.

In this paper, three combinations of S, RS and C are considered that end up with $Z_G(3) = 21$, but the combinations only by S and C (i.e., z=2) were already covered [4] and remaining fifteen cases

$$Z_G(3) - Z_G(2) = 21 - 6 = 15 \tag{2}$$

are treated in numerical examples, as shown as Ex.1-15 in Fig. 2.

For an isotropic rectangular plate ($a/b \neq 1$), a cyclic polynomial becomes

$$Z_G(z) = \frac{1}{4}\left(z^4 + 2z^3 + z^2\right) \tag{3}$$

and the number of combinations increases up to

$$Z_G(3) = 36 \tag{4}$$

for the combination of S, RS and C [23,24].

2.2. Ritz method considering rotational edge springs

A semi-analytical solution is employed here as in Refs.[4,22,23] from the method of Ritz under the classical thin plate theory. The relation between stress and strain in the plate is

$$\begin{Bmatrix} \sigma_x \\ \sigma_y \\ \tau_{xy} \end{Bmatrix} = \begin{bmatrix} Q_{11} & Q_{12} & 0 \\ Q_{12} & Q_{22} & 0 \\ 0 & 0 & Q_{66} \end{bmatrix} \begin{Bmatrix} \varepsilon_x \\ \varepsilon_y \\ \gamma_{xy} \end{Bmatrix} \tag{5}$$

with the matrix elements given by

$$Q_{11} = Q_{22} = \frac{E}{1-\nu^2},\ Q_{12} = \nu Q_{11},\ Q_{66} = G = \frac{E}{2(1+\nu)} \tag{6}$$

where *E* is Young's modulus, *G* is a shear modulus and ν is a Poisson's ratio. When Eq.(5) is integrated through the thickness after multiplying a thickness coordinate *z*, one gets moment resultants

$$\begin{Bmatrix} M_x \\ M_y \\ M_{xy} \end{Bmatrix} = \begin{bmatrix} D_{11} & D_{12} & 0 \\ D_{12} & D_{22} & 0 \\ 0 & 0 & D_{66} \end{bmatrix} \begin{Bmatrix} \kappa_x \\ \kappa_y \\ \kappa_{xy} \end{Bmatrix} \tag{7}$$

in terms of curvature $\{\kappa_x, \kappa_y, \kappa_{xy}\}$.

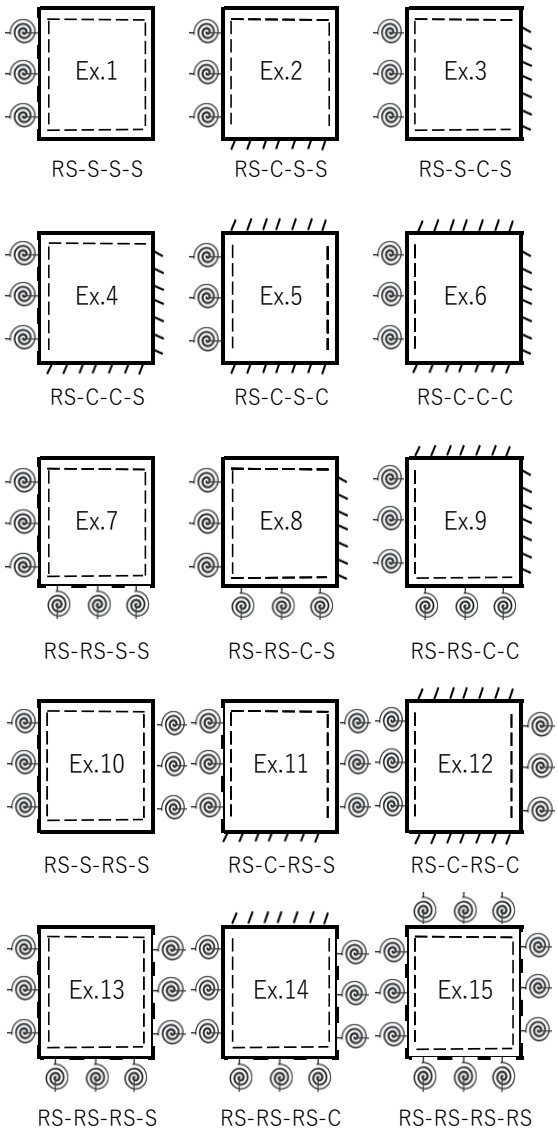

Figure 2. Fifteen numerical examples dealt in the paper

(RS: Rotational Spring, S: Simple support, C: Clamp)

If one considers the small amplitude (linear) free vibration of plate, the deflection w may be written by

$$w(x,y,t) = W(x,y)\sin\omega t \tag{8}$$

where W is the amplitude and ω is a radian frequency of the plate. Then, the maximum strain energy due to the bending is expressed by

$$U_{\max} = \frac{1}{2}\iint_A \{\kappa\}^T \begin{bmatrix} D_{11} & D_{12} & 0 \\ D_{12} & D_{22} & 0 \\ 0 & 0 & D_{66} \end{bmatrix} \{\kappa\}\, dA \tag{9}$$

where the D_{ij} are the bending stiffnesses and $\{\kappa\}$ is a curvature vector

$$\{\kappa\} = \left\{ -\frac{\partial^2 W}{\partial x^2} \quad -\frac{\partial^2 W}{\partial y^2} \quad -2\frac{\partial^2 W}{\partial x \partial y} \right\}^T \tag{10}$$

The maximum kinetic energy is also given by

$$T_{\max} = \frac{1}{2}\rho h \omega^2 \iint_A W^2 dA \tag{11}$$

where ρ [kg/m^3] is the mass per unit volume.

For the sake of simplicity, non-dimensional quantities are introduced as

$$\begin{aligned} &\xi = \frac{2x}{a}, \eta = \frac{2y}{b} \text{ (non-dimensional coordinates),} \\ &\alpha = a/b \text{ (aspect ratio)}, \quad d_{ij} = D_{ij}/D \\ &D = \frac{Eh^3}{12(1-\nu^2)} \text{ (reference stiffness)} \\ &\Omega = \omega a^2 \sqrt{\frac{\rho h}{D}} \text{ (frequency parameter)} \end{aligned} \tag{12}$$

Next, we consider the energy stored in the elastic restraints (rotational elastic springs). The energy equation is written as

$$\begin{aligned} U_r = \frac{1}{2}\times & \left\{ \int_{-b/2}^{b/2} k_{r1} \left[\frac{\partial W(-a/2, y)}{\partial x} \right]^2 dy + \int_{-a/2}^{a/2} k_{r2} \left[\frac{\partial W(x, -b/2)}{\partial y} \right]^2 dx \right. \\ & \left. + \int_{-b/2}^{b/2} k_{r3} \left[\frac{\partial W(a/2, y)}{\partial x} \right]^2 dy + \int_{-a/2}^{a/2} k_{r4} \left[\frac{\partial W(x, b/2)}{\partial y} \right]^2 dx \right\} \end{aligned} \tag{13}$$

where k_{ri} (i=1,2,3,4) are stiffness of rotational springs in unit [Nm/m]=[N] per unit edge length. This energy is added to the plate bending energy (9).

The next step in the Ritz method is to assume the amplitude as

$$W(\xi,\eta) = \sum_{m=0}^{M-1} \sum_{n=0}^{N-1} A_{mn} X_m(\xi) Y_n(\eta) \tag{14}$$

where A_{mn} are unknown coefficients, and $X_m(\xi)$ and $Y_n(\eta)$ are the functions modified so that any kinematical boundary conditions are satisfied at the edges [4,22,23].

After substituting Eq.(14) into these energies, the stationary value is obtained by

$$\begin{aligned} &\frac{\partial}{\partial A_{\bar{m}\bar{n}}} \left\{ T_{\max} - \left(U_{\max} + U_{r,\max} \right) \right\} = 0 \\ &\left(\bar{m} = 0,1,2,..(M-1); \bar{n} = 0,1,2,...(N-1) \right) \end{aligned} \tag{15}$$

Then the eigenvalue equation that contains a frequency parameter Ω is derived as

$$\begin{aligned} &\sum_{m=0}^{M-1} \sum_{n=0}^{N-1} \left[d_{11} I^{(2200)} + \alpha^2 d_{12} (I^{(2002)} + I^{(0220)}) + \alpha^4 d_{22} I^{(0022)} \right. \\ &\left. + 4\alpha^2 d_{66} I^{(1111)} + (\text{Spring term}) - \left(\frac{\Omega^2}{16} \right) I^{(0000)} \right]_{m\bar{m}n\bar{n}} \cdot A_{mn} \\ &= 0 \qquad \left(\bar{m} = 0,1,2,..(M-1); \bar{n} = 0,1,2,...(N-1) \right) \end{aligned} \tag{16}$$

where an integral I is the products

$$I^{(pqrs)}_{m\bar{m}n\bar{n}} = \varphi^{(pq)}_{m\bar{m}} \cdot \varphi^{(rs)}_{n\bar{n}} \tag{17}$$

of the two integrals defined by

$$\phi^{(pq)}_{m\bar{m}} = \int_{-1}^{1} \frac{\partial^{(p)} X_m}{\partial \xi^{(p)}} \frac{\partial^{(q)} X_{\bar{m}}}{\partial \xi^{(q)}} d\xi \tag{18}$$

and (Spring term) is the line integral along an edge.

$$\begin{aligned} (\text{spring term}) = \frac{1}{2}\times & \left[k^*_{r1} \frac{dX_m(-1)}{d\xi} \int_{-1}^{1} Y_n(\eta) d\eta + k^*_{r2} \frac{dY_n(-1)}{d\eta} \int_{-1}^{1} X_m(\xi) d\xi \right. \\ & \left. + k^*_{r3} \frac{dX_m(1)}{d\xi} \int_{-1}^{1} Y_n(\eta) d\eta + k^*_{r4} \frac{dY_n(1)}{d\eta} \int_{-1}^{1} X_m(\xi) d\xi \right] \end{aligned} \tag{19}$$

with nondimensional rotational constant

$$k^*_{r1} = \frac{k_{r1} a}{D}, k^*_{r2} = \frac{k_{r2} a}{D}, k^*_{r3} = \frac{k_{r3} a}{D}, k^*_{r4} = \frac{k_{r4} a}{D} \tag{20}$$

Equation (16) is a set of linear simultaneous equations in terms of the coefficients A_{mn}, and the eigenvalues Ω may be extracted by using existing computer subroutines.

The present approach uses simple polynomials

$$\begin{aligned} X_m(\xi) &= \xi^m (1+\xi)^{bc1} (1-\xi)^{bc3} \\ Y_n(\eta) &= \eta^n (1+\eta)^{bc2} (1-\eta)^{bc4} \end{aligned} \tag{21}$$

(bc1=bc2=bc3=bc4=1) to represent a simply supported plate as a base plate, and the integrals (18)(19) can be exactly calculated.

2.3. Finite element formulation of rotational spring

A finite element is newly developed to include the effect of rotational springs distributed along the edges, and the finite element code (FEM code) is developed by the author to compare the result with the Ritz solution to establish accuracy of both methods. Formulation of plate bending element and kinetic element are already explained in Refs.[22,25]. Here only formulation of the edge spring element is shown.

The amplitude inside the element including boundary is assumed by

$$W(x,y)=\{P\}\{\alpha\} \tag{22}$$

where {*P*} and { α } are (T: transpose)

$$\{P\}=\{1,x,y,x^2,xy,y^2,x^3,x^2y,xy^2,y^3,x^3y,xy^3\} \tag{23}$$

$$\{\alpha\}=\{\alpha_1,\alpha_2,\alpha_3,\alpha_4,\alpha_5,\alpha_6,\alpha_7,\alpha_8,\alpha_9,\alpha_{10},\alpha_{11},\alpha_{12}\}^T \tag{24}$$

The displacement at node i is defined as

$$\{\delta_i\}=\{W_i,(\partial W/\partial x)_i,(\partial W/\partial y)_i\}^T \tag{25}$$

and the displacements of four nodes labelled as *i*,*j*,*k* and *l* in a rectangular element can be expressed as

$$\{\delta_e\}=\{\delta_i \quad \delta_j \quad \delta_k \quad \delta_l\}^T \tag{26}$$

Using [*C*] which is obtained by substituting Eq.(26) into the four sets of node coordinates, *W* is transformed as

$$W(x,y)=\{P\}[C]^{-1}\{\delta_e\} \tag{27}$$

For example, when the rotational spring is distributed uniformly along Edge(2) or Edge(4) at $y=\bar{y}$, equation (27) is substituted into the second or fourth term of Eq.(13) and

$$\frac{1}{2}\int_{-a/2}^{a/2}k_{ri}\left(\frac{\partial W(x,\bar{y})}{\partial y}\right)^2dx=\frac{1}{2}\{\delta_e\}^T\left[K_{ri}\right]\{\delta_e\} \tag{28}$$

(*i*=2,4) is obtained, where [K_{ri}] is the *i*-th finite element of rotational edge spring

$$\left[K_{ri}\right]=k_{ri}\left[C^{-1}\right]^T\left(\int\left\{\frac{\partial P(x,\bar{y})}{\partial y}\right\}^T\left\{\frac{\partial P(x,\bar{y})}{\partial y}\right\}dx\right)\left[C^{-1}\right] \tag{29}$$

with $P(x,\bar{y})$ being a function of *x* at fixed $\bar{y}=-b/2$ or $\bar{y}=b/2$ for Edge(2) and Edge (4), respectively. Spring finite elements along Edge(1) and Edge(3) can be formulated in the same manner.

3. Numerical examples and discussions

3.1. Convergence and comparison of the solution

It is assumed in numerical examples that the material is isotropic with Poisson's ratio ν=0.3. Young's modulus *E* and Poisson's ratio ν are included in the dimensionless frequency parameters Ω in Eq.(12).

Figure 2 illustrates numerical examples Ex.1-Ex.15 with different degree of elastic constraints by rotational springs, and such edge (i.e., simply supported edge with uniform rotational spring attached) is denoted by "RS" (Rotational Spring). In case that the example plates have plural rotational springs on the edges, it is assumed that all the springs have the same degree of constraint.

Table 1 Convergence of (a) Ritz solution and (b)FEM solution for square plates constrained by rotational spring (Ex.1)

	Ω_1	Ω_2	Ω_3	Ω_4	Ω_5
(a) Present Ritz solution					
$k_t^*=100$					
6×6	23.37	51.44	57.75	85.28	101.5
8×8	23.37	51.44	57.74	85.27	100.1
10×10	23.37	51.44	57.74	85.27	100.1
$k_t^*=10000$					
6×6	23.64	51.67	58.65	86.14	101.7
8×8	23.64	51.67	58.64	86.13	100.3
10×10	23.64	51.67	58.64	86.13	100.3
(b) Present FEM solution					
$k_t^*=100$					
10×10	23.24	50.98	57.31	83.61	99.16
15×15	23.31	51.21	57.53	84.47	99.61
20×20	23.33	51.31	57.62	84.81	99.80
$k_t^*=10000$					
10×10	23.51	51.26	58.21	84.63	99.55
15×15	23.58	51.45	58.42	85.32	99.83
20×20	23.62	51.54	58.51	85.65	100.0

Table 2 Comparison of frequency parameters for square plates (Ex.15)

	Ω_1	Ω_2	Ω_3	Ω_4	Ω_5
$k_t^*=1$					
Ritz	21.502	51.191	51.191	80.828	100.58
[17]	21.500	51.187	51.187	80.816	100.58
$k_t^*=10$					
Ritz	28.50	60.22	60.22	90.81	111.19
[17]	28.50	60.22	60.22	90.81	111.19
[16]	28.50	60.22	60.22	90.81	111.2
$k_t^*=100$					
Ritz	34.671	70.781	70.781	104.45	127.03
[17]	34.671	70.780	70.780	104.45	127.02
[16]	34.67	70.78	70.78	104.5	127.0
$k_t^*=1000$					
Ritz	35.843	73.104	73.104	107.79	131.06
[17]	35.842	73.103	73.103	107.79	131.06

$$k_r^*=k_{r1}\left(\frac{a}{D}\right)=k_{r2}\left(\frac{a}{D}\right)=k_{r3}\left(\frac{a}{D}\right)=k_{r4}\left(\frac{a}{D}\right) \tag{30}$$

in the calculation, although they can take any different values as needed.

In the figure, Ex.1-6 are square plates constrained on Edge(1) by one rotational spring, and have different combinations of RS-S-S-S, RS-C-S-S, RS-S-C-S, RS-C-C-S, RS-C-S-C and RS-C-C-C, respectively, on the remaining three edges of Edge(2)-Edge(4). Similarly, Ex.7-12 are plates constrained on two edges constrained by two rotational springs and have different combinations

Table 3 Frequency parameters Ω of square plates
(**Ex.1**, RS-S-S-S, ν=0.3)

kr^*		Ω_1	Ω_2	Ω_3	Ω_4	Ω_5
(0)	Ritz	19.74	49.35	49.35	78.96	98.70
S-S-S-S	FEM	19.71	49.24	49.24	78.54	98.47
1	Ritz	20.18	49.53	50.09	79.43	98.79
	FEM	20.16	49.43	49.99	79.01	98.56
10	Ritz	21.95	50.43	53.74	81.95	99.31
	FEM	21.92	50.32	53.63	81.53	99.07
100	Ritz	23.37	51.44	57.74	85.27	100.1
	FEM	23.33	51.31	57.62	84.81	99.80
10000	Ritz	23.64	51.67	58.64	86.13	100.3
	FEM	23.62	51.54	58.51	85.65	100.0
(infinity)	Ritz	23.65	51.67	58.65	86.13	100.3
C-S-S-S	FEM	23.61	51.53	58.52	85.63	99.99

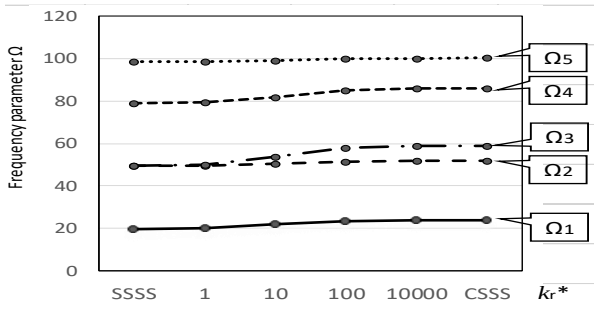

Figure 3 Variation of frequency parameters of square plate with spring stiffness (**Ex.1**).

Table 4 Frequency parameters Ω of square plates
(**Ex.2**, RS-C-S-S, ν=0.3)

kr^*		Ω_1	Ω_2	Ω_3	Ω_4	Ω_5
(0)	Ritz	23.65	51.67	58.65	86.13	100.3
S-C-S-S	FEM	23.61	51.53	58.52	85.63	99.99
1	Ritz	24.02	52.38	58.80	86.57	101.1
	FEM	23.98	52.24	58.67	86.06	100.8
10	Ritz	25.54	55.89	59.57	88.89	105.9
	FEM	25.49	55.75	59.43	88.38	105.6
100	Ritz	26.80	59.75	60.47	92.02	112.8
	FEM	26.75	59.60	60.32	91.46	112.5
10000	Ritz	27.05	60.53	60.78	92.83	114.5
	FEM	27.00	60.38	60.63	92.26	114.2
(infinity)	Ritz	27.05	60.54	60.79	92.84	114.6
C-C-S-S	FEM	27.00	60.37	60.62	92.23	114.2

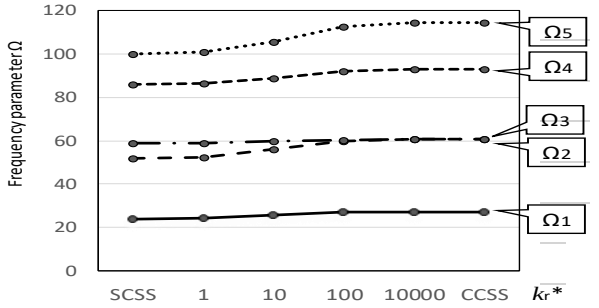

Figure 4 Variation of frequency parameters of square plate with spring stiffness (**Ex.2**).

Table 5 Frequency parameters Ω of square plates
(**Ex.3**, RS-S-C-S, ν=0.3)

kr^*		Ω_1	Ω_2	Ω_3	Ω_4	Ω_5
(0)	Ritz	23.65	51.67	58.65	86.13	100.3
S-S-C-S	FEM	23.61	51.53	58.52	85.63	99.99
1	Ritz	24.21	51.91	59.44	86.67	100.4
	FEM	24.18	51.77	59.31	86.16	100.1
10	Ritz	26.56	53.08	63.48	89.57	101.0
	FEM	26.51	52.93	63.35	89.06	100.7
100	Ritz	28.55	54.42	68.22	93.54	102.0
	FEM	28.50	54.25	68.07	92.98	101.6
10000	Ritz	28.95	54.74	69.32	94.57	102.2
	FEM	28.89	54.57	69.16	94.00	101.9
(infinity)	Ritz	28.95	54.74	69.33	94.59	102.2
C-S-C-S	FEM	28.89	54.55	69.17	93.96	101.9

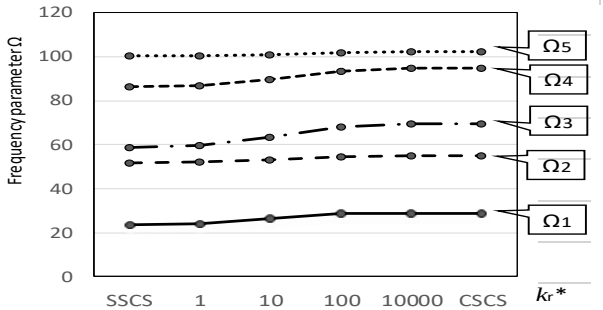

Figure 5 Variation of frequency parameters of square plate with spring stiffness (**Ex.3**).

Table 6 Frequency parameters Ω of square plates
(**Ex.4**, RS-C-C-S, ν =0.3)

kr^*		Ω_1	Ω_2	Ω_3	Ω_4	Ω_5
(0)	Ritz	27.05	60.54	60.79	92.84	114.6
S-C-C-S	FEM	27.00	60.37	60.62	92.23	114.2
1	Ritz	27.55	60.84	61.45	93.33	114.7
	FEM	27.50	60.68	61.28	92.72	114.4
10	Ritz	29.63	61.86	65.35	96.04	115.3
	FEM	29.57	61.69	65.19	95.43	115.0
100	Ritz	31.46	63.04	69.98	99.79	116.1
	FEM	31.39	62.85	69.80	99.13	115.8
10000	Ritz	31.82	63.33	71.06	100.8	116.4
	FEM	31.76	63.13	70.88	100.1	116.0
(infinity)	Ritz	31.83	63.33	71.08	100.8	116.4
C-C-C-S	FEM	31.75	63.11	70.88	100.1	116.0

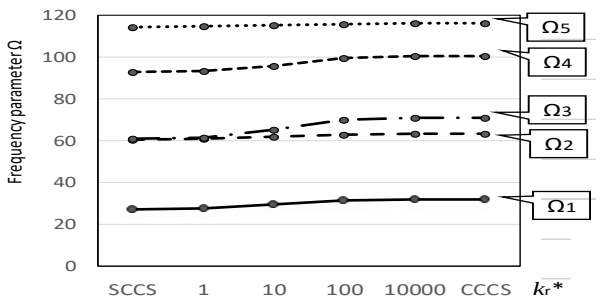

Figure 6 Variation of frequency parameters of square plate with spring stiffness (**Ex.4**).

Table 7 Frequency parameters Ω of square plates

(**Ex.5**, RS-C-S-C, ν =0.3)

kr^*		Ω_1	Ω_2	Ω_3	Ω_4	Ω_5
(0)	Ritz	28.95	54.74	69.33	94.59	102.2
S-C-S-C	FEM	28.89	54.55	69.17	93.96	101.9
1	Ritz	29.26	55.41	69.46	94.98	103.0
	FEM	29.20	55.23	69.30	94.36	102.7
10	Ritz	30.52	58.74	70.12	97.11	107.8
	FEM	30.46	58.56	69.95	96.49	107.4
100	Ritz	31.61	62.47	70.89	100.0	114.5
	FEM	31.54	62.27	70.70	99.35	114.2
10000	Ritz	31.82	63.32	71.07	100.8	116.3
	FEM	31.75	63.12	70.89	100.1	116.0
(infinity)	Ritz	31.83	63.33	71.08	100.8	116.4
C-C-S-C	FEM	31.75	63.11	70.88	100.1	116.0

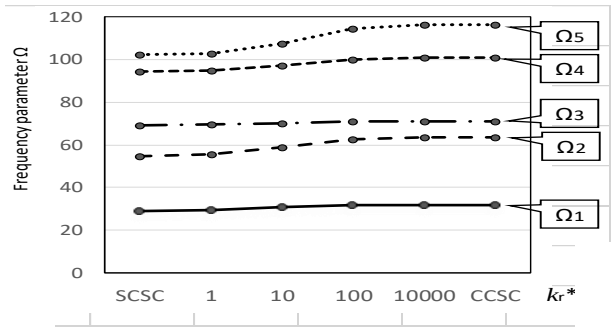

Figure 7 Variation of frequency parameters of square plate with spring stiffness (**Ex.5**).

Table 8 Frequency parameters Ω of square plates

(**Ex.6**, RS-C-C-C, ν =0.3)

kr^*		Ω_1	Ω_2	Ω_3	Ω_4	Ω_5
(0)	Ritz	31.83	63.33	71.08	100.8	116.4
S-C-C-C	FEM	31.75	63.11	70.88	100.1	116.0
1	Ritz	32.25	64.06	71.25	101.2	117.2
	FEM	32.17	63.85	71.05	100.5	116.8
10	Ritz	34.04	67.84	72.11	103.8	122.2
	FEM	33.97	67.63	71.90	103.0	121.8
100	Ritz	35.65	72.33	73.14	107.3	129.7
	FEM	35.57	72.10	72.91	106.5	129.3
10000	Ritz	35.98	73.38	73.39	108.2	131.6
	FEM	35.90	73.15	73.16	107.4	131.1
(infinity)	Ritz	35.99	73.39	73.39	108.2	131.6
C-C-C-C	FEM	35.89	73.15	73.15	107.4	131.1

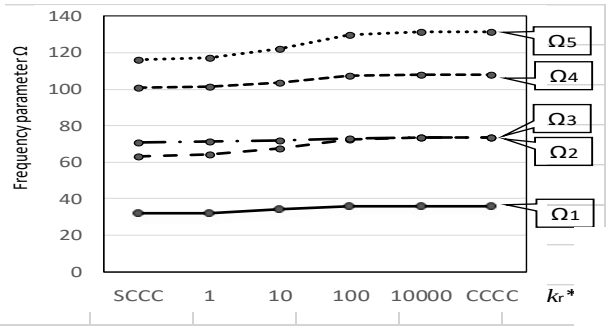

Figure 8 Variation of frequency parameters of square plate with spring stiffness (**Ex.6**).

Table 9 Frequency parameters Ω of square plates

(**Ex.7**, RS-RS-S-S, ν=0.3)

kr^*		Ω_1	Ω_2	Ω_3	Ω_4	Ω_5
S-S-S-S	Ritz	19.74	49.35	49.35	78.96	98.70
1	Ritz	20.62	50.27	50.27	79.89	99.64
10	Ritz	23.96	54.67	54.79	84.83	105.0
100	Ritz	26.55	59.44	59.68	91.19	112.5
10000	Ritz	27.05	60.53	60.78	92.82	114.5
C-C-S-S	Ritz	27.05	60.54	60.79	92.84	114.6

Table 10 Frequency parameters Ω of square plates

(**Ex.8**, RS-RS-C-S, ν=0.3)

kr^*		Ω_1	Ω_2	Ω_3	Ω_4	Ω_5
S-S-C-S	Ritz	23.65	51.67	58.65	86.13	100.3
1	Ritz	24.58	52.62	59.59	87.09	101.2
10	Ritz	28.25	57.19	64.33	92.23	106.6
100	Ritz	31.24	62.18	69.79	99.0	114.3
10000	Ritz	31.82	63.32	71.06	100.8	116.3
C-C-C-S	Ritz	31.83	63.33	71.08	100.8	116.4

Table 11 Frequency parameters Ω of square plates

(**Ex.9**, RS-RS-C-C, ν=0.3)

kr^*		Ω_1	Ω_2	Ω_3	Ω_4	Ω_5
S-S-C-C	Ritz	27.05	60.54	60.79	92.84	114.6
1	Ritz	28.04	61.54	61.72	93.82	115.5
10	Ritz	32.00	66.46	66.48	99.14	121.0
100	Ritz	35.32	72.07	72.07	106.3	129.3
10000	Ritz	35.98	73.38	73.38	108.2	131.6
C-C-C-C	Ritz	35.99	73.39	73.39	108.2	131.6

Table 12 Frequency parameters Ω of square plates

(**Ex.10**, RS-S-RS-S, ν=0.3)

kr^*		Ω_1	Ω_2	Ω_3	Ω_4	Ω_5
S-S-S-S	Ritz	19.74	49.35	49.35	78.96	98.70
1	Ritz	20.64	49.72	50.83	79.90	98.89
10	Ritz	24.51	51.65	58.25	85.09	100.0
100	Ritz	28.17	54.11	67.13	92.52	101.7
10000	Ritz	28.94	54.74	69.30	94.56	102.2
C-S-C-S	Ritz	28.95	54.74	69.33	94.59	102.2

Table 13 Frequency parameters Ω of square plates

(**Ex.11**, RS-C-RS-S, ν=0.3)

kr^*		Ω_1	Ω_2	Ω_3	Ω_4	Ω_5
S-C-S-S	Ritz	23.65	51.67	58.65	86.13	100.3
1	Ritz	24.40	53.09	58.96	87.00	101.9
10	Ritz	27.78	60.25	60.61	91.81	111.6
100	Ritz	31.10	62.76	68.92	98.81	115.9
10000	Ritz	31.82	63.32	71.05	100.8	116.4
C-C-C-S	Ritz	31.83	63.33	71.08	100.8	116.4

of simple support (without spring) and clamped edges. Ex.13 and 14 have three edges with rotational springs, and Ex.15 is a simply supported plate with all edges constrained by rotational springs.

Convergence study is presented in Table 1 for frequency parameters in Ex.1 obtained by the present (a) Ritz method and (b) finite element method. In both sets of results, non-dimensional spring constants are assumed as kr*=100 and 10000. In (a), the number of series terms in Eq.(14) are taken as $M\times N$= 6×6, 8×8 and 10×10, and very fast convergence from above (i.e., this solution is upper-bounded) is observed within the four significant figures. In (b), the number of finite elements is taken as 10×10, 15×15 and 20×20, and slightly slower convergence from below is observed as compared to the Ritz solution. This non-conforming finite element solution seems to give lower bound in this problem, but no theoretical proof is possible due to use of this non-conforming element. The discrepancy between the Ritz 10×10 solution and FEM 20×20 solution is 0.60 percent in the maximum and 0.29 percent on the average. Generally both different solutions agree well.

Table 2 presents a comparison in Ex.15 (uniformly constrained on the four edges) between Refs.[16,17] by Li and co-workers and the present Ritz result. The present solution here is given in the five significant figure to match to the result [17], and clearly they show excellent agreement. Thus in both Tables 1 and 2, validity of the present two methods is well established.

3.2. Frequency parameters of square plates

Tables 3-8 present pairs of frequency parameters obtained by the two different methods for the lowest five modes of square plates (a/b=1) in Ex.1-Ex.6, respectively. The degree of rotational springs is increased as k_r^*=0 (totally simply supported edge), 1, 10, 100, 10000 (almost clamped). In the limiting case of $k_r^*=\infty$ (infinity), the accurate values are available by replacing $k_r^*=\infty$ (S) with clamped edge (C). It is seen in common that the frequencies are monotonically increasing, as RS edge starts from simple support (k_r^*=0) to strongly constrained edge k_r^*=10000=10^4, and this degree of $k_r^*=10^4$ virtually coincide with the clamped edge.

Such monotonical increases in frequency can be seen in the accompanying Figs.3-8 for Ex-1-Ex.6, respectively. Some interesting observations are made in each figure. For example, in Fig.3 (Table 3), the second and third frequencies of S-S-S-S plate are identical (degenerated mode of a square plate) for k_r^*=0, but they become separated as k_r^* being increased and become the second and third frequencies of C-S-S-S plate. In contrast in Fig.8 (Table 8), two distinct second and third frequencies of S-C-C-C plate gradually approach each other and eventually merge into one degenerated mode.

Tables 9-17 list the lowest five frequencies obtained by the Ritz method only, when needed, they can be plotted in figures by using Excel and other software. When one needs frequency value for intermediate stiffness, one can introduce interpolation curves with respect to the stiffness values of k_r^*=0, 1, 10, 100, 10000 and ∞.

Table 14 Frequency parameters Ω of square plates

(**Ex.12**, RS-C-RS-C, ν=0.3)

k_r^*		Ω_1	Ω_2	Ω_3	Ω_4	Ω_5
S-C-S-C	Ritz	28.95	54.74	69.33	94.59	102.2
1	Ritz	29.57	56.08	69.59	95.37	103.9
10	Ritz	32.42	62.91	71.01	99.80	113.3
100	Ritz	35.33	71.29	72.89	106.3	127.7
10000	Ritz	35.98	73.37	73.39	108.2	131.6
C-C-C-C	Ritz	35.99	73.39	73.39	108.2	131.6

Table 15 Frequency parameters Ω of square plates

(**Ex.13**, RS-RS-RS-S, ν=0.3)

k_r^*		Ω_1	Ω_2	Ω_3	Ω_4	Ω_5
S-S-S-S	Ritz	19.74	49.35	49.35	78.96	98.70
1	Ritz	21.07	50.46	51.01	80.36	99.74
10	Ritz	26.33	55.86	59.17	87.87	105.6
100	Ritz	30.88	61.90	68.73	98.0	114.1
10000	Ritz	31.81	63.31	71.05	100.8	116.3
C-C-C-S	Ritz	31.83	63.33	71.08	100.8	116.4

Table 16 Frequency parameters Ω of square plates

(**Ex.14**, RS-RS-RS-C, ν=0.3)

k_r^*		Ω_1	Ω_2	Ω_3	Ω_4	Ω_5
S-S-S-C	Ritz	23.65	51.67	58.65	86.13	100.3
1	Ritz	24.95	53.32	59.75	87.52	102.1
10	Ritz	30.29	61.45	65.30	95.04	112.2
100	Ritz	35.00	71.03	71.82	105.4	127.5
10000	Ritz	35.98	73.37	73.37	108.2	131.5
C-C-C-C	Ritz	35.99	73.39	73.39	108.2	131.6

Table 17 Frequency parameters Ω of square plates

(**Ex.15**, RS-RS-RS-RS, ν=0.3)

k_r^*		Ω_1	Ω_2	Ω_3	Ω_4	Ω_5
S-S-S-S	Ritz	19.74	49.35	49.35	78.96	98.70
1	Ritz	21.50	51.19	51.19	80.83	100.6
10	Ritz	28.50	60.22	60.22	90.81	111.2
100	Ritz	34.67	70.78	70.78	104.5	127.0
10000	Ritz	35.97	73.36	73.36	108.2	131.5
C-C-C-C	Ritz	35.99	73.39	73.39	108.2	131.6

3.3. Frequency parameters of rectangular plates

Plate planform other than a square is considered to see the effect of aspect ratios. Tables 18 and 19 are sets of the lowest five frequencies for aspect ratios of a/b=2/3 and 1.5, respectively. Examples are taken form Ex.1 (one edge constrained by rotational spring), Exs.7 and 10 (two edges

Table 18 Frequency parameters Ω of rectangular plate (a/b=2/3, v=0.3)

kr*		Ω_1	Ω_2	Ω_3	Ω_4	Ω_5
Ex.1 RS-S-S-S						
0	Ritz	14.26	27.42	43.87	49.35	57.02
1	Ritz	14.86	27.74	44.70	49.53	57.67
10	Ritz	17.05	29.14	48.69	50.43	60.93
100	Ritz	18.62	30.41	51.44	52.86	64.72
10000	Ritz	18.90	30.66	51.67	53.77	65.61
C-S-S-S	Ritz	18.90	30.67	51.67	53.78	65.62
Ex.7 RS-RS-S-S						
S-S-S-S	Ritz	14.26	27.42	43.87	49.35	57.02
1	Ritz	15.03	28.12	44.76	50.03	57.86
10	Ritz	17.73	31.03	49.00	53.28	61.98
100	Ritz	19.61	33.52	53.40	56.74	66.68
10000	Ritz	19.95	34.02	54.35	57.50	67.78
C-C-S-S	Ritz	19.95	34.02	54.36	57.51	67.79
Ex.10 RS-S-RS-S						
S-S-S-S	Ritz	14.26	27.42	43.87	49.35	57.02
1	Ritz	15.47	28.07	45.52	49.72	58.31
10	Ritz	20.22	31.14	51.65	53.58	64.99
100	Ritz	24.23	34.37	54.11	62.80	73.44
10000	Ritz	25.04	35.10	54.74	64.98	75.58
C-S-C-S	Ritz	25.04	35.10	54.74	65.01	75.61
Ex.13 RS-RS-RS-S						
S-S-S-S	Ritz	14.26	27.42	43.87	49.35	57.02
1	Ritz	15.64	28.45	45.58	50.21	58.50
10	Ritz	20.81	32.92	53.86	54.44	65.98
100	Ritz	25.01	37.17	59.18	63.26	75.20
10000	Ritz	25.85	38.08	60.29	65.48	77.51
C-C-C-S	Ritz	25.86	38.09	60.30	65.51	77.53
Ex.15 RS-RS-RS-RS						
S-S-S-S	Ritz	14.26	27.42	43.87	49.35	57.02
1	Ritz	15.81	28.83	45.64	50.70	58.69
10	Ritz	21.52	34.83	54.18	57.30	67.04
100	Ritz	26.08	40.48	63.81	64.75	77.22
10000	Ritz	26.99	41.69	66.10	66.50	79.78
C-C-C-C	Ritz	27.01	41.70	66.12	66.52	78.81

Table 19 Frequency parameters Ω of rectangular plate (a/b=1.5, v=0.3)

kr*		Ω_1	Ω_2	Ω_3	Ω_4	Ω_5
Ex.1 RS-S-S-S						
S-S-S-S	Ritz	32.08	61.69	98.70	111.0	128.3
1	Ritz	32.36	62.28	98.79	111.8	128.6
10	Ritz	33.60	65.35	99.31	116.2	130.3
100	Ritz	34.79	69.03	100.1	122.8	133.0
10000	Ritz	35.05	69.90	100.3	124.6	133.8
C-S-S-S	Ritz	35.05	69.91	100.3	124.6	133.8
Ex.7 RS-RS-S-S						
S-S-S-S	Ritz	32.08	61.69	98.70	111.0	128.3
1	Ritz	33.29	62.78	100.1	112.1	129.6
10	Ritz	38.63	68.31	107.8	118.0	137.1
100	Ritz	43.77	74.91	119.2	126.9	149.0
10000	Ritz	44.88	76.53	122.3	129.4	152.5
C-C-S-S	Ritz	44.89	76.55	122.3	129.4	152.5
Ex.10 RS-S-RS-S						
S-S-S-S	Ritz	32.08	61.69	98.70	111.0	128.3
1	Ritz	32.64	62.88	98.89	112.6	128.9
10	Ritz	35.36	69.17	99.98	121.4	132.4
100	Ritz	38.38	77.38	101.7	135.5	138.3
10000	Ritz	39.08	79.50	102.2	139.6	140.2
C-S-C-S	Ritz	39.09	79.53	102.2	139.6	140.2
Ex.13 RS-RS-RS-S						
S-S-S-S	Ritz	32.08	61.69	98.70	111.0	128.3
1	Ritz	33.57	63.38	100.2	112.8	129.9
10	Ritz	40.17	71.98	108.5	123.2	139.1
100	Ritz	46.70	82.72	120.6	139.2	153.8
10000	Ritz	48.14	85.46	123.9	143.9	158.2
C-C-C-S	Ritz	48.16	85.49	124.0	144.0	158.3
Ex.15 RS-RS-RS-RS						
S-S-S-S	Ritz	32.08	61.69	98.70	111.0	128.3
1	Ritz	34.51	63.88	101.4	113.1	130.9
10	Ritz	45.58	75.17	117.0	125.1	145.9
100	Ritz	57.77	89.86	141.4	144.0	171.3
10000	Ritz	60.73	93.79	148.7	149.6	179.5
C-C-C-C	Ritz	60.76	93.83	148.8	149.7	179.6

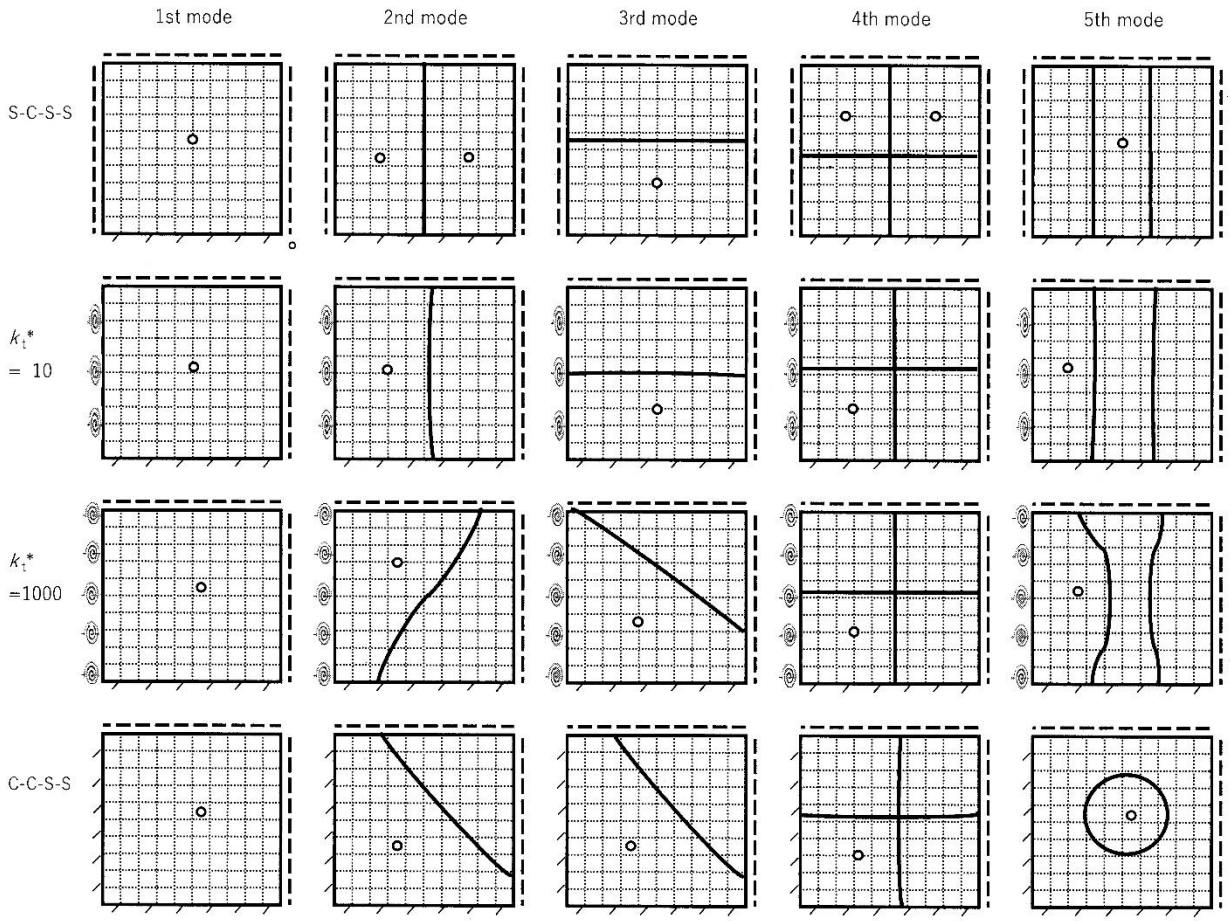

Figure 9 Mode shapes (nodal lines) of square plates (**Ex.2**) (○: Maximum amplitude)

by rotational springs), Ex.13 (three edges) and Ex.15 (four edges), where all examples here start from S-S-S-S plate. Since the present frequency parameter uses the side length a along x axis (Fig.1) in Eq.(12), a rectangular plate (a/b=2/3) appears to have more area than a plate (a/b=1.5), and therefore frequency values of a/b=2/3 in Table 18 have lower values than those of the smaller plate of a/b=1.5. The frequency values for other aspect ratios may be approximated by three-point interpolation or extrapolation curves using values for a/b=2/3, 1 and 1.5 in the paper.

3.4. Vibration mode of square plates

In free vibration analysis, vibration mode shapes are also important technical information. Nodal lines (line of zero amplitude) are plotted in Fig.9, as one example, for a square plate with one rotational spring on Edge(1) (Ex.2 in Fig.2). Variations of nodal lines are illustrated starting from kr*=0 (S-C-S-S plate) to kr*=∞ (C-C-S-S plate) by increasing rotational spring stiffness as kr*=10 and 1000. The maximum amplitude and nodal line are given as a circle ○ and thick solid lines in each figure.

All the first modes are (m*,n*)=(1,1) mode, where m* and n* are half wave numbers to describe modal shapes. There appear no nodal lines in the fundamental modes. The second and third modes are (2,1) and (1,2) modes, respectively. As the stiffness kr* is increased, nodal lines start skewed, and eventually these two modes merge and degeneration of (2,1) and (1,2) mode occurs to show the same nodal pattern. The fourth mode is (2,2) mode and nodal lines are kept almost straight and do not deform much. The fifth mode is (3,1) mode and nodal lines are skewed due to the stiffness increase. A nodal circle is formed by superposing (3,1) and (1,3) mode, as observed for totally clamped (C-C-C-C) square plate [1].

4. Conclusions

The present paper has illustrated a straightforward application of Ritz method to accurately determine the natural frequencies of a rectangular plate with uniform rotational elastic springs located on any of the four edges. A set of additional energy terms due to the springs was added to the plate strain energy in bending. The effects of the rotational springs on determining frequencies of the simply supported rectangular plates were comprehensively investigated through numerical results, including careful convergence and comparison studies. Accurate frequencies were tabulated for all the possible combinations of rotationally constrained edge(s) and other simply supported or clamped edges. It is expected that the comprehensive data is useful for researchers and design engineers.

References

1. Leissa AW, Vibration of Plates, NASA-SP-160, (1969). https://ntrs.nasa.gov/citations/19700009156
2. Gorman DJ, Vibration analysis of plates by the superposition method, World Scientific Pub, (1999).
3. Leissa AW, The free vibration of rectangular plates, *J. Sound Vib*., 31(1973), pp.257-293.
4. Narita Y, Natural frequencies of rectangular plates in improved accuracy, *EPI IJE*, 5 (2022), pp.26-36.
5. Laura PAA, Romanelli E, Vibrations of rectangular plates elastically restrained against rotation along all edges and subject to a bi-axial state of stress, *J. Sound Vibr*., 37 (1974), pp.367-377.
6. Gianetti CE, Diez L, Laura PAA, Transverse vibrations of rectangular plates with elastically restrained edges and subject to in-plane, shear forces, *J. Sound Vibr*., 54 (1977), pp.409-417.
7. Laura PAA, Grossi R, Transverse vibration of a rectangular plate elastically restrained against rotation along three edges and free on the fourth edge, *J. Sound Vibr*., 59 (1978), pp.355-368.
8. Laura PAA, Grossi R, Transverse vibrations of rectangular anisotropic plates with edges elastically restrained against rotation, *J. Sound Vibr*., 64 (1979), pp.257-267.
9. Bapat AV, Venkatramani, Simulation of classical edge conditions by finite elastic restraints in the vibration analysis of plates, *J. Sound Vibr*., 120 (1988), pp.127-140.
10. Grossi RO, Bhat RB, Natural frequencies of edge restrained tapered rectangular plates, *J. Sound Vibr.*, 185 (1995), pp.335-343.
11. Gorman DJ, A comprehensive study of the free vibration of rectangular plates resting on symmetrically-distributed uniform elastic edge supports, *J. Appl. Mech*. ASME, 56 (1989), pp.893-899.
12. Gorman DJ, A general solution for the free vibration of rectangular plates resting on uniform elastic edge supports, *J. Sound Vibr*., 139 (1990), pp.325-335.
13. Gorman DJ, The superposition method for free vibration analysis of rectangular plates with elastic edge support , Finite Elements in Analysis and Design, 18 (1994), pp.155-168.
14. Gorman DJ, A general solution for the free vibration of rectangular plates with arbitrarily distributed lateral and rotational elastic edge support, *J. Sound Vibr*., 174 (1994), pp.451-459.
15. Gorman DJ, Free vibration and buckling of in-plane loaded plates with rotational elastic edge support, *J. Sound Vibr*., 229 (2000), pp.755-773.
16. Li KM, Yu Z, A simple formula for predicting resonant frequencies of a rectangular plate with uniformly restrained edges, *J. Sound Vibr*., 327 (2009), pp.254-268.
17. Li WL, Zhang X., Du J, Liu Z, An exact series solution for the transverse vibration of rectangular plates with general elastic boundary supports, *J. Sound Vibr.*, 321 (2009), pp.254-269.
18. Eftekhari SA, Jafari AA, Accurate variational approach for the free vibration of variable thickness thin and thick plates with edges elastically restrained against translation and rotation, *Int. J. Mech. Sci.*, 68 (2013), pp.35-46.
19. Wan Z, Free vibration analysis of rectangular plates with arbitrary elastic boundary conditions, *INCE Conference Proceedings*, *InterNoise21*, (2021), pp.1891-1898, doi: //doi.org/10.3397/IN-2021-1985.
20. Zhang J, Lu J, Ullah S, Gao Y, Zhao D, Jamal A, Civalek O, Free vibration analysis of thin rectangular plates with two adjacent edges rotationally-restrained and the others free using finite Fourier integral transform method, *Struct. Engng. Mech.*, 80 (2021), pp.455-462.
21. Leng B, Ullah S, Yu T, Li K, New analytical free vibration solutions of thin plates using the Fourier series method, *Appl. Sci*., 12 (2022) , doi.org/10.3390/app12178631.
22. Narita Y, Vibration analysis of free rectangular plates constrained by translational edge spring, *EPI IJE*, 6 (2023), pp.9-17.
23. Narita Y, Combinations for the free-vibration behaviors of anisotropic rectangular plates under general edge conditions, *J. Appl. Mech. ASME*, 67 (2000), pp.568-573.
24. Narita Y, Polya counting theory applied to combination of edge conditions for generally shaped isotropic plates, *EPI IJE*, 2 (2019), pp.194-202.
25. Narita Y, Maximum frequency design of laminated plates with mixed boundary conditions, *Int. J. Solids Struct*., 43 (2006), pp. 4342–4356.

EPI International Journal of Engineering
Volume 7, Number 2, August 2024, pp. 68-74
DOI: 10.25042/epi-ije.082024.04

*p*ISSN 2615-5109
*e*ISSN 2621-0541

Bearing Capacity and Deformation of Timber Pile-Raft Foundation on Soft Soil Deposits

Muhammad Yunus[a,*], Risman Firman[b]

[a]Department of Civil Engineering, Fakfak State of Polytechnic. Email: muhammadyunus@polinef.id
[b]Department of Civil Engineering, Habibie Institute of Technology. Email: risman@ith.ac.id

Abstract

A pile-raft foundation is a type of foundation that combines two different types of foundations, a raft base and a pile foundation. These raft bases are one of the most practical economic solutions for buildings because both the support capacity of the raft and the support capability of the pile both work. The paper presents results of the test bearing capacity of piled-raft foundations made from timber in the laboratory and analyzes numerically the deformations that occur in piled raft foundations made of timber. The results of the loading test on the Bakau piled raft foundations in the laboratory obtained the maximum load that can be held by the foundation before experiencing a failure of 85.00 kN with a deformation value of 21.50 mm. Whereas from the load vs. deformation curve, the ultimate bearing capacity is obtained by the Bakau piled raft foundations at 59.00 kN with an ultimate settlement of 6.00 mm. From the results of the validation between the loading test results of the foundation model in the laboratory and the results of numerical analysis, which compared the results of laboratory tests and the results of plaque analysis, the soil with reinforcement of Timber piled raft foundations gave results that were not much different.

Keywords: bearing capacity, numerical deformation, timber pile-raft foundation, soft soil

1. Introduction

The foundation is a fundamental part of the structure that carries and transfers loads from the superstructure to the bearing ground and is located at a certain depth from the ground surface. Structures ranging from simple residential buildings to skyscrapers have a foundation of the required type. On the basis of type (vertical, lateral, earthquake, wind) and direction of loads on the superstructure and bearing ground properties, the foundation type for the structure changes.

A shallow foundation is preferred for vertical loads and stiff soil, while a deep foundation is preferred for lateral loads and soft soil. The land availability issue in the world causes the construction industry to shift to areas where soil is not suitable for shallow foundations; deep foundations are preferred in such soil types. Pile foundation is given to structures in soft soil, which transfer loads both by bearing and shearing. In some situations, pile foundation alone does not fulfill the requirement of foundation for a structure; in this case, pile and raft are used together to get the required substructure [1].

The raft-pile foundation is a practical economic solution for buildings because both the bearing capacity of the raft and the bearing capacity of the piling are working together. The foundation of the raft-pile acts as a combined construction consisting of three retaining elements, namely: a friction pile, a raft, and soil [2]. When compared with conventional foundations, the design of the raft-pile foundation forms a new dimension of the structure of the interaction of soil particles because the new philosophical design uses piles that are maximized to the carrying capacity based on the interaction of the soil and the pile. The raft-pile foundation of these leads to an economical foundation with a slight decrease if the soil has a soil modulus that increases in proportion to depth [3].

Studies on the effectiveness of the use of raft-pile foundations have been carried out by some of the researchers [4], [5]. Jamil et al. [6] conducted an experimental study of the settlement behavior of piled raft foundations with batter and vertical piles. It is concluded that using a batter pile instead of a vertical pile causes a settlement reduction and an increase in load carrying capacity, and it is recommended to study the settlement and load carrying capacity of a pile raft foundation when a horizontal load is acting on the foundation.

Alhassani et al. [7] conducted research on the on the performance of a piled-raft foundation supported by either connected or unconnected piles. The conclusions can be drawn that, using an unconnected piled raft, the settlement

*Corresponding author. Telp.: +62-811-4212-748
Jalan TPA Imam Bonjol Atas Air Merah, Kelurahan Wagom Fakfak, Papua Barat, Indonesia, 98611

efficiency is approximately constant in the experienced range of displacement and the percentage of load carried by piles.

Jayarajan et. al. [8] conducted research to demonstrates the PDR method for preliminary design and the finite element method for detailed analysis of piled raft foundations. The parametrical study of piled raft is performed through PLAXIS-3D software by considering four different pile configurations. The load-settlement response obtained through PDR method agrees very well with the response calculated through PLAXIS software and hence it can be used effectively during preliminary study to arrive at an optimum pile arrangement required for detailed analysis.

Indonesia is a country that has a tropical climate and has a vast forest area, so Indonesia is a country that is very rich in wood material, both in type and quantity, and can be used as a foundation material for raft- piles [9]. The use of wood as a pile raft foundation material to increase the carrying capacity of the soil and overcome settlement has several advantages, including being an being an easily obtainable material, having a having a relatively lower cost, being simple and easy to implement, and having a relatively short implementation time.

2. Literature Review

2.1. Physical characteristics of timber

Some of the physical characteristics of timber include : a) timber specific gravity, b) natural timber durability, c) timber colour, d) hygroscopic, e) timber structure, f) timber fibre, g) timber weight, h) timber hardness, i) tactile impression, j) odour and taste. k) decorative value.

2.2. Mechanical characteristics of timber

Mechanical characteristics or timber strength is the ability of wood to withstand external loads. What is meant by external loads are forces outside the object that have a tendency to change the shape and size of the object. Timber strength plays an important role in the use of timber as a building material, furniture industry and other uses. Mechanical characteristics of timber include tensile strength, compressive strength, flexural strength, shear strength, compression, split strength, timber ductility and timber hardness.

2.3. Chemical characteristics of timber

The chemical components in timber are important because they determine the usefulness of a particular type of timber. Also by knowing it, we can distinguish the types of timber. The chemical composition of wood is used as an identifier of timber resistance to timber destroying creatures.

2.4. Raft-pile foundation system

Pile raft foundations are a practical economic solution for buildings because the bearing capacity of the raft and the bearing capacity of the piles both work together (see Fig. 1).

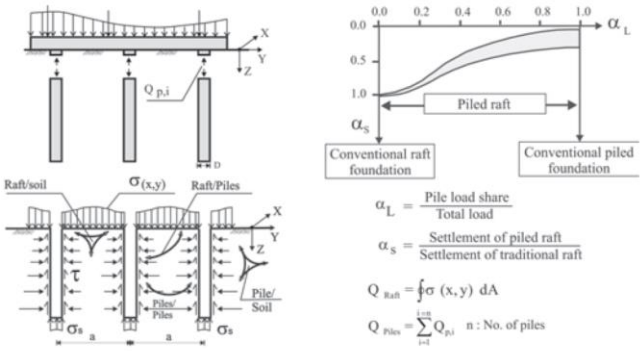

Figure 1. Principle of piled-raft [11]

The pile-raft foundation acts as a combined construction consisting of 3 (three) anchoring elements, namely friction pile, raft, and soil. When compared to conventional foundations, the design of raft-pile foundations forms a new dimension of interaction structure of soil particles due to the new design philosophy of using piles that are maximized to the limit of bearing capacity based on the interaction of soil and piles. The raft-pile foundation leads to an economical foundation with little settlement if the soil has a soil modulus that increases proportionally with depth [10].

Raft foundations are a combination of footings that cover the entire area beneath the structure and support all walls and columns despite very heavy building loads or small soil allowable stresses. In the design of large building foundations in deep compressible soils, it can be found that raft foundations will provide an adequate safety factor against ultimate bearing capacity failure, but the compression will be excessive. When topsoil exhibits very high compressibility values and low shear strength, the raft foundation surface will experience large settlement, even greater than the allowable settlement for that foundation.

Friction piles are used to help increase soil density figures to aid raft foundation work and reduce differential and total settlement. Friction piles prove to be efficient when their shear strength increases with depth and their compressibility decreases with depth. These two actions mean that friction piles reduce settlement even when the foundation receives a high load, and automatically the bearing capacity of the foundation will also increase when the load is channeled into the high shear strength soil beneath the pile.

2.5. Foundation loading test method

In principle, this foundation loading procedure is carried out by applying a vertical load placed on the pile head, and then the amount of vertical deformation that occurs is measured using a dial mounted on the pile [12]. The deformation that occurs consists of elastic and plastic deformation. Elastic deformation is deformation caused by elastic shortening of the pile and soil, while plastic deformation is deformation caused by collapse of the supporting soil at the end or around the pile [13].

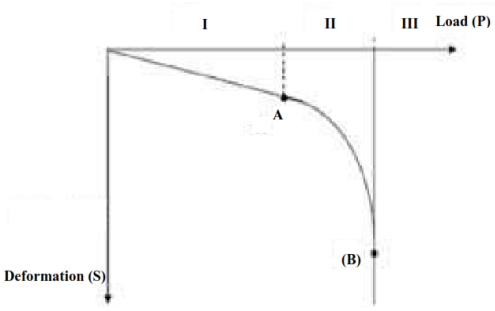

Figure 2. Load vs deformation curve [14]

Thus, this pile loading experiment will give quite precise results if the amount of deformation is carefully measured. Because what we want to know is up to what load the support layer will experience total collapse. Total collapse will occur at a certain load and will experience continuous settlement behavior. If the relationship between deformation and load is depicted in the form of a curve, it will be seen that the curve will consist of 3 (three) parts as shown in Fig. 2.

1. In region I, where up to a certain load the deformation-load curve forms a straight line. This means that up to a certain load, the amount of settlement is proportional to the magnitude of the applied load. Here it can be interpreted that the working loads are mostly used to cause elastic deformation, both in the pile itself and in the supporting soil. The elastic deformation in the pile is elastic shortening, while in the supporting layer it is a consolidation process.
2. In region II, where the parabolically curved section (line AB) occurs, if the settlement that occurs is proportional to the magnitude of the working load. Here the settlement is a function of time, meaning that if a load is allowed to work longer, it will result in greater deformation. In this case, the applied load has caused the supporting soil to collapse.
3. In region III, where the curve is steep to the vertical line. In this section, it can be seen that a certain load of a fixed magnitude will cause continuous or increasing deformation. The load that will result in increasingly larger deformations is called the maximum load.

In the interpretation of axial loading tests, there are several methods used to calculate the allowable load on a single pile foundation [15].

a. Davisson Method
b. Mazurkiewicz Method
c. Chin Method
d. Buttler dan Hoy Method
e. De Beer Method

3. Research Methodology

3.1. Soil characteristics testing

Soil characteristics testing is carried out in the soil mechanics laboratory with testing standards referring to SNI, ASTM, and AASHTO. The types of tests carried out include water content testing, content weight testing, specific gravity testing, Atterberg limits testing, sieve analysis testing, compaction testing, free compressive strength testing, and direct shear testing.

3.2. Testing the characteristics of bakau timber

For testing the mechanical characteristics of bakau timber, it was carried out in the material testing laboratory with testing standards referring to ASTM [16]. The types of tests carried out include tensile strength testing, compressive strength testing, parallel and perpendicular to the fiber, flexural strength testing, and split strength testing. Samples of mangrove wood characteristics testing can be seen in Fig. 3.

Table 1. Test method for laboratory testing of soil characteristics

No.	Testing of type	Test Method	
		ASTM	SNI
1.	Sieve analysis	C-136-06	SNI 03-1968-1990
2.	Atterberg limit		
	a. Liquid limit (LL)	D-423-66	SNI 03-1967-1990
	b. Plastiticity limit (PL)	D-424-74	SNI 03-1966-1990
	c. Plastisticity index (PI)	D-4318-10	SNI 03-1966-2008
3.	Specific gravity (Gs)	D-162	SNI 03-1964-1990
4.	Weight c of soil saturated (γ_{sat})	D-2216-98	SNI 03-1743-1989
5.	Water content (w_c)	D-2216-98	SNI 03-1965-1990
6.	Weight of dry soil (γ_{dry})	D-854-72	SNI 03-1970-2008
7.	Pore value (e)	D-854-72	SNI 03-2473-1991
8.	Porosity (n)	D-7063-11	SNI 13-3604-1994
9.	Degree of saturation (S_r)	D-854-72	SNI 03-2812-1992

Table 2. Test method for testing of bakau timber characteristic

No.	Type of testing	Test Method
1.	Moisture content (w)	ASTM D–143-94
2.	Specific gravity	ASTM D–143-94
3.	Tensile strength parallel to grain	ASTM D–143-94
4.	Tensile strength perpendicular to the grain	ASTM D–143-94
5.	Compressive strength parallel to grain	ASTM D–143-94
6.	Compressive strength perpendicular to the grain	ASTM D–143-94
7.	Shear strength	ASTM D–143-94
8.	Flexural strength	ASTM D–143-94

Figure 3. Bakau timber testing sample

3.4. Foundation modeling in the laboratory

The soft soil in the form of clay that has been tested for its characteristics is put into a testing tub measuring 60 cm x 100 cm x 160 cm. The density of the subgrade was 80% of the maximum density obtained in the standard compacted density test. In this study the subgrade was modeled as 60 cm high.

Then timber piles with a length of 40 cm were staked into the ground with a distance of approximately 25 cm between the poles, after which a timber raft of two layers in the direction of the cross section and longitudinal section was placed on top of the piles that had been staked earlier and tied together using wire. The dimensions of the timber raft used are 50 cm wide and 80 cm long, as shown in Figures 4, 5, and 7. The embankment soil, clay, was then placed on top of the timber raft reinforcement, which was modelled as a 25 cm high embankment.

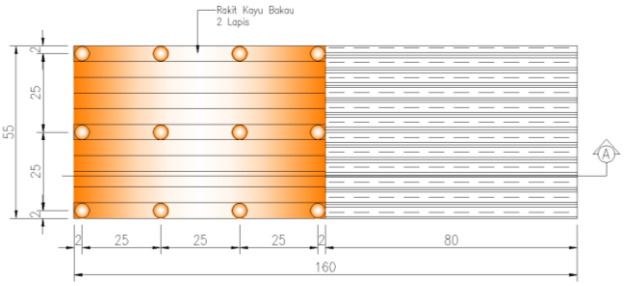

Figure 4. Layout model pile – raft foundation

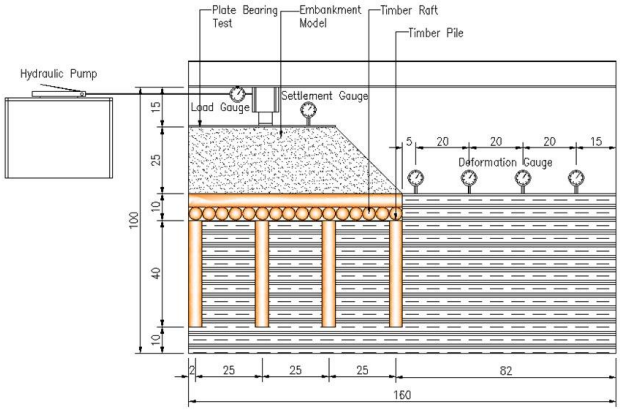

Figure 5. Model testing setup in laboratory

Figure 6. Testing foundation models in the laboratory

The steel plate (plate bearing test) is placed on the surface and will later be loaded using a hydraulic jack. Dial indicators (dial gauges) were placed in five (5) positions. The first was directly above the loading test plate; the second was placed on the subgrade about 5-10 cm to the side of the trial embankment slope, the third on the subgrade 25-30 cm from the slope, the fourth on the subgrade 45-50 cm from the slope, and the last was placed at a distance of 75-80 cm from the trial embankment slope. During the test, the load was added slowly while reading the movement of the dial gauge, observing the settlement pattern and surface deformation.

4. Results and Discussion

4.1. Results

a) Soil characteristics testing results

From the results of tests carried out in the laboratory, soil characteristics data are obtained in Table 3.

b) Test results for bakau timber characteristics

From the test results carried out in the laboratory, the mechanical characteristics of mangrove wood are shown in Table 4.

Table 3. Soil characteristics test results

No.	Type of testing	Unit	Results
1.	Water content (w)	%	36.00
2.	Specific gravity (Gs)	-	2.75
3.	Atterberg limit		
	a. Liquid limit(LL)	%	50.36
	b. Plasticity (PL)	%	37.23
	c. Plasticity index ((PI)	%	13.12
4.	Soil grain analysis		
	a. Coarse-grained soil	%	45.90
	b. Fine-grained soil	%	54.10
5.	Soil classification		
	a. USCS Method	-	MH & OH
	b. AASHTO Method	-	A-7-5
6.	Unconfined compression test (q_u)	kg/cm	0.72
7.	Compaction		
	a. Water content optimum (w_{opt})	%	41.75
	b. Dry weight (γ_{dry})	gr/cm^3	1.22
8.	Direct shear		
	a. Cohesion (c)	kg/cm^2	0.104
	b. Internal shear angle (Φ)	^{0}	17.32

Table 4. Results of bakau timber characteristic test

Types of testing	Unit	Results
Moisture content	%	21.580
Tensile strength	MPa	18.515
Modulus of elasticity tensile strength	MPa	690.423
Compressive strength parallel fiber	MPa	23.757
Modulus of elasticity parallel fiber	MPa	964.596
Compressive strength perpendicular fiber	MPa	14.710
Modulus of elasticity perpendicular fiber	MPa	591.230
Bending strength	MPa	106.224
Strong split	MPa	29.910

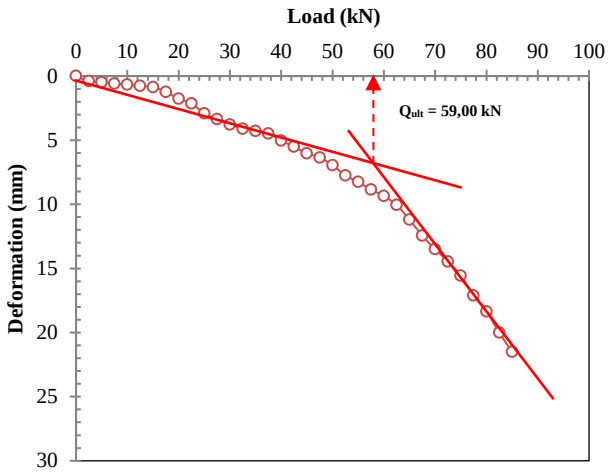

Figure 7. Load vs. deformation curve

c) Results of loading test of timber pile-raft foundation

From the results of loading tests with plate bearing tests in the laboratory, the load vs. deformation relationship curve of the timber raft-pile foundation model was obtained as shown in Fig. 7

In determining the value of the ultimate bearing capacity (Q_{ult}) of the bakau pile-raft foundation model that has been tested for loads, the Butler and Hoy (1977) method is used. This method considers the failure of the load when the load intersects two tangent lines to the curve of the relationship between the load vs. deformation at different points. The first tangent line is the initial straight line which is assumed to be an elastic pressure line. For the second tangent line obtained is limited as a slope of 0.05 kN on the load vs. deformation curve.

From the relation load vs. deformation curve in Figure 7 using the Butler and Hoy method above, the ultimate bearing capacity (Q_{ult}) value of 59.00 kN with an ultimate deformation (δu) was obtained at 6.00 mm.

4.2. Discussion

a. Numerical deformation of timber pile-raft foundation

Numerical analysis description of the pattern of soil failure and areas that have experienced large deformations and shows changes in soil movement due to the influence of the reinforcement of the raft-pile foundation.

Table 5. Deformation readings that occur on the timber pile-raft foundation

Load				Information
20 kN	40 kN	60 kN	80 kN	
-2.15	-7.30	-12.10	-22.50	Settlement
0.40	1.10	3.25	5.00	Dial 1
0.30	1.00	2.00	3.00	Dial 2
0.15	0.80	1.25	1.40	Dial 3
0.00	0.10	0.30	0.50	Dial 4

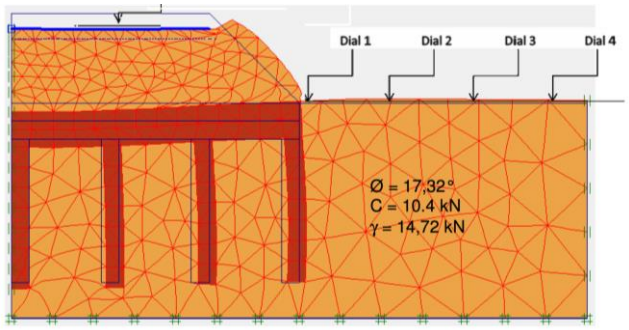

Figure 8. Numerical deformation of timberpile-raft foundation

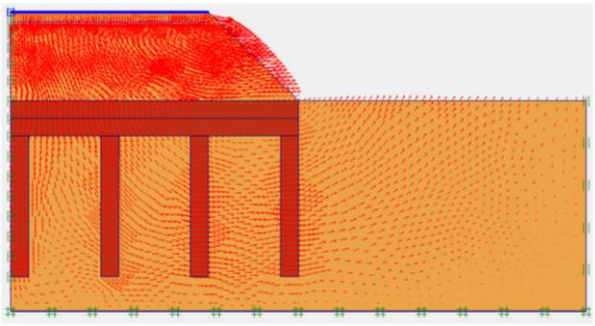

Figure 9. Stress distribution of timber pile-raft foundation

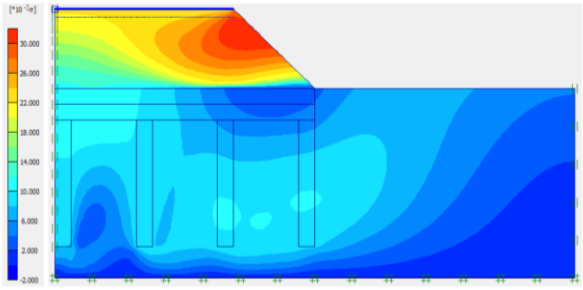

Figure 10. Shading deformation diagram of bakau pile-raft foundation

The results of numerical analysis of the bakau pile-raft foundation with a spacing of 25 cm can be seen in Fig. 8, Fig. 9, and Fig. 10. As for the reading of numerical deformations that occur at loads of 20 kN, 40 kN, 60 kN, and 80 kN, it can be seen in Table 5.

Figure 8 shows that the greater the burden the greater the deformation that occurs in the soil. Deformation that occurs at a load of 20 kN on dial 1 is 0.40 mm, on dial 2 is 0.30 mm, on dial 3 is 0.15 mm and on dial 4 is 0.00 mm. eformation that occurs at a load of 40 kN on dial 1 of 1.10 mm, on dial 2 of 1.00 mm, on dial 3 of 0.80 mm and on dial 4 of 0.30 mm. Deformation that occurs at a load of 60 kN on dial 1 is 3.25 mm, on dial 2 is 2.00 mm, on dial 3 is 1.25 mm and on dial 4 is 0.30 mm. Furthermore, the deformation that occurs at a load of 80 kN on dial 1 is 5.00 mm, on dial 2 is 3.00 mm, on dial 3 is 1.40 mm and on dial 4 is 0.50 m.

b. Numerical validation of timber pile-raft foundation

From the results of the loading test of the raft-pile foundation model in the laboratory and the results of the numerical analysis of the foundation, we obtain a comparison curve of the load vs. deformation relationship, as shown in Fig. 11.

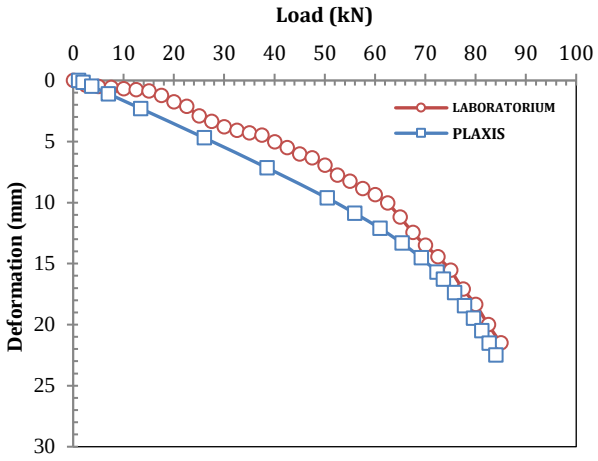

Figure 11. Load vs. deformation curve results laboratory and numerical analysis

From Fig. 11 above, it can be seen that there is a difference between the load and the deformation that occurs in the bakau pile-raft foundation model that is tested for loading in the laboratory and the results of numerical analysis. For loading tests carried out in the laboratory, a maximum load of 85.00 kN is obtained with deformation that occurs at 21.50 mm. As for the results of numerical analysis, the Plaxis 2D program obtained a maximum load of 83.98 kN with deformation that occurred at 22.50 mm.

5. Conclusion

From the results of research and data analysis that has been done, the following conclusions can be written the length of the the loading test of bakau pile-raft foundations in the laboratory obtained the maximum load that can be held by the bakau pile-raft foundation before failure of 85.00 kN with a deformation value of 21.50 mm. While from the load vs. deformation curve, the bearing capacity of the mangrove raft-base foundation is 59.00 kN with an ultimate reduction of 6.00 mm. The validation between the results of the load test model of the foundation in the laboratory and the results of numerical analysis where compared to the results of laboratory testing and the results of the analysis of plaids, the soil with the reinforcement foundation of the bakau pile-rafts gives results that are not much different.

References

[1] W. A. Prakoso and F. H. Kulhawy, "Contribution to Piled Raft Foundation Design," *Journal of Geotechnical and Geoenvironmental Engineering*, vol. 127, no. 1, pp. 17–24, Jan. 2001, doi: 10.1061/(ASCE)1090-0241(2001)127:1(17).

[2] R. Katzenbach, U. Arslan, and Chr. Moormann, "Design and Safety Concept for Piled Raft Foundations," in *Deep Foundations on Bored and Auger Piles*, CRC Press, 2020, pp. 439–448. doi: 10.1201/9781003078517-62.

[3] H. , D. Poulos, *Pile Foundation Analysis and Design*. 1980.

[4] T. Harianto, M. Yunus, and M. A. Walenna, "Bearing Capacity Of Raft-Pile Foundation Using Timber Pile On Soft Soil," *International Journal of GEOMATE*, vol. 21, no. 86, pp. 108–114, Oct. 2021, doi: 10.21660/2021.86.j2294.

[5] M. Mahmood *et al.*, "Experimental Determination of Capacity of Pile Group and Pile Raft Foundation." [Online]. Available: https://www.researchgate.net/publication/335222707

[6] Z. Altaf, S. U. Rehman, and M. H. Arshad, "Experimental Study of Comparison of Settlement Behavior of Pile Raft Foundation with Batter and Vertical Piles," 2019. [Online]. Available: https://www.researchgate.net/publication/335653023

[7] A. M. J. Alhassani and A. N. Aljorany, "Performance of Piled Raft Foundation Supported by Either Connected or Unconnected Piles," in *IOP Conference Series: Materials Science and Engineering*, Institute of Physics Publishing, Aug. 2019. doi: 10.1088/1757-899X/584/1/012045.

[8] P. Jayarajan and K. M. Kouzer, "Analysis of Piled Raft Foundations," 2015. [Online]. Available: https://www.researchgate.net/publication/334732188

[9] M. Yunus, "Model Test Ultimate Bearing Capacity of Bakau Piles Foundation on Soft Soil Deposit," *EPI International Journal of Engineering*, vol. 1, no. 2, pp. 94–99, Nov. 2018, doi: 10.25042/epi-ije.082018.15.

[10] H. G. Poulos, "Piled Raft Foundations: Design and Applications," *Géotechnique*, vol. 51, no. 2, pp. 95–113, Mar. 2001, doi: 10.1680/geot.2001.51.2.95.

[11] Y. El-Mossallamy, "Modelling the Behaviour of Piled Raft Applying Plaxis 3D Foundation Version 2," 2000.

[12] ASTM D 1143 - 81, "Standard Test Method for Piles Under Static Axial Compressive Load 1," 1994. [Online]. Available: http://www.astm.org/

[13] B. M. Das, *Principles of Foundation Engineering*, Eight Edition. Boston: Global Engineering, 2016.

[14] V.N.S Murphy, *Advanced Foundation Engineering - Geotechnical Engineering*, First Edition. New Delhi: CBS Publishers & Distributiors, 2007.

[15] Shamsher. Prakash and H. D. . Sharma, *Pile Foundations in Engineering Practice*. Wiley, 1990.

[16] ASTM D143 - 94, "Standard Test Methods for Small Clear Specimens of Timber," 2000.

EPI International Journal of Engineering
Volume 7, Number 2, August 2024, pp. 75-82
DOI: 10.25042/epi-ije.082024.05

*p*ISSN 2615-5109
*e*ISSN 2621-0541

Performance and Capabilities of Small Qualification Contractors on the Sustainable Construction Regulations Implementation

Mochamad Choir[a], Nusa Sebayang[b], Maranatha Wijayaningtyas[c,*], Wiwik Wiharti[d]

[a]Civil Engineering, National Institute of Technology Malang, 65145, Indonesia. Email: mchoir.fahri.333@gmail.com
[b]Civil Engineering, National Institute of Technology Malang, 65145, Indonesia Email: nusasebayang@lecturer.itn.ac.id
[c]Civil Engineering, National Institute of Technology Malang, 65145, Indonesia. maranatha@lecturer.itn.ac.id
[d]Civil Engineering, Sebelas Maret University, 57126, Indonesia. Email:wiwikwiharti1@gmail.com

Abstract

The construction sector is important in Indonesia's economic and social development. With the increasing awareness of the importance of sustainability, implementing sustainable construction principles has become necessary. On the other hand, construction service businesses with small qualifications face various challenges in meeting strict regulations and adapting to sustainable practices. This study aims to analyze the performance and capabilities of sustainable construction services businesses in small qualification contractors in East Java on implementing sustainable construction services business regulations. The research method used is mixed methods, as well as qualitative and quantitative methods. As many as 100 respondents are members of the Gapeksindo East Java association with small qualifications. The results showed that construction service businesses with good management (high managerial ability) tend to be more able to comply with sustainable construction regulations. In addition, the descriptive analysis results show recommendations and strategies to improve the implementation of construction services regulations among small businesses, such as training and education, financial support, Simplification of Regulations, technology and innovation, Increased Market Awareness, and technical assistance. With these strategies, it is expected that small construction service businesses in East Java can be more effective in implementing sustainable construction regulations to improve their performance and contribution to sustainable development.

Keywords: Capabilities, construction service, sustainable construction regulation, performance, small qualification

1. Introduction

The construction sector is vital to Indonesia's economic and social development. With increasing awareness of the importance of sustainability, implementing sustainable construction principles has become necessary. On the other hand, construction services businesses with minor qualifications face various challenges in meeting strict regulations and adapting to sustainable practices. Construction is a sector that plays a vital role in the country's development and significantly impacts the environment, so structured efforts are needed to reduce its harmful effects, such as sustainable construction practices. Implementing these practices must consider the environmental, social, and economic aspects of the development stages. The government has issued the Construction Services Law and its derivatives to support the implementation of the Indonesian Green Taxonomy in the construction sector, hopefully making it easier for construction service businesses to perform well. Figure 1 shows the Circular Economy Performance of the Construction Sector.

The performance of a construction services business is said to be excellent and successful if it can complete the project at the correct cost, on time, with the right quality, and with adequate resources by applicable laws. However, implementing the law regarding construction services to increase sustainable construction services businesses is not as expected. Because there has been a decline in the number of small qualified construction service business actors in East Java. According to the Gapeksindo DPD East Java Construction Services Association, members complained and had difficulty complying with regulations so that their businesses could survive and get through difficult times when the law was implemented. The number of small-scale entrepreneur members in 2018 was recorded at 850 bodies, becoming 340 bodies in 2023.

So, this research aims to analyze the performance factors and capabilities of sustainable construction services businesses of small qualified contractors in East

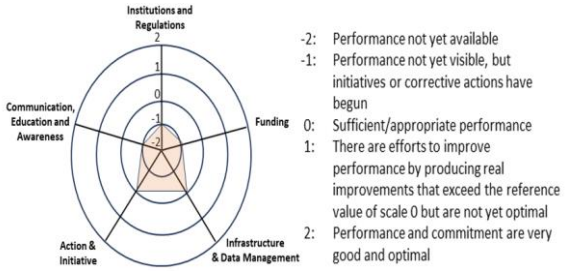

Figure 1. Circular Economy Performance of the Construction Sector [1]

*Corresponding author. Telp.: +62 812-3353-815
Jl. Sigura - Gura No.2, Sumbersari, Kec. Lowokwaru, Kota Malang, Jawa Timur Indonesia 65152

Java regarding the implementation of sustainable construction services business regulations.

2. Theoretical Basis

2.1. Construction project

The construction project is a series of activities that are only carried out once and have a generally short duration. In this series of activities, a process processes project resources into an activity that results in the building. The method in this series of activities certainly involves related parties, both directly and indirectly [2]. Construction projects occur in ever-changing and complex environments, often with high-risk levels. Buildings, roads, residential units, healthcare facilities, utility infrastructure, oil and gas, and other industrial facilities may seem typical, but each project presents challenges and risks. Construction projects are not always built at the performing organisation's primary place of business. Still, they can be built in remote environments, sometimes across the open sea, beneath the earth's surface, and soaring high into the sky [3].

2.2. Sustainable construction

In Presidential Regulation of the Republic of Indonesia no. 111 of 2022, the Sustainable Development Goals are implemented by setting national Sustainable Development Goals [4], which are prepared referring to the global goals and targets of the 2030 Sustainable Development Goals and the national targets of the national medium-term development plan for the current period [5].

The General Concept of Sustainable Construction is developed to explain the construction industry's responsibility in realising sustainable development. Sustainable development focuses on three main pillars: environmental friendliness, social life and economic prosperity [6]. Sustainable construction is a series of development processes that improve the quality of life and provide satisfaction to project customers, give the possibility and potential for future changes in the function of buildings, and provide a social environment that maximises the use of resources [5].

2.3. Elements of sustainable construction

Elements of Sustainable Construction The definition of sustainable first appeared in 1987 in the “Brutland Report” Sustainable development is development to meet the needs of the present generation without sacrificing future generations in meeting their future needs [7]. In the context of future development, sustainable development includes three things, as in Fig. 2.

2.4. Construction service

According to the National Construction Services Development Institute Regulation No. 10 of 2013 [8], a construction services business is a type of construction services business that provides construction work implementation services, which are differentiated according to the form of business, classification, and

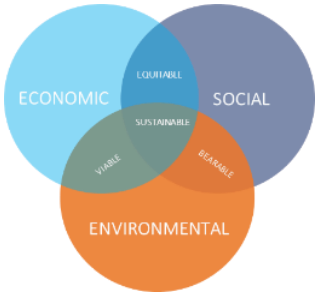

Figure 2. Three elements of sustainable development

qualifications of the construction services business [6]. Construction service qualifications are as follows:

a. Minor Qualifications

Minor Qualifications (K1, K2, and K3) are the qualifications of a company, construction service business entity, or contractor capable of efficiently carrying out work—risk small, simple, high technology, or at a small cost.

b. Intermediate Qualification

Intermediate Qualifications (M1 and M2) are the qualifications of a company, construction services business entity, or contractor capable of carrying out work with high risks, technology, and high costs.

c. Big Qualifier

Significant Qualifications (B1 and B2) are the qualifications of a company or construction services business entity or contractor capable of carrying out work with high risks, technology and significant costs.

2.5. Regulation of sustainable construction services businesses in Indonesia

Fulfilment of green criteria for the construction services sector includes appropriate land use, energy conservation, water conservation, use of environmentally friendly materials, maintaining air and noise quality, waste management, disaster adaptation, community empowerment, gender-responsive development, supporting community interaction and local businesses and protection of protected areas and cultural heritage [8], [9] called the Indonesian green taxonomy (THI) of the construction sector.

With the preparation of the THI for the construction sector, it is hoped that it can support the holistic implementation of sustainable construction in the construction sector nationally. This is in line with PP Number 14 of 2021 concerning Amendments to Government Regulation Number 22 of 2020 [10] Concerning Implementing Regulations of Law Number 2 of 2017 concerning Construction Services, which mandates that the provision of construction services for constructing buildings and civil structures must comply with sustainable principles. Across the resource and life cycle of the building [11].

3. Research Methods

This research method uses descriptive analysis. Descriptive research attempts to describe phenomena that

occur realistically, naturally and contemporarily because this research consists of making systematic, factual and precise descriptions, drawings or paintings regarding the facts, characteristics and relationships between the phenomena being studied [12]. This research is expected to reveal the experiences of informants to understand views regarding the performance of sustainable construction service businesses from the perceptions of association members (Gapeksindo in East Java) with low qualifications, association DPD administrators, experts in the field of sustainable construction management and academics regarding their influence on the implementation of service business regulations. Applicable construction. Viewpoints are also taken from the perspective of sustainable construction experts and academics to look for discoveries and information that will contribute to science.

The research process is explained in Fig. 3.

Based on information from Gapeksindo, there are approximately 500 members with small qualifications, so using the purposive sampling method, it was found that the minimum number of respondents was 100. The survey was carried out by distributing questionnaires offline, and the link was sent to selected respondents (Gapeksindo East Java members) using a Likert scale of 1 to 5. Then, this research will be analyzed using descriptive analysis.

Research variables are anything in any form that the researcher determines to be studied so that information about it can be obtained and conclusions drawn. Meanwhile, indicators are concrete measurement tools closely related to research variables. The variables in this study are shown in Table 1, and Table 2 shows sub-variables and research indicators.

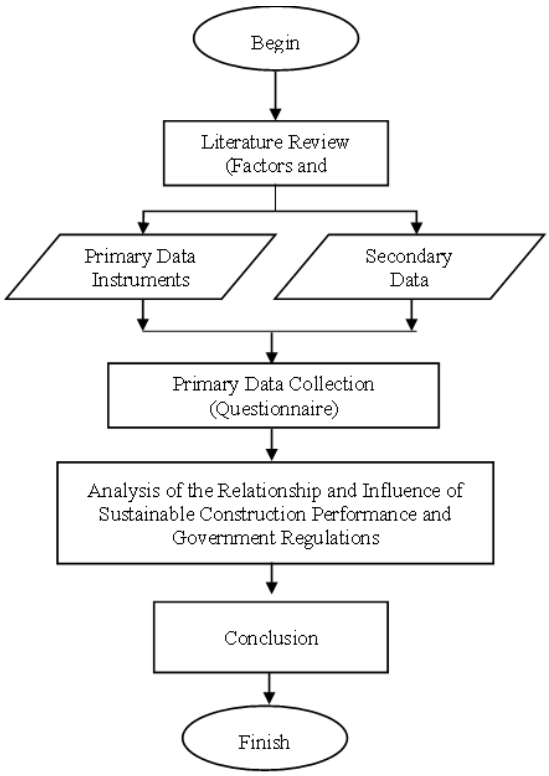

Figure 3. Research flow diagram

Table 1. Research variables

Variable	Symbol
Construction Services Business Performance	X1
Construction Services Business Capabilities	X2
Regulatory Compliance	Y

Table 2. Subvariables and research indicators

Construction Services Business Performance (X1)
Construction Services Productivity (X1.1)
Number of projects in the last one year (X1.1.1); Number of projects completed on time (X1.1.2); Labor productivity ratio (X1.1.3);.
Project Quality (X1.2)
Client satisfaction (X1.2.1); Number of complaints after project completion (X1.2.2); Periodic evaluation to maintain the quality of construction projects (X1.2.3);
Finance (X1.3)
Annual income growth (X1.3.1); Net profit margin (X1.3.2); Current cash ratio (X1.3.3); Project capital capability (X1.3.4);
Work Security and Safety (X1.4)
Frequency of work accidents (X1.4.1); Labor compliance with safety SOPs (X1.4.2); Availability of accident insurance (X1.4.3); Implementation *of reward* and *punishment* related to the implementation of safety first(X1.4.4);
Sustainability (X1.5)
Use of environmentally friendly materials (X1.5.1); Implementation of *zero waste* (X1.5.2); Implementation of projects related to water efficiency (X1.5.3); Implementation of projects related to energy efficiency (X1.5.4); The work environment prioritises the health and comfort of the work environment (X1.5.5).
Construction Services Business Capabilities (X2)
Managerial Ability (X2.1)
Implementation of continuous project management (X2.1.1); Manager's education level related to sustainable construction services businesses (X2.1.2); Project leaders can integrate project constraints, manage time, manage costs, manage human resources, and handle *stakeholders (X2.1.3).*
Technology Capability (X2.2)
Application of the latest technology to the project (X2.2.1); Number of technologies applied (X2.2.2); Nominal investment in the latest equipment (X2.2.3);
Human Resources (X2.3)
Workforce education level (X2.3.1); Certified labor ratio(X2.3.2); Level of worker satisfaction (X2.3.3);
Financial Capability (X2.4)
Debt to Equity Ratio (X2.4.1); Stability *Cash flow* on the company (X2.4.2); Accuracy of payment of wages to the workforce (X2.4.3);.
Regulatory Compliance (Y)
Compliance with company regulations (Y1); Renewal of legality requirements for construction services businesses in each period (Y2); Certification owned by the company (Y3);

4. Results and Discussion

4.1. Sustainable construction

Descriptive statistical analysis based on respondent characteristics :

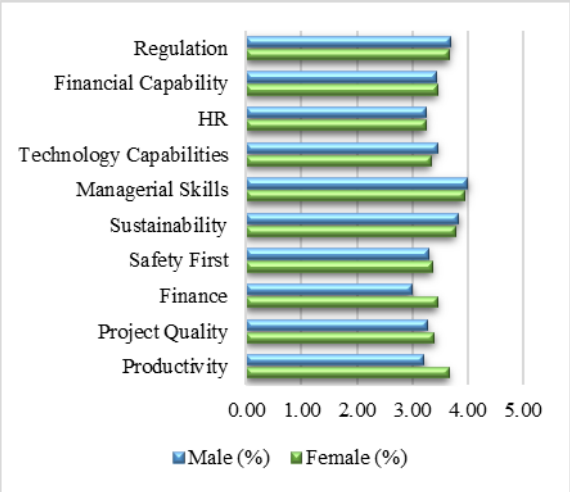

Figure 4. Graph of gender characteristics

Table 3. Gender characteristics

Variable	Mean	
	Woman	Man
Construction Services Business Performance		
Productivity	3.67	3.21
Project Quality	3.40	3.27
Finance	3.45	3.00
Safety First	3.36	3.30
Sustainability	3.78	3.84
Construction Services Business Capabilities		
Managerial Ability	3.94	4.00
Technology Capability	3.33	3.46
HR	3.25	3.24
Financial Capability	3.46	3.43
Regulations	**3.67**	**3.70**

a. Gender

Figure 4 and Table 3 show no significant differences in the perceptions of female and male respondents regarding all research indicators. In the construction service business performance variable, all genders have the highest mean value on the sustainability indicator.

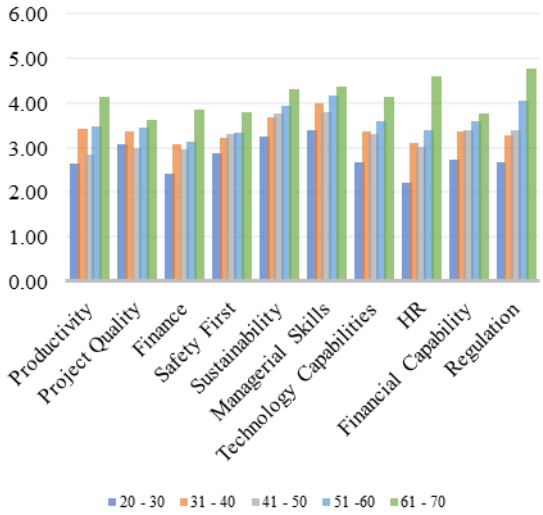

Figure 5. Graph of respondent age characteristics

Table 4. Age characteristics of respondents

Variable	Age				
	20 - 30	31 - 40	41 - 50	51 -60	61 - 70
Construction Services Business Performance					
Productivity	2.63	3.42	2.86	3.47	4.15
Project Quality	3.07	3.36	2.99	3.44	3.63
Finance	2.43	3.08	2.96	3.13	3.86
Safety First	2.88	3.22	3.31	3.34	3.81
Sustainability	3.24	3.69	3.77	3.95	4.31
Construction Services Business Capabilities					
Managerial Ability	3.40	4.00	3.81	4.16	4.37
Technology Capability	2.67	3.36	3.29	3.59	4.15
HR	2.20	3.11	3.03	3.39	4.59
Financial Capability	2.73	3.38	3.40	3.58	3.78
Implementation of Regulations					
Regulations	2.67	3.27	3.40	4.07	4.78

b. Respondent's Age

Based on Fig. 5 and Table 4, the age characteristics of respondents show that perception is highest with a mean value of 4.31 on the Sustainability performance variable, age range 61-70. Meanwhile, the highest mean value was 4.59 for the construction services business capability variable, with an age range of 61-70. This condition shows that length of experience is important in determining the performance and ability of construction service businesses to implement sustainable construction regulations.

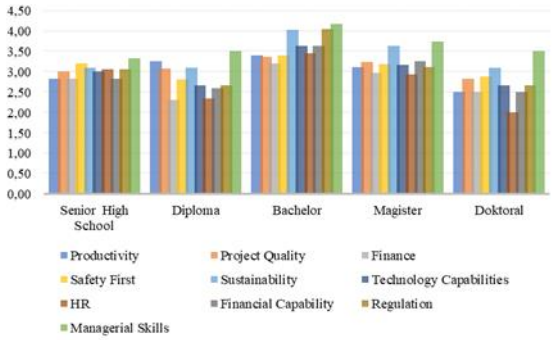

Figure 6. Variable characteristics and respondents' education level

Table 5. Variable characteristics and educational level of respondents

Variable	Level of education				
	SMA/SMK	D3	S1	S2	S3
Construction Services Business Performance					
Productivity	2.83	3.25	3.40	3.11	2.50
Project Quality	3.00	3.08	3.36	3.24	2.83
Finance	2.83	2.31	3.20	2.97	2.50
Safety First	3.21	2.81	3.40	3.18	2.88
Sustainability	3.10	3.10	4.02	3.64	3.10
Construction Services Business Capabilities					
Managerial Ability	3.33	3.50	4.17	3.74	3.50
Technology Capability	3.00	2.67	3.64	3.17	2.67
HR	3.06	2.33	3.45	2.94	2.00
Financial Capability	2.83	2.58	3.63	3.26	2.50
Implementation of Regulations					
Regulations	3.06	2.67	4.05	3.11	2.67

c. Level of education

Characteristics of Educational Level respondents whose last education was at Bachelor/S1 level showed the highest perception of the construction service business performance variable, with the highest mean value of 4.02 on the Sustainability indicator in Fig. 6 and Table 5. This shows that the majority of respondents have a high level of understanding and expertise in the field of sustainable construction. High perception is also demonstrated in the construction services business capability variable in the managerial capability indicator, amounting to 4.17. This condition illustrates that a minimum education level of a Bachelor's degree requires good basic organizational skills to implement sustainable construction regulations.

4.2 Descriptive analysis based on research variables

a. Construction Services Productivity Variables

Regarding construction services productivity indicators, as shown in Fig. 7, respondents' perceptions were highest in the productivity ratio sub-indicator, with a 70-80% range. This condition illustrates that most contractors have a relatively high level of productivity.

b. Project Quality Variables

Figure 8 illustrates that the project quality of the majority of respondents is a crucial factor in determining the performance of their construction services business. The results are excellent. As many as 88% of respondents stated that all their clients were satisfied, even very satisfied, with the company's performance on completed projects and the lack of complaints received. Additionally, 86% of respondents stated that they carry out periodic evaluations to maintain the quality of their work.

X1.1.1 and X1.1.2	1 = 0 Projects 2 = 1 – 2 Projects 3 = 3 – 4 Projects 4 = 5 – 6 Projects 5 = > 7 Projects
X1.1.3	1 = <50% 2 = 50 % - 60% 3 = 60% - 70 % 4 = 70% - 80 % 5 = > 80%

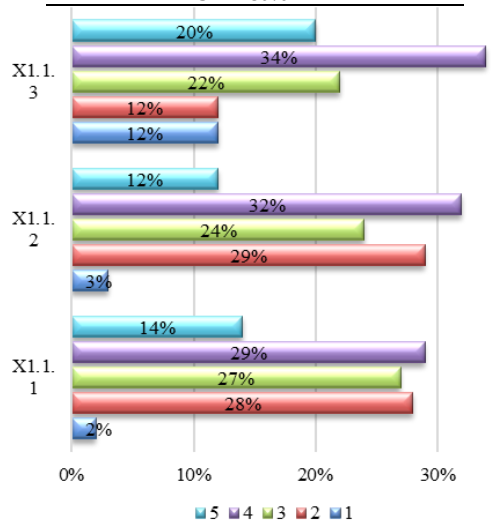

Figure 7. Descriptive graph of construction services productivity

X1.2.1 and X1.2.3	1 = Very dissatisfied 2 = Dissatisfied 3 = Neutral 4 = Yes 5 = Very satisfied
X1.2.2	1 = 0 Projects 2 = 1 – 2 Projects 3 = 3 – 4 Projects 4 = 5 – 6 Projects 5 = > 7 Projects

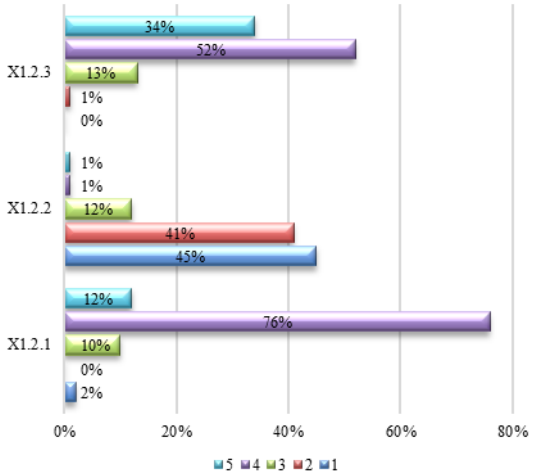

Figure 8. Project quality variable

X1.3.1 X1.3.2 X1.3.3 X1.3.4	1 = 0% - 5% 2 = 5% - 10% 3 = 10% - 15% 4 = 15% - 20% 5 = > 20%

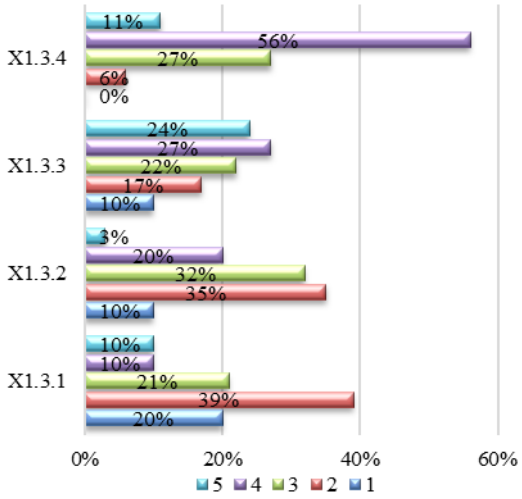

Figure 9. Descriptive graph of financial variables

c. Financial Variables

Based on Fig. 9, descriptive results of financial indicators show that most respondents have income growth of up to 10% every year with a margin or profit of 5-20% from each completed project. Apart from that, the current cash ratio is also around more than 10% each year, and the majority of respondents, 67%, stated that they have good and very good capital capabilities. However, around 27% did not respond to the condition of the project's capital capabilities.

X1.4.1	1 = 0% - 5% 2 = 5% - 10% 3 = 10% - 15% 4 = 15% - 20% 5 = > 20%
X1.4.2 **X1.4.3** **X1.4.4**	1 = Very bad 2 = Not good 3 = Neutral 4 = Good 5 = Very good

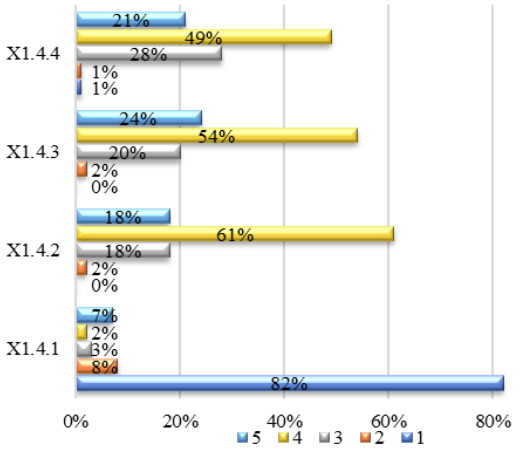

Figure 10. Descriptive graph of work safety and security

X1.5.1	1 = 0% - 5% 2 = 5% - 10% 3 = 10% - 15% 4 = 15% - 20% 5 = > 20%
X1.5.2 X1.5.3 X1.5.4 X1.5.4	1 = Strongly disagree 2 = Disagree 3 = Neutral 4 = Agree 5 = Strongly agree

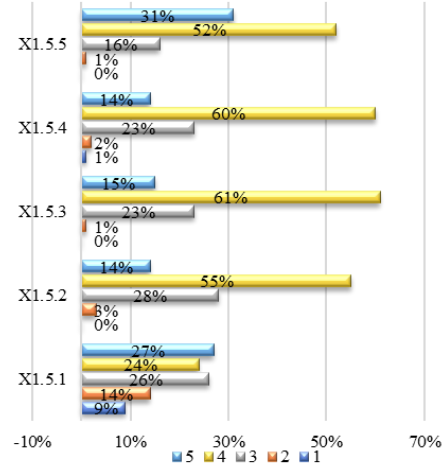

Figure 11. Descriptive graph of sustainability variables

d. Work Safety and Security Variables

Construction service business performance variables are also shown by implementing safety first in each project. The respondent's perception positively responded to this indicator, as illustrated in Fig. 10. More than 90% of the total respondents had no work accidents because the workforce complied with the safety first SOPs implemented. In addition, the Company guarantees the safety and health of workers by providing insurance and *rewards and punishments* for workers when implementing safety first. The informal construction workers must be better organised and activated, and social change attempts to force the government to protect society better [13]. Management that considers humans, processes and places in the organisation's context include an efficient physical environment, technology, safety, comfort and occupational health to achieve optimal work productivity [14].

e. Sustainability Variables

Most respondents have implemented the concept of sustainability in their businesses. More than 70% of respondents have used environmentally friendly materials, which comprise more than 10% of the total project implementation needs. In addition, more than 60% of contractors stated they had implemented sustainable construction concepts such as *zero waste*, carrying out water and energy efficiency projects, and strictly implementing safety first. Conditions The description of respondents regarding sustainable construction is shown in Fig. 11.

f. Managerial Ability Variable

The majority's perception of the contractor's managerial ability states agree and strongly agree, as shown in Fig. 12; the manager's education level influences the ability of a sustainable construction services business; as much as 71% answered in the affirmative. The highest agreement and strongly agreed statements were 85% of respondents on the indicator that project leaders can integrate project boundaries, manage time, manage costs, manage human resources, and handle stakeholders. These results show that the leader's ability is critical to support the contractor's ability to implement and follow sustainable construction services regulations. Many experts have complexly defined social capital.

X2.1.1 – **X2.1.3**	1 = Strongly disagree 2 = Disagree 3 = Neutral 4 = Agree 5 = Strongly agree

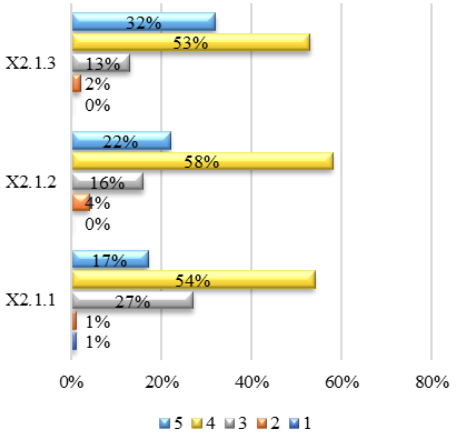

Figure 12. Descriptive graph of managerial ability variable

X2.2.1	1 = Strongly disagree 2 = Disagree 3 = Neutral 4 = Agree 5 = Strongly agree
X2.2.2	1 = 0 technology 2 = 1 – 2 technologies 3 = 3 – 4 technologies 4 = 5 – 6 technologies 5 = > 7 technologies
X2.2.3	1 = 0 2 = 0 – 5 million 3 = 5 – 10 million 4 = 10 – 15 million 5 = > 15 million

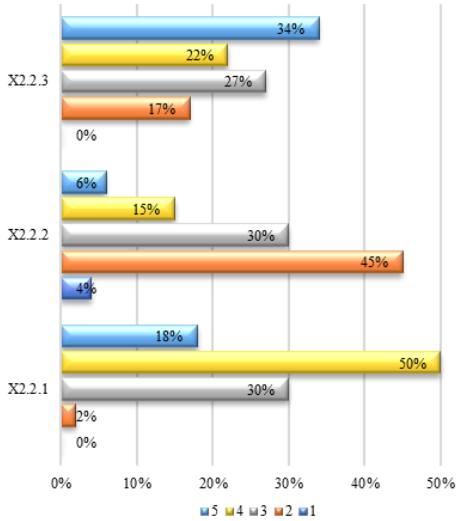

Figure 13. Descriptive graph of technological capability variable

g. Technology Capability Variable

Figure 13 shows that most respondents highly perceive the ability of construction service businesses to apply the latest technology in the projects they undertake and invest in purchasing and using the latest technology. More than 50% of respondents stated that they had invested more than 15 million rupiahs each year to purchase tools to help implement construction projects. One of the technologies that can be utilised to implement sustainable construction is Building Information Modeling (BIM). BIM is one of the promising developments in the field of AEC (Architecture, Engineering and Construction). The successful use of BIM in the construction sector illustrates that BIM can handle the development process through digitisation, with the use of an integrated BIM system that can assist and provide these management needs [12].

h. Human Resources Variables

Respondents gave a high perception regarding the qualifications of their human resources; more than 90% of respondents stated that their human resources consisted of at least two people with a Bachelor's degree, and more than 70% of respondents had more than 60% of the total number of human resources who had certified competency according to the field of work they were engaged in. In addition, as many as 74% of respondents stated that staff and employees felt satisfied joining their business, as shown in Fig. 14.

X2.3.1	1 = 0 workforce 2 = 1 – 2 Workforce 3 = 3 – 4 Workforce 4 = 5 – 6 Workforce 5 = > 7 Workforce
X2.3.2	1 = < 50% 2 = 50% - 60% 3 = 60% - 70% 4 = 70% - 80% 5 = > 80%
X2.3.3	1 = Very dissatisfied 2 = Dissatisfied 3 = Neutral 4 = Yes 5 = Very satisfied

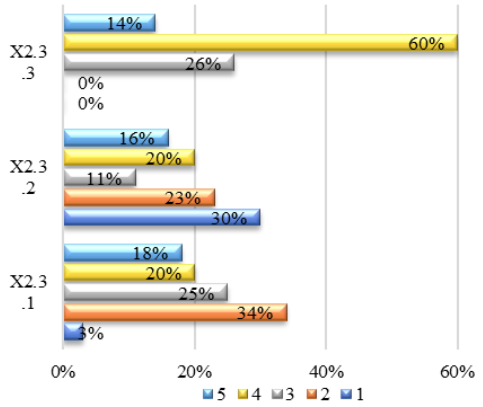

Figure 14. Descriptive graph of human resources variable

i. Financial Capability Variable

Financial capability is also an important factor in measuring the capability of a construction services business. The analysis results in Fig. 15 show that most respondents, more than 50%, have a debt ratio below 10%, and as many as 64% have stable cash flow. In addition, almost 80% of respondents stated that they were never late in paying their obligations to pay workers' wages.

X2.4.1	1 = 0% - 5% 2 = 5% - 10% 3 = 10% - 15% 4 = 15% - 20% 5 = > 20%
X2.4.2 and X2.4.1	1 = Strongly disagree 2 = Disagree 3 = Neutral 4 = Agree 5 = Strongly agree

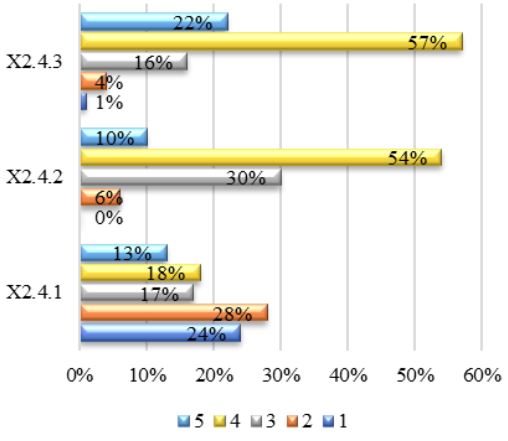

Figure 15. Descriptive graph of financial capability variable

Y1 and Y2	1 = Strongly disagree 2 = Disagree 3 = Neutral 4 = Agree 5 = Strongly agree
Y3	1 = 0 Certification 2 = 1 – 2 Certifications 3 = 3 – 4 Certifications 4 = 5 – 6 Certification 5 = > 7 Certification

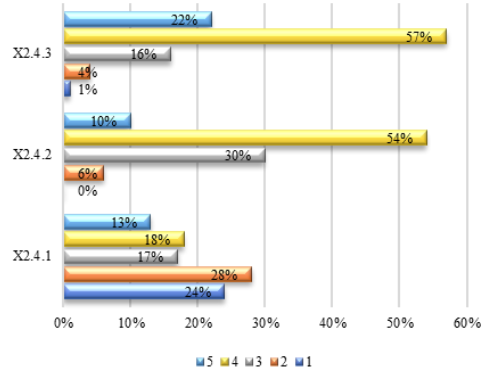

Figure 16. Descriptive graph of compliance with regulations variable

j. Variable Compliance with Regulations

Referring to the results of the presentation of respondents' statements as in Fig. 16**,** as many as 70% of respondents stated that they had adopted and implemented the regulatory rules for sustainable construction services businesses. Apart from that, as many as 84% of contractors also gave the same perception that they constantly update the Company's terms and legality according to the latest construction services business regulations. On average, respondents have 3-4 competency certifications as required by construction services regulations.

5. Conclusion

The research found that construction service businesses with good management (high managerial ability) tend to be more able to comply with sustainable construction regulations (positive correlation). The construction sector plays an important role in Indonesia's economic and social development. With increasing awareness of the importance of sustainability, implementing sustainable construction principles has become necessary. On the other hand, construction services businesses with small qualifications face various challenges in meeting strict regulations and adapting to sustainable practices. Based on the survey results, evaluate the extent to which construction services regulations are implemented.

References

[1] Kementerian Perencanaan Pembangunan Nasional / Badan Perencanaan Pembangunan Nasional, "Peta Jalan & Rencana Aksi Nasional Ekonomi Sirkular Indonesia 2025-2045," 2015.

[2] W. I. Ervianto, *Manajemen Proyek Konstruksi Edisi Revisi*. Yogyakarta: Andi, 2005.

[3] Project Management Institute Inc., "Construction Extension To The PMBOK Guide," 2016.

[4] Presiden Republik Indonesia, "Peraturan Presiden Republik Indonesia No. 111 Tahun 2022 tentang Pelaksanaan Pencapaian Tujuan Pembangunan Berkelanjutan," 2022.

[5] D. Pangemanan, R. U. Latief, S. Hamzah, and R. Arifuddin, "Study on the Application of Sustainable Construction in the Development of the Likupang Special Economic Zone," *Int. J. Eng.*, vol. 36, no. 1, pp. 50–59, 2023.

[6] D. Pangemanan, R. U. Latief, R. Arifuddin, and S. Hamzah, "Literature Review and Conceptual Framework: Sustainability Construction of Implementation in Development of Special Economic Zone (SEZ) Likupang," in *IOP Conference Series: Earth and Environmental Science*, 2023.

[7] United Nations, "Report of the World Commission on Environment and Development," Oslo, 1987.

[8] Lembaga Pengadaan Jasa Konstruksi Nasional, "Peraturan LPJKN Nomor: 10 Tahun 2013 tentang Registrasi Usaha Jasa Pelaksana Konstruksi," 2013.

[9] N. S. A. Adiwoso and S. P. Prasetyoadi, "Towards Indonesia Sustainable Future through Sustainable Building and Construction," in *Green Building Council Indonesia*, 2010.

[10] Pemerintah Republik Indonesia, "Peraturan Pemerintah Republik Indonesia No. 14 Tahun 2021 tentang Peraturan Pelaksanaan Undang-undang No. 2 Tahun 2017 tentang Jasa Konstruksi," 2021.

[11] M. Agnes and R. H. Koestoer, "A Review on Sustainable Construction Regulations in Asian Countries: Savvy Insights for Indonesia," *J. Ilmu Lingkung.*, vol. 19, no. 2, pp. 459–464, 2021.

[12] A. Rukajat, *Pendekatan Penelitian Kualitatif (Qualitative Research Approach)*. Yogyakarta: Deepublish, 2018.

[13] M. Wijayaningtyas, K. Lukiyanto, E. Nursanti, and D. I. Laksmana, "The Effect of Economical phenomenon on Informal Construction Workers Earnings within Covid-19 Pandemic: A Mixed Method Analysis," *Heliyon*, vol. 8, 2022.

[14] I. Gunawan, M. Wijayaningtyas, D. Kartika, and L. A. R. Winanda, "Factors Influencing the Application of Health Management Systems of Occupational Safety and Environment on Green Construction Projects," in *AIP Proceeding*, 2024.

EPI International Journal of Engineering
Volume 7, Number 2, August 2024, pp. 83-87
DOI: 10.25042/epi-ije.082024.06

*p*ISSN 2615-5109
*e*ISSN 2621-0541

Analysis of the Performance of a Solar Water Heating System Utilizing a Flat-Plate Absorber with Integrated Thermal Storage

M. Anis Ilahi Rahmadhani[a], Jalaluddin[b,*], A. Amijoyo Mochtar[b]

[a]Mechanical Engineering Department, Engineering Faculty, Hasanuddin University.
[b]Mechanical Engineering Department, Engineering Faculty, Hasanuddin University. Email: jalaluddin_had@eng.unhas.ac.id
[c]Mechanical Engineering Department, Engineering Faculty, Hasanuddin University. Email: andijoyo@unhas.ac.id

Abstract

Solar water heaters (SWHs) are widely used all over the world since they use solar energy to power themselves. Solar water heaters that use aluminum-alumina (AL_2O_3) thermal storage at the collector base are the focus of this experimental evaluation. To maximize the efficiency of the heat transfer process and the water heating system, it is essential to incorporate thermal storage within the collector. An investigation of the efficiency of a solar water heater with AL_2O_3 thermal storage has been conducted. Tests are conducted on two different types of absorber plates: the standard flat-plate (SFP) collector and the SFP with AL2O3 as thermal storage. The tests are carried out over the course of a period of 180 minutes and under conditions of constant solar intensity. When the SFP and SFP-TS models are compared, the results indicate that the SFP-TS type has a greater outlet temperature than the traditional SFP. The SFP-TS model delivers a thermal efficiency boost of around 6% when compared to the SFP model with the same specifications. Adding AL_2O_3 to the absorber plate as a thermal storage material improves the thermal efficiency of the plate collector, increases the duration that heat is stored in the collector, and improves the absorption of radiant heat energy.

Keywords: Solar Water Heater (SWH), Aluminum-alumina (AL_2O_3), Standard Flat Plate (SFP), Standard Flat Plate with Thermal Storage (SFP-TS)

1. Introduction

Solar water heaters (SWHs) are devices that harness solar energy as their primary power source, widely utilized in various countries worldwide. While significant progress has been made in this field, challenges remain in improving the performance of existing solar water heaters. One notable approach to address this involves integrating solar collectors with thermal storage systems. This integrated design aims to reduce energy consumption in residential water heating systems cost-effectively [1].

Some examples of recent developments in solar water heating technology include the use of porous materials, changes to the geometries of absorber plates, and modifications to clear cover glass using fluorine-doped tin oxide nanoparticles [2]. The latest developments in Solar Water Heater Systems (SWHS) have explored enhancements to Flat-Plate Collectors (FPC). For instance, Jalaluddin et al. [3] examined the thermal efficiency of solar water heaters equipped with V-shaped absorber plates, revealing an efficiency improvement of 3.6–4.4% compared to conventional designs. Furthermore, subsequent research incorporating phase change materials (PCM) into V-shaped solar water heating systems demonstrated substantial increases in efficiency, achieving gains of 20%, 14%, and 13% at discharge rates of 0.5, 1, and 1.5 L/min, respectively [4]. Despite these advancements, challenges such as fluid leakage persist.

The elevated temperatures on the absorber plate's surface often result in significant heat loss, underscoring the need for thermal energy storage systems to enhance collector efficiency. Experimental studies, such as those conducted by Pisut Thantong et al. [5], have demonstrated that combining collectors with thermal storage improves energy efficiency under tropical conditions. The same holds true for shell-and-tube energy storage systems; experiments comparing horizontal and vertical designs [6] and integrating shell and finned-tube latent heat storage devices [7] have demonstrated daily efficiencies of up to 65%.

The utilization of porous materials to improve heat transfer is the subject of a new strategy for collector development. One promising approach involves using metal foams sandwiched between the absorber plate and the insulator. These foams can store heat for long periods of time before transferring it to the working fluid. Foam blocks made of aluminum, copper, nickel, reticulated vitreous carbon, and ceramic are among the porous materials that have been used as collectors.

*Corresponding author. Tel.: +62 821-9226-7077
Jalan Poros Malino km. 6 Bontomarannu
Gowa, Sulawesi Selatan
Indonesia 92171

Geometry, placement, and fluid flow rate are three aspects that have been the focus of numerous simulation- and experiment-based investigations of foam's function in collectors. Thermodynamic efficiency and heat transfer area are both improved when foam is placed inside the collector channel, according to research by Gunjo et al. [8]. When comparing parabolic collector designs with and without metal foam, Valizade et al. [9] discovered that the former had better thermal efficiency. The use of aluminum foam on the top and bottom plates considerably improves efficiency when compared to designs lacking foam, according to trials conducted by Basri et al. [10].

Based on these findings, incorporating thermal storage into collectors significantly improves heat transfer processes and water heating system performance. The porous structure of metal foams provides excellent thermal conductivity and heat retention capabilities. However, their metallic properties also facilitate rapid heat dissipation, limiting their efficiency as heat storage materials. Ceramics, on the other hand, are less efficient overall but absorb heat better and retain it for longer. Composite constructions made of these materials show potential for improving collector efficiency, heat transfer, and retention. Two absorber plate types are examined in this study: the Standard Flat-Plate (SFP) collector and the SFP-TS, which combines the SFP with AL_2O_3 thermal storage.

2. Methodology

Chemical energy, sensible heat, and latent heat are the three main forms of energy storage. Both heating and cooling fluids, as well as keeping a constant temperature, are possible with the help of these sources of stored energy. The main areas of concentration in the field of thermal storage materials research at the moment are sensible and latent heat [11]. Latent heat storage involves substances undergoing phase changes, such as melting, boiling, or solid-to-crystal structure transformations, where heat is absorbed or released without changing the temperature. Phase change material (PCM) or heat of transformation describes the amount of energy needed for this shift. The equation for the heat required during phase change is expressed as [12]:

$$Q = m\text{Le} \quad (1)$$

Where is the heat required for phase change (J), m is the mass of the substance (kg), and Le is the specific latent heat capacity (J/kg). The schematic representation of a solar water heater with composite thermal storage is shown in Fig. 1.

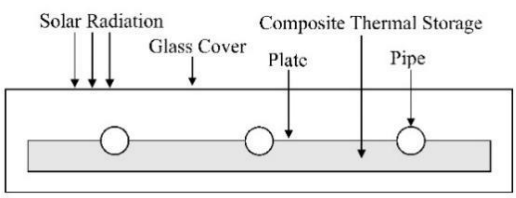

Figure 1. SWH integrated composite thermal storage

Composite materials combine two or more distinct constituents to achieve enhanced mechanical, thermal, and physical properties. These composites contain reinforcement materials and a binder (matrix), such as metals, ceramics, or polymers. Factors like geometric configuration, phase morphology, concentration distribution, matrix alignment, and volume percentage influence the properties of composites [13].

A steady-state energy balance describes the performance of a solar collector by dividing incident solar energy into thermal losses, optical losses, and usable energy gain. The net usable energy produced by a given collector area is the sum of its solar energy absorption and thermal losses A_c [14]:

$$Q_u = A_c[s - U_L (T_{pm} - T_a)] \quad (2)$$

Q_u, Useful energy can also be determined from the temperature measurements of inlet and outlet water in the collector using the equation [14].

$$Q_u = \int Q_u dt = \dot{m} C_p (T_o - T_i) \quad (3)$$

where $\dot{m}$ is the mass flow rate (kg/s), C_p is the specific heat capacity (kJ/kg·K), T_o is the outlet fluid temperature (°C), and T_i is the inlet fluid temperature (°C).

Collector efficiency is defined as the ratio of useful output to the incident solar energy over a specific time period [15]:

$$\eta = \frac{\int \mathrm{Q_u} dt}{A_c \int \mathrm{I_T} dt} \quad (4)$$

$\mathrm{I_T}$ where represents solar intensity (W/m²) and A_c is the collector surface area (m²).

The Hasanuddin University Department of Mechanical Engineering's Renewable Energy Laboratory was the site of the research. A solid insulator, a collector, and a lighting unit serving as the heat source made comprised the experimental setup's ET-202 solar thermal energy unit. Several sensors were installed to monitor the water temperature at the intake and outflow, as well as the surrounding air temperature, the amount of solar radiation, the flow rate, and the water pump's ability to circulate air within the storage reservoir.

Rectangular containers with absorber plates and heat storage medium made up the test components. We put the Standard Flat Plate (SFP) and the Standard Flat Plate with AL2O3 Thermal Storage (SFP-TS) absorber plate designs to the test. Both prototypes were tested experimentally for 180 minutes under the same conditions. Data such as flow rates, water temperatures at the intake and outflow, and solar intensity were recorded. Followed the steps outlined in the ET-202 manual for performance analysis and measurement [16].

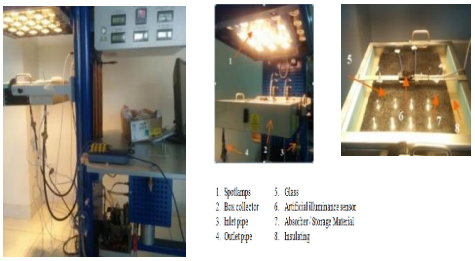

Figure 2. Solar thermal energy unit

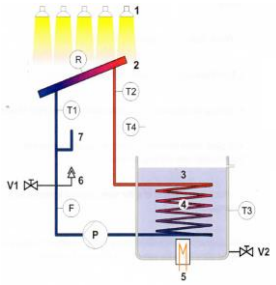

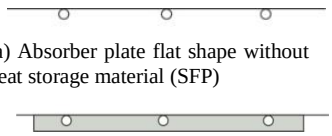

(a) Absorber plate flat shape without heat storage material (SFP)

(b) Absorber plate flat shape with the addition of heat storage material (SFP-TS)

Figure 3. Experimental set-up

Table 1. Solar thermal energy unit specifications

Description	Dimension	Unit
ET 202 FPC		
Absorbing surface	0.32 x 0.34	m
Angle adjustment	0	deg
Height adjustment	0.5	m
Lighting unit		
Illuminance	1	kW/m^2
Peristaltic Pump		
Flow rate	10	L/h

Figure 4. Composite Thermal Storage

Table 2. Specifications Composite Thermal Storage

	Alumina 65%	Aluminum 35%
Density (kg/m^3)	3720	2700
Melting point (^{o}C)	2049	660
Thermal Conductivity (W/m.K)	38	220

3. Results and Discussion

AL_2O_3 composite integrated absorber plates were the subject of this experimental investigation. Two models were teste with SFP and SFP-TS. To ensure accuracy, data collection for each model was repeated three times.

3.1. Solar intensity

The intensity of solar radiation during testing was provided by a lighting unit and measured using an artificial solarimeter. Both SFP and SFP-TS models were subjected to a consistent solar intensity of 1 kW/m² for 180 minutes. After 60 minutes, the lighting unit was turned off, rendering the solar intensity unreadable. Figure 5 shows the solar intensity during testing.

3.2. *Temperature of absorber plate*

Figure 6 illustrates the temperature profiles of the SFP and SFP-TS models throughout the test. The absorber plates' copper substance has a strong heat absorption capability, therefore the temperatures increased gradually from an initial reading of around 40°C. That the absorber plate gets even hotter thanks to the AL_2O_3 thermal storage

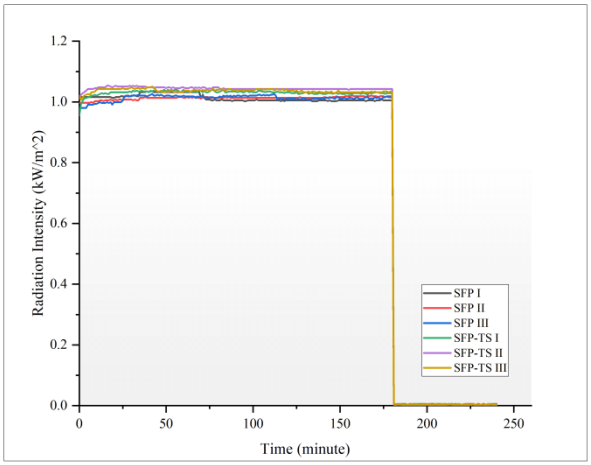

Figure 5. Radiation intensity

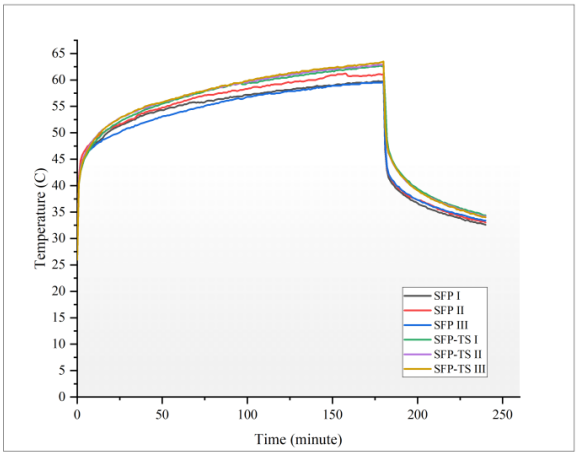

Figure 6. Absorber plate temperature

is evident from this. After 180 minutes, the SFP-TS model reached a maximum temperature of around 63°C, while the SFP model peaked at 60°C, indicating a 3°C difference. The SFP-TS model retained heat more effectively, cooling at a slower rate after the lighting was turned off. This behavior highlights the advantage of thermal storage in heat retention.

3.3. Temperature of inlet and outlet water

Figure 7 shows a graph with constant flow rate of 10 L/h comparing entrance and exit temperatures for every data collecting point. Every model's inlet temperature runs from 27°C in the early minutes to 38°C around 180 minutes before the lights go out. The output temperature of the SFP-TS variation shows higher than that of the SFP model. During 180 minutes of illumination, the SFP-TS type's maximum outlet temperature is about 48°C. The input and output temperatures seem to be exactly same at a given point when the illumination is turned off. Still, the SFP-TS model's temperature drop seems to be more gradual than that in the SFP. Thermal storage in the SFP-TS model helps it to retain heat for around thirty minutes after lights deactivation. Heat retention is improved by including AL_2O_3 thermal storage at the base of the absorber plate. Measuring an artificial solarimeter, the lighting unit determines the strength of solar radiation on

the test equipment. Figure 5 shows the two SFP models' received solar intensity. SFP-TS models For 180 minutes, both models were tested under a fixed solar intensity of 1 kW/m². The lighting unit is turned off sixty minutes later, hence the measurement instrument cannot read the solar intensity.

Figure 7 shows the water temperatures for the outlets and inlets for both models. Beginning at 27°C and rising to 38°C over 180 minutes, the inlet temperature was 10 L/h constant flow rate. Reaching a maximum of 48°C, the SFP- TS model routinely attained greater outlet temperatures than the SFP model. The SFP-TS model showed a sustained heat retention capacity once the lighting unit was turned off, preserving higher temperatures for an extra thirty minutes.

3.4. *Energy Absorption*

Figure 8 contrasts the energy absorbed by the SFP and SFP-TS absorber plates throughout the 240-minute test. The energy rises over the first 30 minutes and subsequently stabilizes until the 180th minute. The SFP-TS model can absorb up to 103 watts of energy, however the SFP model can only absorb approximately 93 watts, indicating a notable difference between the two types. This demonstrates that AL_2O_3 thermal storage is highly effective in energy absorption up to a differential of 10 watts.

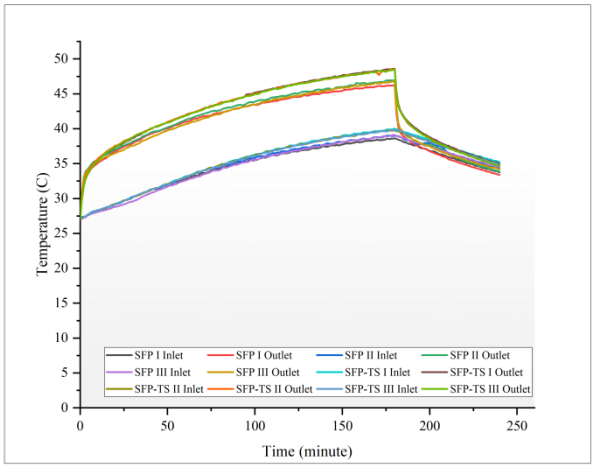

Figure 7. Inlet and outlet water temperature

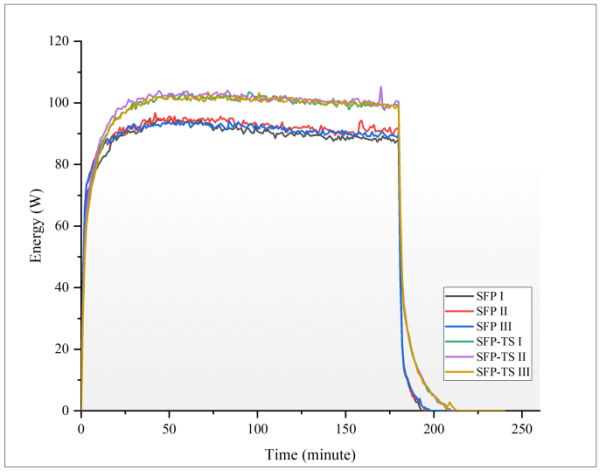

Figure 8. Energy absorption

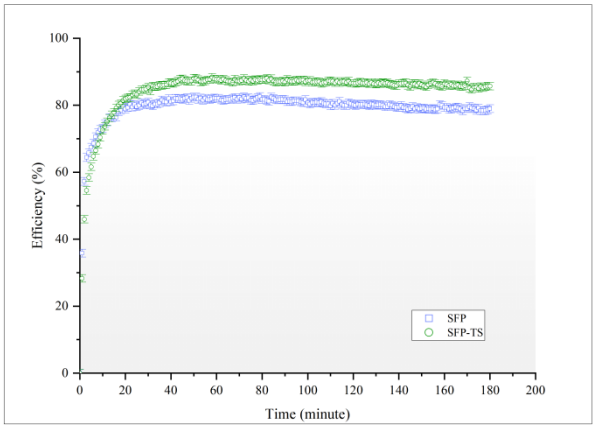

Figure 9. Efficiency

3.5. *Collector Efficiency*

Figure 9 shows the comparison of operational lifetime with thermal efficiency. Over the first three hours, the thermal efficiency of the SFP model stabilises after around 20 minutes of operation at an efficiency of about 80%. Concurrently, the SFP-TS type requires around sixty minutes to attain a continuous thermal efficiency of about 85%. The stop of radiation intensity causes the collector's thermal efficiency to zero after 180 minutes of running. Nevertheless, as Figures 6 and 7 show, the thermal energy in the SFP-TS stays kept in thermal storage for about 30 minutes even with the reduction of radiation intensity. The SFP-TS model shows an efficiency value somewhat higher than that of the SFP model—about 6%. Underlying the collecting plate with thermal storage greatly improves heat absorption, storage, andretention.

Alumina thermal storage combined with the absorber plate improves heat absorption, storage, and retention. Acting both as a heat absorber and reservoir, the thermal storage medium enhances the general performance of the system.

4. Conclusions

A solar water heater and AL_2O_3 thermal storage have been studied for their potential effectiveness. Experimental evaluations were conducted for two kinds of absorber plates under continuous solar intensity for 180 minutes. One model was the standard flat-plate (SFP) collector, and the other was the SFP with AL_2O_3 thermal storage (SFP-TS). The SFP-TS model's water temperature outlet is higher than the SFP model's. Additionally, compared to the SFP model, the SFP-TS model's thermal efficiency rises by about 6%. By adding AL_2O_3 to the absorber plate's base for thermal storage, radiant heat energy is better absorbed, the collector's heat storage time is extended, and the plate collector's thermal efficiency is raised.

Acknowledgment

This research was supported and financed by the Directorate of Research, Technology and Community Service, Ministry of Education, Culture, Research and Technology, and the Institute of Research and Community

Service (LP2M) of Hasanuddin University with contract number 020/E5/PG.02.00.PL/2023.

References

[1] C. Garnier, T. Muneer, and J. Currie, "Numerical and Empirical Evaluation of a Novel Building Integrated Collector Storage Solar Water Heater," *Renew. Energy*, vol. 126, pp. 281–295, 2018.

[2] V. Msomi and O. Nemraoui, "Improvement of the Performance of Solar Water Heater Based on Nanotechnology," in *IEEE 6th International Conference on Renewable Energy Research and Applications*, 2017.

[3] Jalaluddin, E. Arif, and R. Tarakka, "Experimental Study of an SWH System with V-Shaped Plate," *J. Eng. Technol. Sci.*, vol. 48, no. 2, pp. 207–217, 2016.

[4] Jalaluddin, R. Tarakka, M. Rusman, and A. A. Mochtar, "Performance Investigation of Solar Water Heating System with V-Shaped Absorber Plate Integrated PCM Storage," *Int. J. Eng. Appl.*, vol. 8, no. 5, 2020.

[5] P. Thantong and P. Chantawong, "Experimental Study of Solar - Phase Change Material Wall for Domestic Hot Water Production under the Tropical Climate," *Energy Procedia*, vol. 138, pp. 38–43, 2017.

[6] S. Seddegh, X. Wang, and A. D. Henderson, "A Comparative Study of Thermal Behaviour of a Horizontal and Vertical Shell-and-Tube Energy Storage Using Phase Change Materials," *Appl. Therm. Eng.*, vol. 93, pp. 348–358, 2016.

[7] S. M. Shalaby, A. E. Kabeel, B. M. Moharram, and A. H. Fleafl, "Experimental Study of the Solar Water Heater Integrated with Shell and Finned Tube Latent Heat Storage System," *J. Energy Storage*, vol. 31, 2020.

[8] D. G. Gunjo, P. Mahanta, and P. S. Robi, "CFD and Experimental Investigation of Flat Plate Solar Water Heating System Under Steady State Condition," *Renew. Energy*, vol. 106, pp. 24–36, 2017.

[9] M. Valizade, M. M. Heyhat, and M. Maerefat, "Experimental Study of the Thermal Behavior of Direct Absorption Parabolic Trough Collector by Applying Copper Metal Foam as Volumetric Solar Absorption," *Renew. Energy*, vol. 145, pp. 261–269, 2020.

[10] M. H. Basri, Jalaluddin, R. Tarakka, M. Syahid, and M. A. I. Ramadhani, "Experimental Study of Modified Absorber Plate Integrated with Aluminium Foam of Solar Water Heating System," *Int. J. Renew. Energy Res.*, vol. 12, no. 2, pp. 993–999, 2022.

[11] Jalaluddin, E. Arief, and R. Tarakka, "Analisis Performansi Kolektor Surya Pemanas Air dengan Pelat Kolektor Bentuk-V," in *Seminar Nasional Tahunan Teknik Mesin Indonesia XIV*, 2015.

[12] A. Sharma, V. V. Tyagi, C. R. Chen, and D. Buddhi, "Review on Thermal Energy Storage with Phase Change Materials and Applications," *Renew. Sustain. Energy Rev.*, vol. 13, no. 2, pp. 318–345, 2009.

[13] A. K. Sharma, R. Bhandari, A. Aherwar, and R. Rimašauskienė, "Matrix Materials Used in Composites: A Comprehensive Study," in *MaterialsToday: Proceeding*, 2020.

[14] J. A. Duffie, W. A. Beckman, and N. Blair, *Solar Engineering of Thermal Processes, Photovoltaics and Wind*. John Wiley & Sons, Inc., 2020.

[15] N. Roonprasang, P. Namprakai, and N. Pratinthong, "Experimental Studies of a New Solar Water Heater System Using a Solar Water Pump," *Energy*, vol. 33, no. 4, pp. 639–646, 2008.

[16] K. Boedecker and J. Rohweder, "Experiment Instructions: ET 202 Principles of Solar Thermal Energy," 2015.